Enhancement of Energy Efficiency in Stirred Tank Reactors by Use of Computational Fluid Dynamics

Dissertation

zur Erlangung des akademischen Grades eines
Doktors der Naturwissenschaften
– Dr. rer. nat. –

vorgelegt von

Alexander Stefan

geboren in Sarafschan, Usbekistan

Fakultät für Chemie
der
Universität Duisburg-Essen

2018

The work presented here was performed from November 2014 till October 2017 at the University of Applied Sciences Niederrhein in the work group of Prof. Dr.-Ing. H. J. Schultz. It was done in cooperation with the Lehrstuhl für Technische Chemie II of the University of Duisburg-Essen and supervised by Prof. Dr. M. Ulbricht.

Date of oral examination: December 20, 2018

Referents: Prof. Dr. Mathias Ulbricht

Prof. Dr.-Ing. Heyko Jürgen Schultz

Chairman: Prof. Dr. Georg Jansen

Statement

I declare that this dissertation represents my own work, except where it is stated by acknowledgements and references. I only used the materials and references named and this work was not submitted to any other university before.

Düsseldorf, December 2018

Contents

Abstract

The research subject of this work is the fluid and heat flow in a stirred tank reactor with immersing internals like heating elements and baffles. On the basis of an industrial esterification process, the investigation is focused on the efficiency improvement of the reactors unit operations and the interaction between stirrer and static elements. Since flow field measurements are not possible on the industrial precedent, the investigation is approached by computational fluid dynamics (CFD) simulation. Additionally, appropriate downscale models are constructed for flow pattern measurements via particle image velocimetry and serve as an essential validation instrument for the simulation results.

The analysis of the flow conditions of the industrial reactor reveals considerable dead zone formations within the reactor. Those zones included substantial parts of the heater and therefore facilitated heat accumulation and product overheating. Moreover, the phase boundary shows very insufficient movement that delays particle suspension. Those issues are approached in a simulation study by varying the stirrer configuration. As a result, an optimized modification of the stirrer is implemented in the industrial reactor and shows significant improvement on operating utility consumption, heating characteristics, product quality and process control. The production capacity is augmented by up to 12 % higher batch sizes at 6.5 % shorter runtime.

In order to maximize the heat transfer and to homogenize the temperature distribution in the reactor, a novel approach to heater design development is introduced where the kinetic energy that is generated by the stirrer is maximally exploited for incident flow towards the heat exchange surface. An iterative algorithm for adaptive design of the heater is formulated and successfully applied to systems with a radial pumping impeller. The result is a heater element, that achieves the same heat transfer as conventional helical heater coils – however with substantially lower exchange area and significantly improved temperature homogeneity. The realization of the final design in the laboratory demonstrates the validity of the model and opens the way for a new heater design and further development on a novel basis.

1. Introduction

1.1. Agitated vessel reactors in chemical engineering

In process engineering and especially in chemical and biotechnological industry, agitated vessels like fermenters and chemical reactors are commonly used for various applications. These can be characterized by unit operations like heating or cooling, mixing and blending, homogenizing, suspending, gassing and performance of chemical reactions and biological fermentations. Due to the great importance of agitated vessels for the industry and science, they have been investigated in various papers and monographs. In most of the research works, the investigation focuses on a particular basic operation and derives statements concerning this special operation. As a matter of fact, promoting measures for one operation can be counterproductive for another one. However, due to the production process or logistical and economic reasons, various basic operations have to be performed in one single apparatus in industrial practice. It is thus necessary to observe the process holistically under given circumstances. The handling of an agitated reactor is even more complicated in industrial reality because further aspects like product quality, side reactions, production time as well as material and energy consumption have to be considered then.

It is good engineering practice to use common design specifications from relevant regulations and literature. The individual character of the given production aim is often neglected. Since it is mostly not possible to investigate the transport and flow phenomena inside an industrial plant, engineers have to rely on experience and common statements. This often leads to misjudgment of the influences of individual features inside the apparatuses and can impede unexpected issues in the whole process as well as unrecognized and hidden potentials for higher efficiency. Closer “looks” inside individual features are rare and either limited to scientific research on a lab scale level or hosted by companies who protect these expansive investigations. However, several reference projects like that presented in this work, impressively demonstrate the potential, the benefits and the importance of such investigational effort.

1.2. CFD as an engineer's tool

Fluid dynamics is omnipresent in chemical industry. Processes of arbitrary complexity involve handling with material and energy fluxes. Several works serve as basis for practical planning and designing of instruments and apparatuses of production plants. In compliance with given requirements, dimensioning and designing are performed according to pertinent specifications given in standards, monographs or guidelines. Process simulations are very common in chemical industry, too. Due to high complexity, simplified and semi-empirical models were developed for commonly used apparatuses. Those models are the basis for underlying algorithms in process simulation software. A multitude of software applications serve as aid for design and operating of chemical plants.

Computational fluid dynamics simulation (CFD) tools, however, still occupy a niche in chemical industry. Big success of CFD in e.g. aviation or race sports industry is explainable with the fact that it optimizes the final product. In chemical industry, on the other hand, the optimized object is a tool itself. Due to high implementation effort as well as computational and monetary cost of commercial CFD, chemical engineers still mostly prefer well-established process simulation tools. As open and free-to-use CFD tool, OpenFOAM® provides an economic solution and reveals huge potential for optimization of chemical industry utilities.

Individual production plants with very specific requirements can be designed and optimized holistically. However, CFD results have to be verified before serving as a valid tool for apparatus design and optimization. A further hurdle for common establishment of CFD in chemical industry is the high license cost for commercial software. At least this hurdle can be overcome by the free program OpenFOAM®, which competes with the performance of commercial simulators but is less user-friendly, however. Nevertheless, it undergoes continuous development and has the potential to achieve a breakthrough in the industrial use, if supported well by successful cooperation projects like the present.

1.3. State of the art

Like the most areas of processing engineering, stirring technology became scientifically important in the middle of the last century. Ever since, huge progress has been made. By the end of the last century, eminent authorities like Zlokarnik [1]

stated, that classical stirring technology is mostly explored and reliable design rules ensure valid dimensioning for industrial scale apparatuses. The focus of mixing and stirring technology science was expected to shift towards computational methods. As a matter of fact, the computational approach becomes more popular in the scientific investigation area. Besides, new measurement methods allow noninvasive and qualitative determination of flow fields inside the apparatuses. Numerical methods and results can be validated, though.

1.3.1. Measurement technology

Flow field measurements can be performed by means of invasive and non-invasive methods. Of course, invasive methods like pressure drop sensors imply an influence to the flow field. Huge care has to be taken concerning the implementation of the sensors, though. Thus, the limits of invasive methods are narrow and lack for validity due to the impact of the invasion. Non-invasive methods, on the other hand, require huge implementation effort and generally highly expansive measurement technology. Usually, those methods need for a model setup and are generally not applicable in a "living" process. Nowadays, non-invasive measurements pose a fixed component in flow field research. The most widespread methods including the relevant literature are listed in Table 1.

Table 1: Overview of the relevant non-invasive methods for flow field measurements [2]

Method	Measurable	Measurement room	Reference
Laser Doppler Anemometry	1D-velocity 2D-velocity 3D-velocity	point point point	[3]–[6]
Phase Doppler Anemometry	particle size, 1d-velocity particle size, 2d-velocity	point point	[7]–[10]
Holographic Interferometry	temperature and concentration	volume	
Two-Color-Photometry	2 concentrations	volume	
Particle Image Velocimetry PIV	2D-velocity	plane	[11], [12]
Stereo-PIV	3D-velocity	plane	[11], [12]
Volumetric PIV	3D-velocity	volume	[11], [12], [13]
Laser-Induced Fluorescence - LIF	temperature, concentration, etc.	plane	[12], [14]

1.3.2. Computational methods

The behavior of fluids obeys the Navier-Stokes-Equations. These are differential expressions that are mutually coupled and non-linear. As there is no general solution to those equations, numerical methods are developed for the approximation and prediction of the observed fields like velocity, pressure, temperature, etc. Generally, the numeric approach approximated differential operators by difference quotients. This is called discretization, since the calculation occurs at discrete spots (nodes) of the observed domain and time and involves discrete differences instead of a continuous field description. Of course, spatial and temporal resolutions play a role in the solution accuracy. Different discretization methods have been established for the solution of differential equations:

- Finite differences method (FDM): simple and fast method for the solution of strictly structured problems. The differential expression is replaced by the difference expression in each node. The expression for one node involves implicitly the field values of neighbor nodes. Together, the expressions for all nodes form a system of algebraic equations which can be solved by matrix solvers. However, this method is useless for complex flows due to accuracy issues.

- Finite volume method (FVM): takes advantage of the conservation law. An integral form of the differential equations allows the enforcement of mass conservation, since fluxes are calculated and implicitly balanced at each finite volume (cell). Arbitrary cell shapes, structured as well as unstructured, can be used for this method. The discrete field values are valid for the whole cell, though. Hence, the fields are not continually throughout the domain, which is the main difference to the finite element method.

- Finite element method (FEM): is an extension on the finite volume method. Inside an element (volume or area cell), the field values are described by a function and not only by a value. In addition to mass conservation, this guarantees field continuity throughout the domain even beyond single elements.

In computational fluid dynamics (CFD), FVM is commonly used, since it is an appropriate compromise between accuracy and calculation and implementation

costs. Today, CFD is a quick growing business area that covers various areas of industry and science like aerodynamics of aircrafts and vehicles, hydrodynamics in naval architecture, turbomachinery, heat transfer problems, chemical reactions, combustion, meteorology, oceanography, etc. Detailed information can be reviewed in relevant literature like [15]–[19].

For the mathematical description of flow conditions inside an agitated vessel, various empirical and semi-empirical models were derived for characteristic reactor types. However, these models serve as generic information and have little benefit for concrete applications and optimization work.

Nowadays, in the commercial use of CFD, it usually comes embedded in a whole computer aided engineering (CAE) workspace. Whenever possible, it is used to optimize products regarding its aerodynamics, hydrodynamics, resilience etc. A multitude of software applications from CAD (computer aided design) to CFD and FEM analysis, as well as process simulations are employed in this scope. Several special methods like the discrete element method (DEM) and population balances (PB) are being developed lately and also find their way into practical use.

1.4. Aims of this work

The investigations in the area of stirring technology often are done in laboratory scale only. This leads to a lack of transfer to industrial applications. Besides, experimental work is expensive when it comes to measurement technology and construction of prototypes. On the other hand, computational methods have little value when there is no verification to its validity. This work takes these issues up and combines those three aspects (industrial process, laboratory measurements, and the fluid simulations) – however, keeping the focus on CFD calculations.

To guarantee successful transfer from scientific results to industrial applications, an existing production plant was chosen as a reference object for investigation. One of the main aims of this work is to identify the main problems of the existing process which is supposed to be representative for the actual state of the art. The perceptions should lead to concrete measures which are realizable in the industrial practice and serve for tangible improvement of the current process. Furthermore, this work should seek for general problems in this type of apparatuses and formulate general

statements regarding the interaction between the stirrer and various internals. Special attention should be paid to heat transfer phenomena, mixing time and general flow pattern homogeneity. Detached from the reference process, different internals and stirrer types have to be investigated with the same focus. The aim is to give recommendations concerning optimal operating parameters and optimal internals design.

In the scope of this work, efficient methods for simulation, measurement, industrial transfer and a symbiotic relationship between those aspects must be found and realized. Each of the disciplines must benefit from this collaboration. The industrial process provides a basis for investigation with practical relevance and becomes improved. The simulation reveals important trends, potential problem zones and not measurable effects but on the other hand benefits from measurement validation. The measurement technology allows reliable statements about the flow conditions and benefits from the simulation since experimental load is reduced significantly.

1.5. Concept and scope of this work

Since it is the perspective of this work to involve an industrial reference process, a geometric down scale model of it serves as a basis for the laboratory investigations which themselves serve as validation tool for simulations. The focus of this work lies in the implementation of the observed problem in the CFD workspace and running numerical studies with the aim to improve both, the operating parameters as well as developing optimal designs for future apparatuses. Thereby, different abstraction levels of modelling are used and assessed via consistency inspection and comparison to measurement results.

Following the main tasks of an agitated vessel, this work investigates the efficiency of heat transfer, and it approaches the mixing characteristics and the flow patterns. Available design specifications are scrutinized and reviewed. The conclusions from the simulation studies are transferred to the laboratory scale models for validation with measurements. Valid methods then are used for the optimization of the industrial process.

After the exploration of the reference process and other commonly used designs, novel shapes are sought for to handle identified problems which occur with the classical construction design.

The theoretical background will treat the basics of stirring technology as well as the physical and numerical principles that are important for this work. Chapter 3 will describe in detail how particular investigation methods are implemented and set up in the used CFD tools. Analogically, the implementation of measurement technology will be described in chapter 4. The flow fields of observed cases will be discussed in chapter 5. Chapter 6 will extensively treat heat transfer and chapter 7 will discuss energy consumption problematics. Chapter 8 deals with the implementation of a method definition for mixing time investigations. In every chapter the numerical results will be validated by means of numerical criteria and measurement data as far as they are available and comparable.

2. Theoretical background

2.1. Aims of stirring technology

In chemistry, the crucial condition for reactions is to bring reactants into contact. The most classical way to do so is stirring, as we see not least in our daily life. Transferred to the technical view, stirrer and a vessel are needed for it, which together pose an agitated apparatus. Since such an apparatus is an investment for the operating company, it is endeavored to provide versatile application possibilities. By installation of special internals in the vessel, basically any energy and material transport process can occur in the agitated tank. The main tasks of a stirred vessel reactor can be classified into the following basic operations:

- mixing and blending
- heating and cooling
- generation of emulsions, suspensions and dispersions
- homogenization

Those basic operations can be performed subsequently or simultaneously, depending on the process requirements and conditions. In the course of the enhancement of energy efficiency, further aspects like power consumption of the agitator unit and heat efficiency play a crucial role.

2.1.1. Homogenization

Material as well as temperature inhomogeneities often lead to negative implication on the whole process. At worst, huge gradients entail cavity, uncontrolled or chain reactions, substance damaging etc. Apart from material and energy transport, the process should ensure quick and efficient homogenization, hence. Within the meaning of stirring technology, homogenization is the generic term for mixing and blending. In this work, however, the concept of mixing is rather orientated on the temporal material transfer inside an apparatus, whereas homogenization is a term of the current or at least the temporal averaged (over a short period) state, regarding both, the velocity and the energy fields. An appropriate mathematical measure for homogeneity has to be derived for use in the temporally resolved mixing

investigations. I.e. homogenization is the prerequisite term for any mixing investigation. The focus of homogenization is moreover not only in the pure distribution of field values but also in the detection of problem zones and areas of big gradients.

2.1.2. Mixing and blending

Different types of mixing can be distinguished: micro and macro mixing. Macro mixing regards a certain state (material distribution, temperature, etc.) all over the domain, whereas micro mixing looks into a small scale volume down to molecular level. Both of these aspects deserve consideration; different phenomena dominate the respective mixing type, though. In this work, macro mixing is referred to when mixing is mentioned. Micro mixing is not really covered in the scope of this work since it is a generic matter of substance systems and not specific to stirring technology, whereas this work takes a rather technical point of view considering agitated processes. Fundamentally, mixing is a transformation operation of a physical system with an impact on the degree of homogeneity. Generally, mixing is achieved by convective transport and is decisive for chemical reactions and the efficiency of other unit operations like heat and material transfer, emulsification, dispersion and suspension. The most prominent example of mixing is clearly the blending of different substances. However, mixing also includes the temporal homogenization of energy profiles by means of convective transport. One way of qualifying and quantifying the mixing characteristics is the determination of mixing time. Some kind of a homogenization degree is required for it, which, plotted against time results in a convergent curve. The time spot when the curve becomes convergent is defined as mixing time.

2.1.3. Heating and cooling

The process conditions of an agitated process usually require the preservation of a certain temperature inside the chemical reactor. For the most reactions, temperature has a huge influence on the thermodynamics, kinetics, selectivity, side reactions and product quality. Often, the margin for temperature deviations is quite narrow and a tight spatial temperature profile is required. Furthermore, temperature can be used as a control mechanism for processes and reactions by use of a temporal temperature profile. In a closed vessel, energy originally enters the system by conductive

transport and then is distributed by mixing, i.e. convective transport. In addition, radiative heat transport is to be mentioned, but will not be discussed in the scope of this work due to inferiority in the observed cases compared to conductive and convective transport.

In an agitated vessel, heat exchange can be performed by jacket heating or heat exchange internals (cooling is also possible, when heating is referred to but will not be explicitly mentioned henceforth). Zlokarnik [1] summarizes commonly used variants of jacket heating in Fig. 1. Widespread internal heat exchangers are different types of heating coils. The most common ones are shown in Fig. 2. However, in recent time other types of heat exchangers become more popular like tube baffles and heating plugs, which pose an elegant union of heater and baffles, but have significantly lower exchange area in comparison with heating coils, on the other hand.

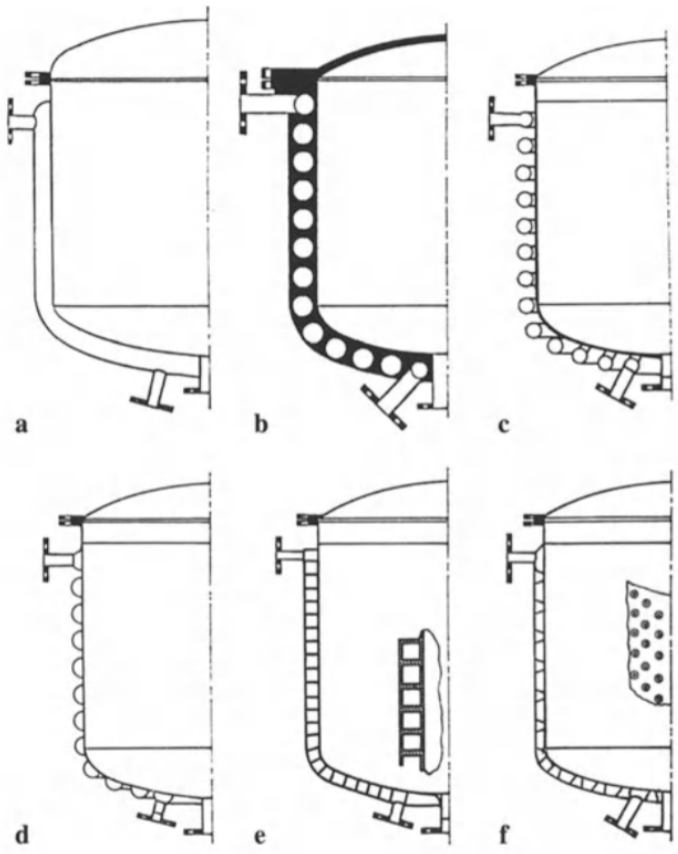

Fig. 1: Variants of jacket heating for reactors and vessels. a) full jacket, b) cast-iron with molded pipes, c) welded pipe coil with copper interlayer, d) welded half-pipe coil, e) welded channels from angle profiles and f) double-wall-studs-welding [20]

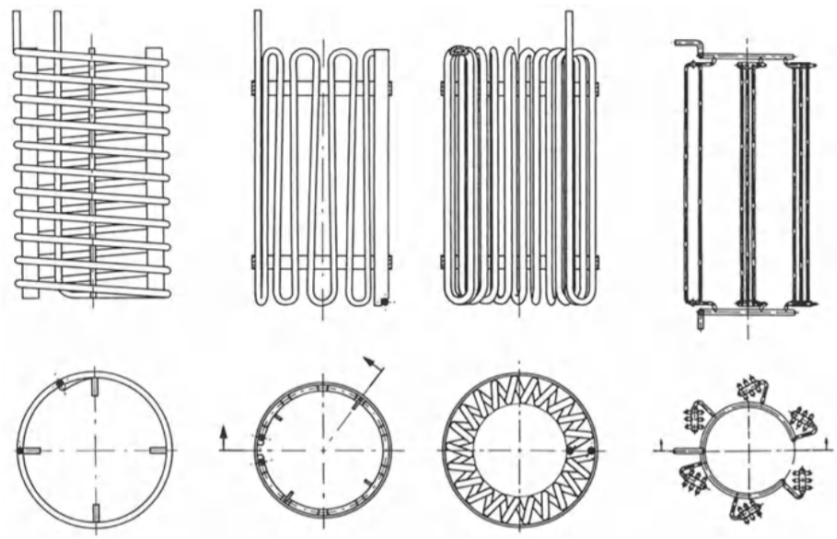

Fig. 2: Variants of heating coils for reactors and vessels. From left: helical coil, single meander coil, double meander coil, register pipes.

The choice of the heater type is always influenced by the used stirrer, the required heat exchange quantity and the availability and costs of the respective heater design. In practice, some combinations of stirrers, internals and reactor types are not feasible, since maintenance and repair work would imply too high effort and costs. Depending on the heat exchange task, further aspects have to be considered. The heat medium is decisive for the direction of the current. Especially in the case of steam heating, the selection of possible heater designs is very limited and requires special operating arrangements. The temperature, however, is nearly constant along the whole heater due to latent heat.

2.1.4. Power consumption of stirred processes

For the purpose of energy analysis and efficiency enhancement, it is necessary to observe the power consumption of the agitator unit. From the practical point of view, not only the agitator power is relevant but also the power loss at the gear and the shaft bearing and seal. Additionally, the start power has to be considered, but can be neglected if the stationary process is comparatively long, which is usually the case in chemical industry. Power losses of stirrer drives are generally well known by the manufacturers of the agitator units, this work focuses on the pure agitator power *P*, hence. The generic formula for power consumption is a product of the torque *M* and the angular speed ω of the stirrer:

$$P = M \cdot \omega \tag{2.1}$$

where $\omega = 2\pi n$, n is the rotational frequency of the stirrer.

The agitator power is handled differently for homogeneous and gassed processes as well as for Newtonian and non-Newtonian fluids. Gassed processes and non-Newtonian fluids occupy separate fields of research which is why only homogeneous processes with Newtonian fluids are observed in the scope of this work.

The Newton number Ne is a characteristic key figure for power consumption of an agitated process. Considering the influence of given parameters like installation conditions (bottom clearance of the stirrer, filling level of the fluid, dimensioning of the reactor, etc.) and the impeller type, the power consumption is derived as a function of the impeller diameter d, the rotation frequency and the transport properties of the substance (density ρ, kinematic viscosity ν, etc.) by means of dimensional analysis:

$$Ne = \frac{P}{\rho n^3 d^5} \tag{2.2}$$

In the course of the dimensional analysis, a second relevant key figure – the Reynolds number – comes out:

$$Re = \frac{nd^2}{\nu} \tag{2.3}$$

The Newton number is referred to as the target key figure and the Reynolds number as the process key figure, respectively. A plot of those key figures is known as “performance characteristics” (see Fig. 3). It clearly shows different sections of the plot, namely the laminar, the turbulent and the crossover section.

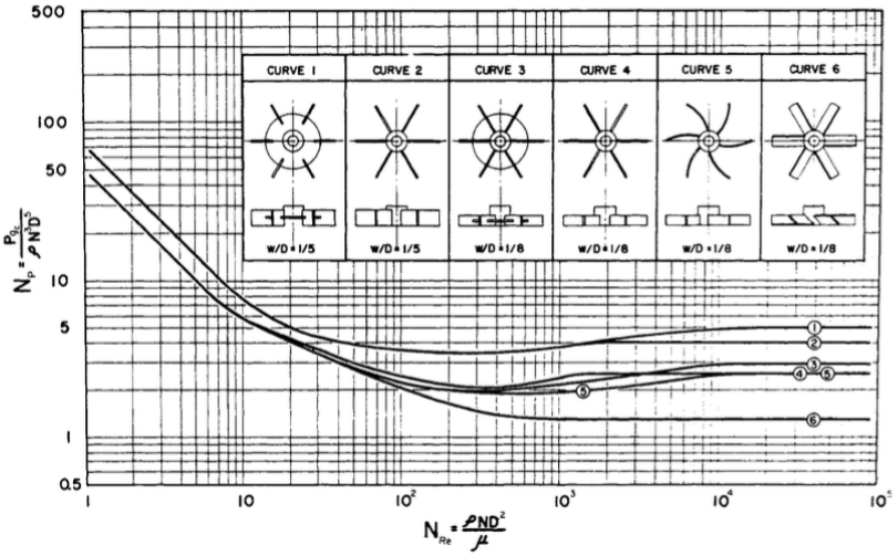

Fig. 3: Performance characteristics for different stirrer types [21].

The performance characteristics are well documented for a multitude of stirrer types and installation conditions – baffled as well as unbaffled.

2.2. Theoretical background on heat exchange

Heat can be brought into a system in different ways. Actually, three fundamental methods of heat transport are distinguished: convective, diffusive and the radiative heat transport. The radiative transport is not objective of this work; hence it will not be discussed here. Since batch processes are observed here, no heat enters the system by convection. The heat is exchanged at special surfaces of the heater which is heated by a heat carrier, itself. Hence, a double heat transfer occurs at both sides of the heater and the heat flows in a diffusive manner through the solid heater wall. The total heat transfer from heat carrier to the fluid in the vessel domain is illustrated in Fig. 4 in a generic and schematic way.

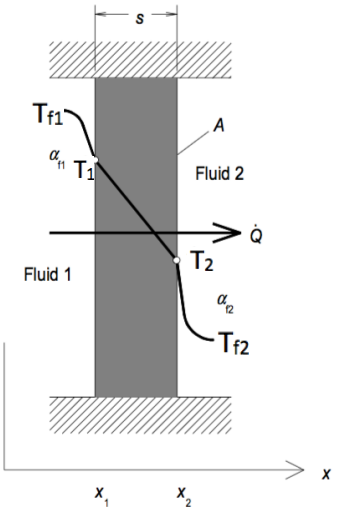

Fig. 4: Heat transfer through a solid wall [22].

The curved black line shows the temperature course throughout the wall. It starts and ends tangentially to the fluids on both sides of the wall. Those points demark the so-called thermal boundary layer δ^*. This is a layer, where the fluid is laminar due to the flow resistance at the wall. The thickness of that layer decreases with increasing turbulence intensity, since high kinetic energy sheers off the laminar structure. Within this layer, heat is transported by diffusion, since no convective transport is possible towards the wall due to the laminar character of the layer. Diffusive transport is by scales slower than convective; therefore, the heat transfer is dependent on the boundary layer thickness. Beyond the boundary layer, heat transfer is dominated by convection and is assumed to be generally constant due to turbulent mixing. This is why the temperature course expires tangentially at those points. The general heat

transfer coefficient can be approximated to normal conduction with the thermal conductivity of the fluid λ:

$$\alpha = \frac{\lambda}{\delta} \tag{2.4}$$

Of course, this linear expression contradicts the curvy course in Fig. 4. However, the transition between laminar and turbulent domains is vague. δ is an easy to handle and valid approximation of the full boundary layer thickness δ^*, though.

For the augmentation of the heat flux $\dot{Q}$, the aim is to produce high flow intensity towards the heater surface A. The heat flux can be calculated via the principal conductance law by use of the heat transfer coefficient and the temperature difference between the fluid and the heater surface $\Delta T = T_2 - T_{f2}$ [22], [23]:

$$\dot{Q} = \alpha \cdot A \cdot \Delta T \tag{2.5}$$

This formula is basically the starting point for the dimensioning of heaters. Since the desired heat flux and the temperature difference are normally predefined and heat transfer coefficients can be looked up for certain material-liquid couples in tables, the exchange area is the calculated design value. Of course, this good engineers practice is a pragmatic and fast way to dimension the heater size. However, the local heat transfer is not considered in this method and can lead to unforeseen effects. In industrial practice, design and dimensioning often is performed by use of characteristic equations which contain dimensionless numbers.

2.2.1. Nusselt number

This number *Nu* characterizes the exchange efficiency of a heater. It is the ratio between the thermal boundary layer δ and the characteristic length d of the heater as e.g. the diameter of a heating pipe. Application of this (cf. eq. (2.4)) leads to the formulation of the Nusselt number:

$$Nu = \frac{\alpha \cdot d}{\lambda} \tag{2.6}$$

2.2.2. Reynolds number

This is the most relevant number in fluid dynamics. It characterizes the turbulence of the flow. Turbulence emerges by demolition of the laminar structure of hypothetic layers which slide at each other and layer become winded to eddies due to the friction between the layers – this resistance is referred to as viscosity. The Reynolds number is a ratio between inertia and friction forces:

$$Re = \frac{\bar{u} \cdot d}{\nu} = \frac{nd^2}{\nu} \tag{2.7}$$

The middle part of the equation is for use in pipes where a mean velocity is known by total flux. The characteristic length is the pipe diameter. The right side of the equation is for use in stirred processes and involves the rotational frequency n. The characteristic length is the stirrer diameter. According to the relevant literature [1], [24]–[26], full turbulence is reached at a Reynolds number of 10,000.

2.2.3. Prandtl number

This is the ratio of two transport numbers, the momentum and the conductive thermal transport. The momentum transport is described by the kinematic viscosity which is the dynamic viscosity η, normalized by the density. The thermal transport a, on the other hand is the conductivity λ, multiplied by the density and divided by the heat capacity c_p of the fluid:

$$Pr = \frac{\nu}{a} = \frac{\eta \cdot c_p}{\lambda} \tag{2.8}$$

An illustrative description of the Prandtl number is the ratio between the thicknesses of laminar boundary layer at a wall and the thermal boundary layer. The Prandtl number is obviously magnitudes higher for liquids than for gases [22].

2.2.4. Heat transfer characterization

Each of the presented numbers are characteristic for one aspect of a process. The Prandtl number consists of material values and is a material number, hence. It is determined by the system and allows least influences. The Reynolds number is determined by the size of the apparatus and depends on the mechanical operation parameters like flow velocity or stirrer frequency. A direct impact can be generated by

these parameter adjustments. The Nusselt number has a thermal character and is the most complicated to determine. It is a function of the material and operating influences; hence $Nu = f(Re, Pr)$. For different heat exchange situations, there are multiple equations formulated in [23], however the following is the most generic and very well applicable to stirred processes:

$$Nu = C \cdot Re^{c_{Re}} \cdot Pr^{c_{Pr}} \cdot \left(\frac{\eta}{\eta_w}\right)^{c_{Vis}} \tag{2.9}$$

where the coefficients C, c_{Re}, c_{Pr} and c_{Vis} can be looked up for different heated systems. The last factor is the ratio between the viscosities in the main fluid domain and in the immediate heater surface vicinity. c_{Vis} is generally low and is not observed in this scope.

2.3. Numerical simulation

In this work, computational fluid dynamics with the finite volume method is meant whenever “numerical simulation” is mentioned. The basis for numerical simulation is the Navier-Stokes-Equation (NSE) system.

2.3.1. Physical principles of fluid dynamics

A fluid element is observed in time and space and described mathematically. Since it can undergo deformation and distortion, extension and shrinking, acceleration and deceleration, the mass element *m* (control mass CM) is described in the integral way, namely as the volume *V* integral of its density ρ:

$$m = \int_{V_{CM}} \rho \, \mathrm{d}V \tag{2.10}$$

This equation can be understood as a relationship between the extensive Φ (quantified by mass) and intensive ϕ (standardized by mass) description of a conserved physical size, where, of course, the intensive size stands in the integral. To observe the development i.e. the dynamics of this mass element, it is differentiated by time *t*. Since the observed CM volume deforms by time, it is expedient to transform the volume integral of the CM to the sum of a control volume (CV) integral and the fluxes of the observed CM through the CV boundary:

$$\frac{\mathrm{d}\Phi}{\mathrm{d}t} = \frac{\mathrm{d}}{\mathrm{d}t}\int_{V_{CM}} \phi\rho \,\mathrm{d}V = \frac{\mathrm{d}}{\mathrm{d}t}\int_{V_{CV}} \phi\rho \,\mathrm{d}V + \int_{S_{CV}} \phi\rho(\boldsymbol{u} - \boldsymbol{u_b}) \cdot \boldsymbol{n} \,\mathrm{d}S, \tag{2.11}$$

where S is the CV boundary surface, $\boldsymbol{n}$ its normal, $\boldsymbol{u}$ the mass flux velocity and $\boldsymbol{u_b}$ the boundary velocity of the CV. Hereinafter, the CVs are assumed to be stationary, hence the boundary velocity to be zero and the differential operator becomes partial. This generalized equation (2.11) is known as the Reynolds theorem. This form already shows the finite volume character. Obviously, the mass is conserved if all cells of the flow domain (all CVs) are contiguously connected and neighboring cells share congruent faces. The integral form can also be reduced to an integral and discretization free form by use of the Gaussian theorem[1] and shrinking of the CV down to infinitesimal scale $V_{CM} \to \mathrm{d}V$:

$$\frac{\partial \Phi}{\partial t} = \frac{\partial}{\partial t}\phi\rho + \phi\rho\nabla \cdot \boldsymbol{u} \tag{2.12}$$

The **mass conservation** equation can be derived when setting $\Phi = m$. The time differential of it must be zero since the mass conservation guarantees continuity. Hence, the continuity equation reads

$$\frac{\partial}{\partial t}\rho + \nabla \cdot (\rho\boldsymbol{u}) = 0 \tag{2.13}$$

Moreover, for the description of a fluid flow, **momentum conservation** is needed. Since the momentum $\boldsymbol{J} = m\boldsymbol{u}$ is a vectorial size, applied in the Reynolds theorem it results in a three-dimensional equation. Furthermore, the time differential of the momentum is the force $\boldsymbol{f}$:

$$\frac{\partial \boldsymbol{J}}{\partial t} = \frac{\partial}{\partial t}\int_{V_{CV}} \rho\boldsymbol{u} \,\mathrm{d}V + \int_{S_{CV}} \rho\boldsymbol{u}\boldsymbol{u} \cdot \boldsymbol{n} \,\mathrm{d}S = \sum \boldsymbol{f} \tag{2.14}$$

Two types are to be distinguished: volume forces like gravitation and surface forces like shearing. It is important to distinguish those types before simplifying the equation (2.14) to the integral-free form. Surface forces have then to be transformed by the Gaussian theorem, first. Only Newtonian fluids are observed in this work, so the surface forces are described by the stress tensor **T**:

[1] Gaussian divergence theorem, applied to the surface integral of equation (2.11): $\int_S \phi\rho\boldsymbol{u} \cdot \boldsymbol{n} \,\mathrm{d}S = \int_V \phi\rho\nabla \cdot \boldsymbol{u} \,\mathrm{d}V$

$$\mathbf{T} = -\left(p + \frac{2}{3}\nu\nabla \cdot \boldsymbol{u}\right)\mathbf{I} + 2\nu\mathbf{D} \tag{2.15}$$

where p is the pressure, ν the kinematic viscosity, **I** the unit tensor and **D** the deformation tensor:

$$\mathbf{D} = \frac{1}{2}(\nabla\boldsymbol{u} + (\nabla\boldsymbol{u})^T) \tag{2.16}$$

The volume forces can be represented by the volume integral of the product of the density and the intensive force, which is acceleration $\boldsymbol{b}$. Therefore, the momentum differential generally is described as

$$\frac{\partial \boldsymbol{J}}{\partial t} = \sum \boldsymbol{f} = \int_{S_{CV}} \mathbf{T} \cdot \boldsymbol{n}\,\mathrm{d}S + \int_{V_{CV}} \rho\boldsymbol{b}\,\mathrm{d}V. \tag{2.17}$$

In the integral-free form, equation (2.14) finally reads

$$\frac{\mathrm{d}(\rho\boldsymbol{u})}{\mathrm{d}t} + \nabla \cdot (\rho\boldsymbol{u}\boldsymbol{u}) = \nabla \cdot \mathbf{T} + \rho\boldsymbol{b} \tag{2.18}$$

In the **conservation of scalar quantities**, the transport can also occur by other mechanisms than convection or divergence. In general, it is diffusion transport f_D. Analogue expressions for material and heat serve for the description of diffusion – Fick's and Fourier's laws, respectively. In both cases, it is the product of a certain diffusion coefficient Γ and the driving force $\nabla\phi$ over the observed surface. In the case of a finite volume, diffusion is described as follows

$$f_D = \int_{S_{CV}} \Gamma\nabla\phi \cdot \boldsymbol{n}\,\mathrm{d}S \tag{2.19}$$

Further temporal changes can occur in the finite volume due to generation or destruction. For example, chemical reactions can lead to sources and sinks of both, material and heat. Generally, such phenomena follow certain laws like kinetics or thermodynamics and are summarized as source terms q_ϕ. The whole conservation equation for scalar quantities is a combination of the source term and equations (2.12) and (2.19):

$$\frac{\partial(\rho\phi)}{\partial t} + \nabla \cdot (\rho\phi\boldsymbol{u}) = \nabla \cdot (\Gamma\nabla\phi) + q_\phi \tag{2.20}$$

The terms of this equation obtain labels due to their physical meaning. The terms are named from left: temporal, convective, diffusive and source terms. Strictly speaking, equation (2.20) has the same, although extended, shape as the expressions for mass and momentum conservation. Together, the conservation equations, which are nonlinear, coupled and differential, form the Navier-Stokes-Equation- (NSE) system. Therefore, some authors like [27] and [17] represent the NSEs in a single vectorial equation, that contains all conserved quantities. The NSE -system is used to calculate mainly the pressure and velocity fields. Depending on the physical problem complexity, further fields like density, temperature and viscosity become relevant, although.

A generalized and united form of (2.20), where the temporal solution vector $\boldsymbol{U}$, the convective fluxes $\boldsymbol{F}$ and the diffusive fluxes $\boldsymbol{G}$ (including turbulence modelling) are involved into the respective terms, reads [27]:

$$\frac{\partial(\boldsymbol{U})}{\partial t} + \nabla \cdot (\boldsymbol{F}) - \nabla \cdot (\boldsymbol{G}) = \boldsymbol{q}_{\phi} \tag{2.21}$$

where $\boldsymbol{U}$, $\boldsymbol{F}$ and $\boldsymbol{G}$ are five-dimensional vectors (mass, momentum and energy).

2.3.2. Operating principles of the finite volume method

Flow fields are often calculated on complex geometries. Unlike very simple and straight geometries used in the FDM, the spatial discretization of complex geometries produces nodes, which are non-orthogonal to each other and therefore need for special handling. The differential terms cannot just be transformed to differences like it is done in the FDM, since numerical inaccuracy leads to highly unstable computation. In the FVM, flux control suppresses high instabilities and allows arbitrary cell shapes. Therefore, the integral form of the conservation equations is used and the flux serves as a balancing mechanism. Equation (2.21) can be transformed to the integral form by use of the Gaussian theorem:

$$\frac{\partial}{\partial t}\int_{V} \boldsymbol{U}\,\mathrm{d}V + \int_{S} (\boldsymbol{F} - \boldsymbol{G}) \cdot \boldsymbol{n}\,\mathrm{d}S = \boldsymbol{q}_{\phi} \tag{2.22}$$

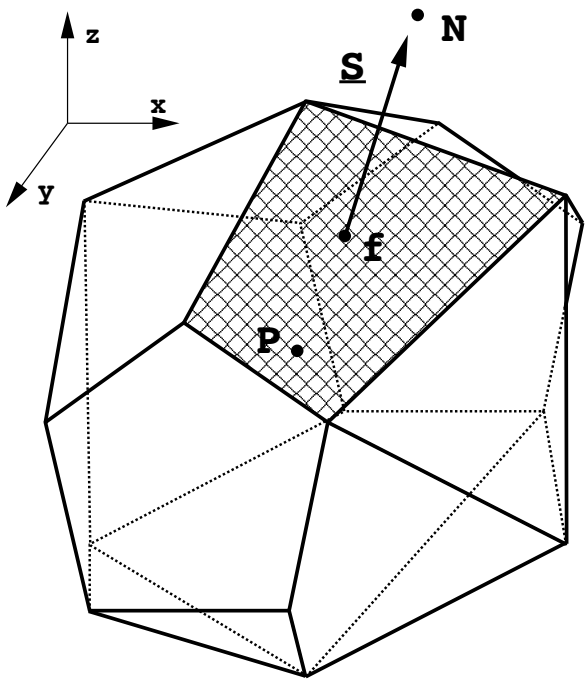

Fig. 5: A typical FVM-cell [28]

The handling of this form becomes straightforward realizable, when the volume element is framed in easily computable planar faces. The most primitive volume is a cube, hence. The integration of the volume as well as of the faces can be implemented without hard effort.

2.4. Turbulence

This term originates from the Latin word *turbare* which means spin, trouble or distract. In fluid dynamics, it describes a state of the flow, where vortices and eddies of different scales are formed and transported. Kolmogorov [29], [30] developed a physical theory on the generation and decay of eddies. According to this theory, eddies witch emerge behind blades or due to high sheering forces, decay into smaller eddies, which then decay into even smaller ones until they reach a certain size where the cannot decay furthermore and dissipate as thermal energy in the fluid (Kolmogorov scale [31]). This process is entropic and therefore irreversible.

Turbulence provokes a three-dimensional flow field, that varies temporally and locally in a manner that is apparently randomly. For a certain location in the domain of turbulent flow, the temporal plot of velocity appears like a base curve with noise (Fig. 6).

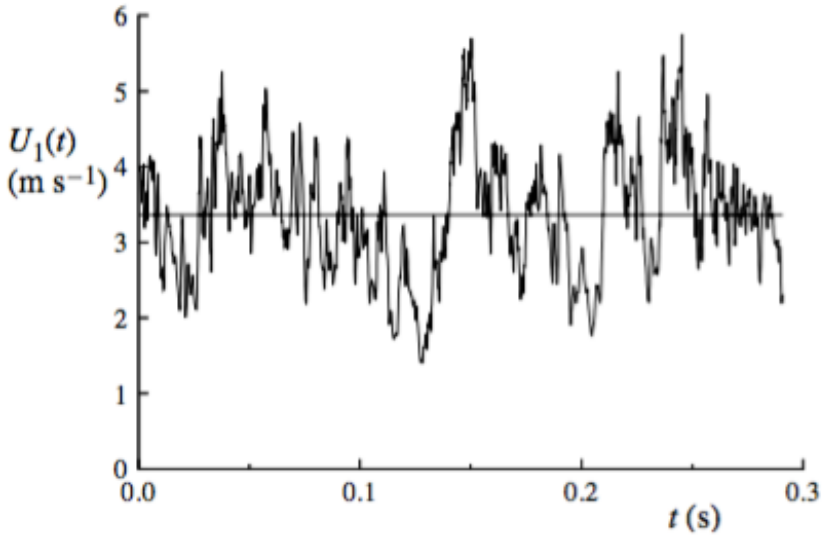

Fig. 6: Temporal plot of local velocity in a turbulent flow [31]

2.4.1. Reynolds-averaged Navier-Stokes Equations

The absolute velocity $\boldsymbol{u}$ at that point $\boldsymbol{x}$ and time t can be described by an apportionment into a temporally averaged part $\overline{\boldsymbol{u}}$ and the deviation part $\boldsymbol{u}'$, respectively:

$$\boldsymbol{u}(\boldsymbol{x},t) = \overline{\boldsymbol{u}}(\boldsymbol{x},t) + \boldsymbol{u}'(\boldsymbol{x},t) \tag{2.23}$$

whereas the averaged part can be calculated via the integral mean value theorem:

$$\overline{\boldsymbol{u}}(\boldsymbol{x},t) = \frac{1}{\Delta\tau}\int_{\tau}^{\tau+\Delta\tau} \boldsymbol{u}(\boldsymbol{x},t)\,\mathrm{d}t \tag{2.24}$$

$\Delta\tau$ is a period of time that is sufficiently large for averaging the value of $\boldsymbol{u}$ but small enough to avoid discrimination of possible flow unsteadiness. Obviously, t has to lay in the interval $[\tau, \tau+\Delta\tau]$. The same apportionment can be performed with the pressure and the resulting formulations are applied to the NSE. This formulation is used for the development of the so-called Reynolds-averaged Navier-Stokes (RANS) equations which are also used for computation of turbulence without the need to resolute the grid down to the Kolmogorov scale. It is referred to as Reynolds-averaged simulation (RAS). The deviation part of the velocity is temporally seen, of course, balanced out. However, if the mean square root of the velocity deviation is calculated, the result is an extent that stands for turbulence intensity. It is basically the standard deviation of the velocity, normalized by the mean velocity. The

additional unknowns in the RANS formulation are expressed by the Reynolds stress tensor **R**:

$$\mathbf{R} = \rho \begin{bmatrix} u_x'u_x' & u_x'u_y' & u_x'u_z' \\ u_y'u_x' & u_y'u_y' & u_y'u_z' \\ u_z'u_x' & u_z'u_y' & u_z'u_z' \end{bmatrix}, \boldsymbol{u}' = \begin{pmatrix} u_x' \\ u_y' \\ u_z' \end{pmatrix} \tag{2.25}$$

Under the assumption of isotropic turbulence (no direction is preferred), the six unknowns are reduced to one only. The resulting variable has the shape of kinetic energy. Since it is the result of turbulent fluctuations, it is called the turbulent kinetic energy:

$$k = \frac{1}{2}\left(u_x'u_x' + u_y'u_y' + u_z'u_z'\right) \tag{2.26}$$

This formulation is used for the development of turbulence models, see [31].

2.4.2. The k-ϵ turbulence model

Due to the apportionment of the velocity and pressure and their application to the NSE, additional sizes appear in the equation systems. The additional terms have the shape of the viscous term and are connected to it, hence. Therefore, the effective viscosity ν_{eff} is described as a sum of standard physical viscosity ν and the additional turbulent viscosity ν_t. The turbulent viscosity can be calculated via two additional equations – one for the turbulent kinetic energy k (2.26) and one for the dissipation energy ϵ:

$$u_x'u_y' = \nu_t \frac{\partial \overline{u_x}}{\partial y} = 0.09 \frac{k^2}{\epsilon} \frac{\partial \overline{u_x}}{\partial y} \tag{2.27}$$

The equations for k and ϵ are applied to the Reynolds theorem and result in an augmentation of the NSE-system. Since turbulence models are not objects of the research in the scope of this work, further information is referred to in the relevant literature like [31]–[34].

2.5. Special mesh treatment at stirring problems

During the implementation of a stirred system, the moving element has to be considered. This matter of fact poses a serious problem to the numerical system, since the flow domain is not static anymore and hence requires special treatment. In

a case where the domain boundaries remain static in relation to each other (e.g. the domain of a sloshing tank), solely additional pseudo forces have to implemented. If this is not the case, individual cells have to be deformed during the time. This has to be considered at the face flux correction and volume integration steps. Oscillatory movement can be handled this way usually satisfactorily. In the case of exaggerated squeezing, deforming and unphysical twisting of a cell, special mechanisms for generation and deletion of cells have to be implemented and are generally numerically elaboration as well as highly expensive regarding the calculation cost and memory demand.

There have been established some applicable methods for handling the issue of a rotor-stator system:

- multiple reference frame (MRF)
- arbitrary mesh interface (AMI) or sliding mesh
- clicking mesh
- distortion and remeshing
- overset mesh

Clicking mesh is suitable for highly structured grids which cannot be provided due to a very high degree of complexity. Distortion and remeshing is the method which was mentioned above. It is not pursued due to high demand for resources on the one hand and the lack of significant benefit on the other hand. The overset mesh method is a new development in OF. It uses multiple grids (static and moving grids) which overlap and allow smooth interpolation between the reference frames of each. It cannot be discussed in the scope of this work, but deserves to be mentioned due to its promising potential, seen in other CFD software.

2.5.1. Multiple reference frame

The multiple reference frame (MRF) method is described in [35]. A good overview description is also given in [36]. It is a method, which allows different zones of the grid to move with different velocities. Rotational and translational speeds can be applied to different zones. The grid connectivity remains close, only the mathematical

system and the governing equations for the cells in the different zones change. The interfaces between stationary and moving zones have to be treated in a special way, though. A local transformation is necessary to make flow variables of one zones cells to be used for the calculation of fluxes towards the attached cells of the other zone. Actually, the boundaries inside the respective zones do not move, hence there is no actual relative movement between different geometry parts. The full interaction of for example rotor and stator parts of the geometry cannot be discussed by means of this method. However, if the interaction is relatively weak, the use of the MFR method shows valid results. Since the interaction of the impeller blades with the stationary internals of a stirred vessel do not show transient effects observed over a long time scale – i.e. the transient effects are balanced out over a certain period of time – the MRF model can be used for the simulation of stirring processes, even though it is a huge simplification and clearly an approximation of the physics.

Some limitations have to be considered, when implementing a MRF zone. The internal boundary – i.e. the interface between stationary and rotational zones – has to “move” with a velocity that is orthogonal to its orientation. This is the case when a cylinder is implemented as rotational cell zone and the rotation axis coincides with the cylinder axis. In practice, the boundary is described by a set of cell faces. The described condition has to be good for each of those faces; otherwise huge numerical errors occur and can lead to a crucial loss of stability.

As mentioned before, short time transient effects are ignored by this method. If there is the need to temporally resolute the flow field, the AMI method is privileged. Since the MRF method generates something similar to temporally averaged flow fields, the fields can be interpreted as averaged screenshots, or “frozen flow fields”. This poses a problem, if physical particles have to be traced throughout the MRF domains since short time transient effects play a crucial role on the particle path. Strictly mathematically, this effect disappears for mathematical particles – i.e. particles with zero mass – since the short time effects are balanced out statistically. This is not the case for physical particles (with no zero mass) since inertia forces are involved and the particles do not only follow the flow field.

In the case of a stirrer, a cylinder is implemented around the stirrer geometry. The size of the cylindrical MRF zone is not exactly straightforward. Strictly seen, the zone of rotation is limited to the revolution volume of the stirrer itself – which has not

necessarily got to be a cylinder. In practice, such an approach often leads to instabilities and difficulties at mesh generation. Following the main principle of MRF method, the interaction between stator and rotor has to be minimal. This is evidently the case in the middle between rotor and stator. One has to be careful with a too large cylinder – if it is magnitudes larger than the stirrer itself, the relative movement will be calculated in a wide too large domain and predict the stirrers pumping effect exaggerated. In the observed cases, the stirrer has a diameter of about 1/3 of the vessel diameter. The middle between stirrer tip and stator baffles is a good choice for the MRF, hence. Fig. 7 shows an exemplary grid with an MRF zone implementation.

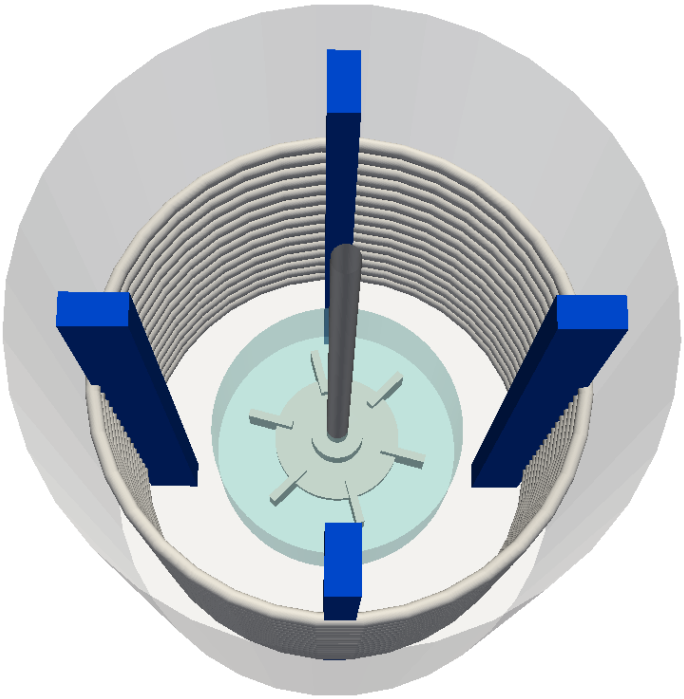

Fig. 7: Exemplary rotor, stator and MRF zone. The stirrer blades are completely inside the MRF zone which extends beyond the stirrer radius and poses a frontier between stator and rotor.

2.5.2. Arbitrary mesh interface

In contrary to the MRF method, the sliding mesh method – called arbitrary mesh interface (AMI) in OpenFOAM® (see 3.1) and general grid interface (GGI) in foam-extend – performs a “real” movement of a geometry part. The grid, therefore, has to be disconnected at a certain point between the stator and the rotor. Actually, not only the geometries move relatively to each other but also the surrounding parts of the grid. Of course, one of the most important characteristics gets lost by this method – namely the conservation nature of the FVM. In order to keep the subsequent continuity errors small, it is important to guarantee a gapless mesh. The boundary

between the adjacent domains has to be as congruent as possible and remain this during the movement. This also explains the name “sliding interface”. A cylindrical AMI inherits the congruency due to its axisymmetric character. However, the actual domain representation consists of cells which have planar faces and therefore only approximate a real cylinder. By definition, the grid is not gapless, though. A grid refinement in the vicinity of the AMI is recommended, hence. The fluxes between the domains cannot simply be calculated via a transformation like in the case of MRF method. An interpolation is needed not only to calculate the field values on the boundary faces but also to account for the shift between faces and the non-congruent character of adjacent faces. The principal of flux calculation across the AMI is visualized in Fig. 11. For simplicity reasons, it is shown two-dimensional.

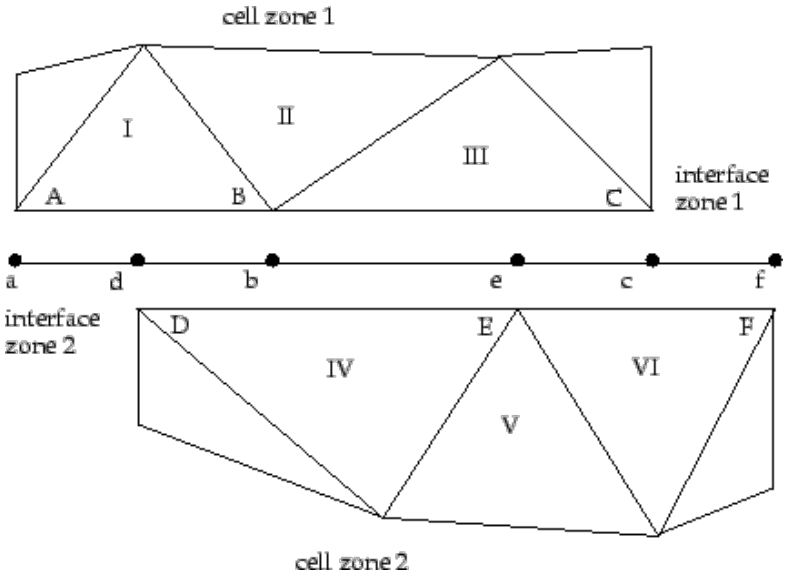

Fig. 8: Two-dimensional AMI principle [36]

As the faces of adjacent sliding cells partially overlap with various cells on the other side of the AMI, more than one cell is used for flux calculation. The boundary faces are notionally split into several parts along the overlap area which allows a weighted interpolation. The weighting corresponds to the partial of the face areas. In Fig. 11, the flux into cell III is calculated from cells IV and VI, but instead of actual cell faces DE and EF, the fictional faces “be” and “ec” are used.

The AMI method is indeed very demanding concerning computational time and memory occupation but the most accurate method concerning temporally resolved results and effects.

2.6. Quality criteria of CFD

The numerical prediction of flow fields basically is done in the following steps:

- Mathematical description of the physical problem by differential equations and application of acceptable simplifications. Generation of a mathematical system.
- Discretization of the mathematical system, use of a certain discretization method, choice of approximation schemes and solution algorithms. Generation of a numerical system.
- Flow domain description by generation of a grid.
- Solution of the numerical system involving linearization, coupling and approximation on a computing machine.

Each of those steps entails errors for the numerical prediction.

2.6.1. Mathematical system

At the mathematical description, the difficulty lies in the choice of proper simplifications of the generic description, which is proved to be valid but is, however, extremely hard to handle from the numerical point of view. The characteristics of the flow problem play a crucial role involving the following questions:

- Does energy play a role for the flow? Do thermal effects influence the flow?
- Is the flow compressible? Is the density constant?
- Does thermodynamics play a role?
- What kind of rheology is present? Is the flow laminar or turbulent?
- Is the domain static, are there moving elements? Does fluid-structure-interaction exist?
- Is the flow stationary or transient?
- Is it a single or a multiple phase system? Does miscibility play a role?

For some special cases, the mathematical system is being simplified to such point that an analytical solution can be formulated like in the case of Bernoulli's equation. The formulation of a valid mathematical system poses the greatest challenge to the user of CFD. It is therefore recommended to investigate a problem from bottom to top, i.e. to start with the simplest possible system and compare it to the next stage of complexity. Often, it is not necessary to obtain an exact solution to a problem but for example to see trends in a parameter variation study. The costs and benefits of simulation work have to be considered well.

2.6.2. Numerical system

After the definition of a mathematical system, basically there is a system of coupled, non-linear partial differential equations which somehow contain the desired field sizes like pressure and velocity. A computer is not capable to calculate with differentials, so they have to be approximated by differences. This implies approximation errors that generally become smaller with increasing temporal and spatial resolution. Generally, the fineness of a grid minimizes the approximation error, but rises the calculation effort by usually even higher order. The non-linear and coupled character of the equations is handled by neglecting or primitive prediction of the non-linear compounds and iterative correction until the calculated fields become sufficiently consistent with the underlying numerical system. The remaining inconsistency is called the discretization error. It also includes the errors of the actual field solution of linearized equations (linear matrix solver errors). The machine errors caused by floating point representation of numbers in the computer is comparatively low considering the errors made by discretization and mathematical system setup.

2.6.3. Spatial resolution

The mesh (discrete representation of the spatial flow domain) has a huge impact on the quality of numerical results. Of course, the cell size has a direct influence on the approximation error, but other criteria play an important role, too. Since the FVM uses interpolation, numerical differentiation and numerical integration in the process of linearization, the mesh shape influences the numeric accuracy in variate ways. For example, the FVM implies the interpolation of field values from the nodes to the cell faces, where flux and gradients are calculated. Skewness, non-orthogonality and inhomogeneous cell aspect ratios lead to incorrect interpolation and entail

differentiation and integration errors. The estimation of the resulting error originating from non-orthogonality and skewness has the shape of the diffusion term in the NSE. Especially in areas, where diffusion is crucial like at heat transfer, this leads to augmented diffusion and entails numerical over-prediction. Special care has to be taken at heat and material transfer regions, though. In order to manage this issue, mechanisms like cell layer addition become a significant part of mesh generation. Since the mesh resolution determines the spatial step size (differential approximation), the approximation error can be reduced by reducing the cell size, i.e. augmenting the total number of cells. When the refinement is done sufficiently, the numerical results should converge to the analytical solution. In practice, the results of several refinement levels are compared and the so-called “spatial consistency” is reached when there is no significant difference in the results between two refinement levels. Therefore, the numerical error can be handled by means of CFD itself, namely by achieving spatial consistency. However, this is no guarantee to the results’ validity, since it merely verifies the numerical system to converge to the mathematical.

2.6.4. Numerical solution characteristics

As mentioned before, consistency is a decisive property of the numerical solution. A simulation is basically worthless without this verification. However, other quality criteria have to be considered in CFD, although. For a suitable estimation of the computational costs, the used approximation schemes, linear solvers and solution strategies have to be well defined. All of those aspects entail different convergence orders and solution stabilities. Of course, high convergence order is desirable due to lower refinement necessity, but on the other hand often corrupts the stability or, in the worst case levers conservation properties of the FVM. The stability is basically the tolerance of the solution progress to numerical or physical disruption (accuracy issues, pressure shocks, etc.). The main obstacle to stability is the numerical system. The errors that appear during the linearization and iteration process should be decreased during the solution. Methods, that magnify these errors, are classified as unstable and will seldom lead to convergent solutions. The boundedness of a numerical solution is an important criterion for the physical validity of the results. Non-physical results usually cannot be excluded by the discretization method.

2.7. Laser-optical measurement technology

2.7.1. Particle Image Velocimetry (PIV)

The particle image velocimetry is a noninvasive method for measuring velocity fields inside of optically accessible geometries. The principle of PIV measurements is schematically shown in Fig. 9. A pulsed laser beam is transformed into a thin cutting plane which illuminates a sheet inside the observed flow domain. The flow itself carries small particles which scatter the laser light. In an orthogonal position to the laser plane, a camera records this image. By means of a special software, the particles inside the observed laser sheet can be detected and localized. Two shots taken at a predefined, short time period (acquisition delay) are compared by the software and the particles displacement serves as the starting point for velocity field calculations.

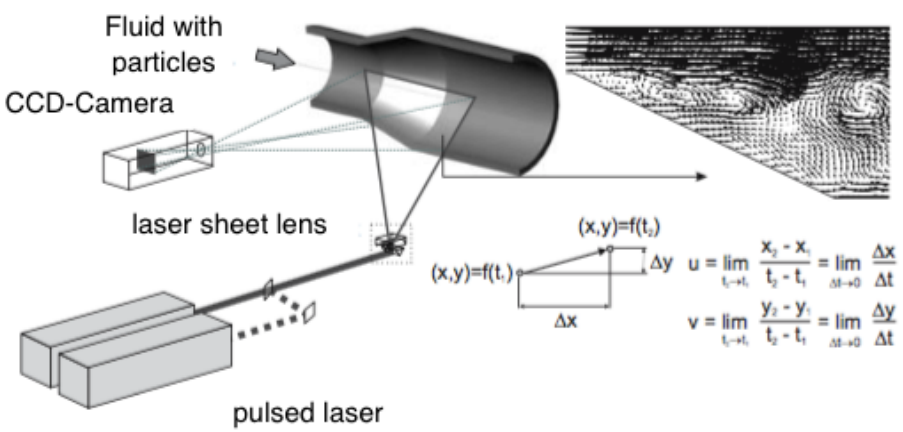

Fig. 9: PIV principle on the example of a wind tunnel [3]

Several requirements – physical, technical and operational – have to be considered for the PIV technology.

Physical and technical requirements: The tracer (or seeding) particles are supposed to follow the flow field without influencing it by inertia, buoyancy or collision interactions. The particle size is on the one hand decisive for scattering and detection, on the other hand it has an influence on the before mentioned characteristics and has the potential to affect the flow field. The latter issue is crucial for the whole method and has to be avoided or suppressed as far as possible. Detection, on the other hand can be improved by increase of the laser intensity. Of course, it implies higher effort concerning security and requires special care for the

sensitive cameras and primarily for the user health. The above shown experimental setup is quite simple and does not imply problems with optical distortion, since the ray path is mainly orthogonal to refraction spots. For more complex geometries, however, it is necessary to counteract the refraction which occurs at geometry boundaries. The method of refraction index matching (RIM) has become established for complex geometries. The principle is, to adapt the refractive index of the fluid inside the flow domain to that of the geometry material. However, the limits for both, the choice of the material as well as of the fluid are very tight since the refractive index ranges of solid materials and liquid substances overlap in very small areas. The system of acrylic glass and ammonium acetate solution could prove to meet this requirement.

Operative requirements: Besides the particle size, the particle density plays a crucial role for the analysis and result accuracy of the PIV. Since it is not possible to track each particle individually, the displacement of particles is treated statistically. The whole observed area is split into so-called interrogation areas (IA). Each IA of the resulting lattice is evaluated individually. The average displacement of the particles located inside the respective IA is calculated by means of cross correlation. Its principle is shown in Fig. 10. In contrast to individual tracing, where each particle has an own path, the cross correlation reveals the movement of a particle cluster. Since in the acquisition delay, particles can leave or enter the observed plane, individual tracing would fail at this point, whereas the cross correlation tolerates irregularities of individual particles. For statistical accuracy, it is important to adjust the acquisition delay, the particle density and the size of IA in such manner that five particles are located in one IA, on average. A rough estimation of flow velocity has to be assumed before the measurement, hence.

The size of IAs is important for profound investigation of the flow, since PIV – by definition – detects only linear trajectories, which correspond to a first order approximation of an arbitrary trajectory. Especially in turbulent flows, the IA has a crucial role when it comes to resolve vortex structures and derive turbulent quantities like the energy dissipation rate. The adaptive cross correlation picks this issue up by iterative decrease of the IA and comparison to the previous result. This is done until a numerically infinite IA size is reached. The spatial resolution (size of interrogation areas) depends on the particle density, the laser intensity, and the camera characteristics, the laser pulse clocking and the data processing capacities. Each of

these aspects can pose tight limitations which has to be considered when setting up the PIV experiment.

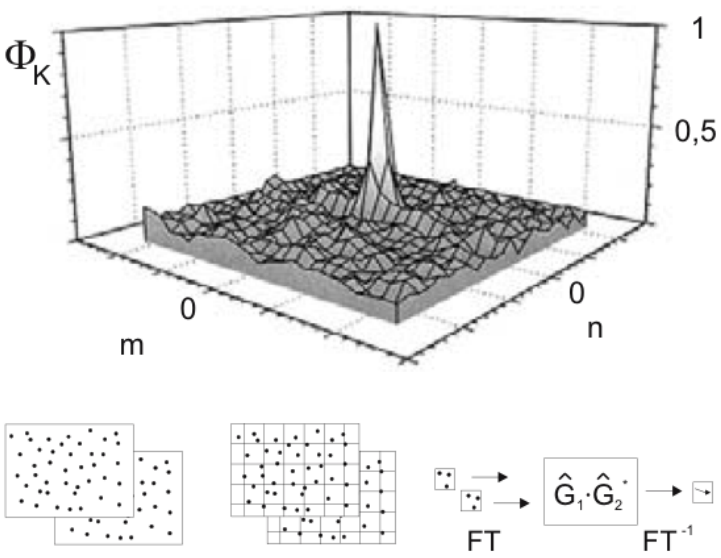

Fig. 10: Principle of particle displacement calculation by means of cross correlation. [3]

The described method is valid for detection of the flow field components, that are projected to the observed plane. The out-of-plane (OOP) component is neglected in the classical PIV. In flow problems with strong OOP components, this can lead to the failure of cross correlation since not enough particles remain in the IA during the acquisition delay. An extension to the classical PIV by the expansion of the laser sheed thickness and the use of two cameras enables even the detection of the OOP component. This method is called Stereo-PIV.

2.7.2. Stereo-PIV

For the purpose of extending the PIV capacities by three-dimensional velocity detection, it is necessary to expand the laser plane thickness, since the OOP movements of particles need to be detectable throughout the acquisition period. It is now important to distinguish between the laser sheet which is the zone of detection with a certain thickness and the laser plane, which is a strict two-dimensional term – it serves as the reference plane and is defined to lie in the center of the sheet. However, one single camera sees the particles movement through the sheet as a projection to the laser plane. The view of two cameras from different angles to the

laser plane allows a reconstruction of the real particle movement from the projections. The principle of stereo-PIV is shown in Fig. 11. It follows the fundamental principle of the human eye.

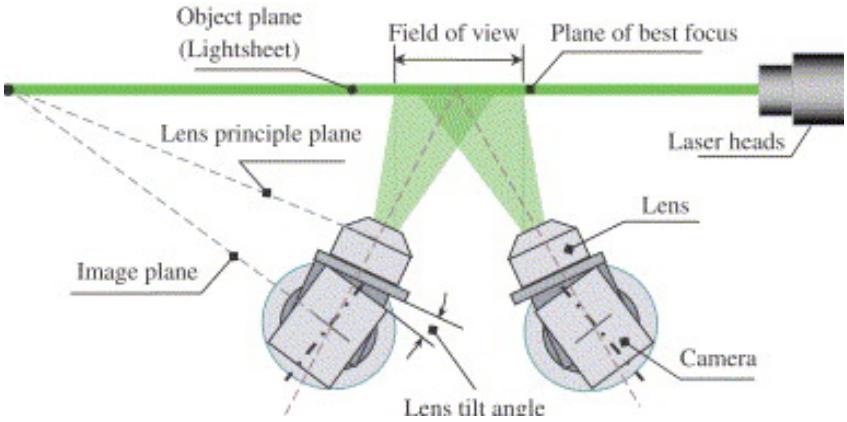

Fig. 11: Principle of the Stereo-PIV. [37]

Since the cameras do not orthogonally look at the laser plane, the so-called Scheimpflug principle has to be considered. It is a geometric rule that allows the plane of focus (the laser plane) to be not orthogonal to the image (camera chip or film). The camera, however, must be capable of adjusting the lens relatively to the image. The Scheimpflug condition is that the intersecting point of the lens and the chip plane has to be located on the object plane, as it can be seen in Fig. 11. Due to the Scheimplug adjustment, it is possible to achieve the necessary depth of focus for the cameras over the whole laser plane. An adequate adapter is imaged in Fig. 12.

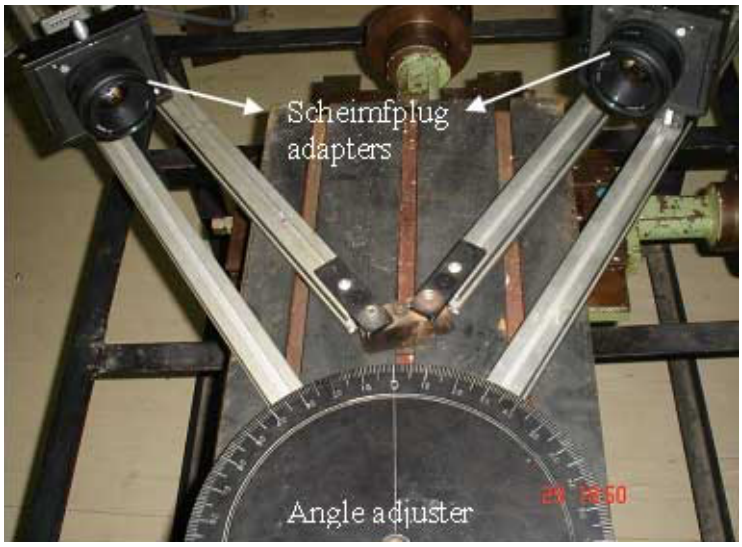

Fig. 12: The Scheimpflug adapter. [38]

2.7.3. Laser-induced fluorescence (LIF)

Fluorescence is the spontaneous emission of light. The emission duration is just a few nanoseconds, which differentiates it from the other type of luminescence – the phosphorescence. The precondition for fluorescence is the absorption of light rays by a fluorophore substance. The absorption causes the transformation of an electron to an exited state. Due to the short life time of the exited state, the electron returns to the ground state quasi simultaneously and emits light that usually has a lower frequency than the absorbed and cannot be absorbed by the same substance. This effect is used by the LIF, whereby a monochromatic laser light is used as stimulator. The camera is equipped with a filter that cuts of the lasers' frequency. In this manner, only fluorescing light is detected. In accordance with the Lamberts-Beer law, the fluorescence intensity is proportional to the fluorescent substance concentration, if the concentration range is small enough. Within a calibration, the fluorescence intensity can be correlated with the substance concentration, though. From the technical point of view, the intensity is detected as greyscale on the camera image. The range of detectable grayscales and its resolution (number of distinguishable grayscales) is therefore an important quality criterion of the camera – regarding LIF. The analysis can then be performed on a pixel basis in contrast to the PIV, where a number of pixels is needed to detect a single particle.

3. Implementation of numerical fluid dynamics

The CFD software used in this work is the open source and free-to-use program OpenFOAM® [39] by OpenCFD Ltd. OpenFOAM (OF) is a widespread CFD-tool in science due to its open source character, since the user is able to implement mathematical models and methods by augmenting the existing code by his own. A domain specific language (DSL) provides the basis for standardized development even by a wide user and developer community. OF is based on the original CFD code FOAM by Henry Weller [40]. After the program language transformation from FORTRAN [41] to C++ [42], the development of the OF project took variate forks, the most important of which are the here used official OpenFOAM® and the rather community development orientated foam-extend-project [43].

3.1. Overview of standard CFD software

In the world of computational fluid dynamics, mainly three software providers stand out. In the commercial segment, ANSYS (Fluent and CFX) [44] as well as CD-adapco – Siemens (Star-CCM+) [45] dominate the scientific as well as the commercial area. The open source segment is mainly occupied by the here used software OpenFOAM®. Especially in the commercial segment, CFD usually comes as a package with additional software for geometry design, mesh generation, assistance for simulation setup, postprocessing, visualization and even integrating software for parameter studies and shape optimization. Multidisciplinary design exploration (MDX) is the new trend in the commercial software. The highlights are explicitly set in the area of product design optimization. Huge efforts are made to provide user-friendly interfaces and stable solvers as well as intuitive and consistent handling. In the free-to-use and open source segment, on the contrary, all of those aspects are covered by different packages, that have to be integrated individually. Often, the interfaces between different packages are not adequate, the handling, use and operation is completely different and lack for suitable integrability. Most of all, the automation of processes is complicated then. Moreover, many of the available packages come without a graphical user interface (GUI). The communication takes place via specified text files and commands in the shell prompt. The user is obliged to learn the grammar and syntax on the uncomfortable way. Often, the user is faced with a lack of information about possible options and settings. The absence of an all-embracing

and plain documentation poses a huge hurdle of a fast and pleasant software handling acquisition. Since OF is mostly used in scientific environment, the development focuses mostly on the physical, numerical and program-related issues. Descendants of OF which provide some comfort for the user are usually commercial variants. HELYX® [28], cfFLOW [47] and the embedded OF in the CAE (computer aided engineering) software SimScale [48] are the most prominent examples. Further programs specialize on certain aspects of simulation like grid generation or heat transfer phenomena. A comprehensive overview of both, commercial as well as free software is given in [49]. Packages for solvers, grid generation, visualization etc. can be looked up here. For the free software – available for Linux Ubuntu systems – a short overview is given in [50].

3.2. Concept and operating principle of OpenFOAM®

Like every CFD software, OF is organized in the three fundamental areas of preprocessing, solving and postprocessing, see Fig. 13. However, the way of handling in each of this areas can differ from other – especially commercial – software. During the visualization part, it is rather comparable and outsourced to ParaView, the residual steps are performed by the typical OF-concept.

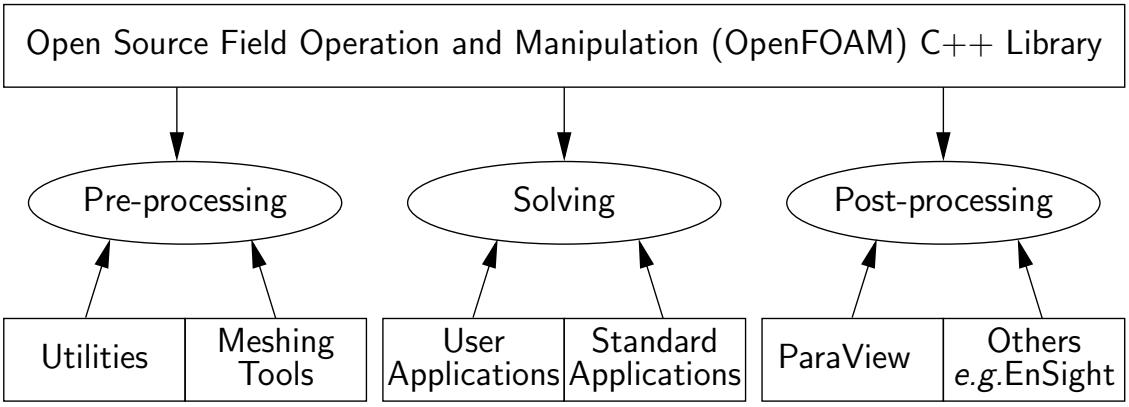

Fig. 13: Overview of OpenFOAM structure [51]

3.2.1. Fundamental concept

OF was developed in the scientific environment and is therefore not orientated to a good and easy handling. From the point of logic and organization it is a well-structured package, though. The whole package is organized a way that enables the

user not only to use the utilities and solvers, but also to interact with the structure and use it for further development and modification. Is not only a collection of executables, but also provides a domain-specific language (DLS), which is closely leaned on the object-orientated character of the programming language C++ itself. This includes a high level of abstraction. The principle of hesitation from class to class and the possibility to separate implemented operators for different contexts by use of different namespaces makes the manipulation and development of OF possible for even those who are not deeply familiar with programming in C++. After a first hurdle of the unusual handling, the software appears to be a flexible instrument especially when it comes to implement new functionality.

3.2.2. Handling and interfaces

Most of the users of OF have to learn the principles of command line instructions on the computer, before they can start with the first simulation. Due to the absent graphical user interface, one has to create a roadmap of actions in mind and transfer it to the language of OF. This language is a combination of direct shell commands and manipulation of certain text-files which are used for specifications and adjustments. Generally, a utility is called by a shell command and then looks up in the specified so-called dictionary-file for the adjustments. To accomplish a certain task – like for example the generation of a grid – there often has to be performed a series of several utilities. The exact procedure depends on the complexity of the mesh and the requirements to it. In contrast to usual commercial software, there are no hints and obvious proceedings in OF, which calls for experience of at least similar cases from where to take over the procedure. Within the dictionary files, a special grammar guarantees a consistent communication structure. OF provides a user guide for the first steps and principal handling [51].

3.2.3. Development of a user workspace

Due to the non-existing graphical user interface (GUI) of OpenFOAM®, it is at times quite challenging to perform studies of many simulations “by hand”. A well-organized workspace is needed for a tidy structured investigation work. In the world of OpenFOAM-based software developer and user community, several packages have been established, that augment the functionality of OF, implement new applications, facilitate interaction with further software and help organize and manage simulative

investigation work. At this point, it is fair to mention packages like pyFoam [52] and swak4Foam [53] by Bernhard F.W. Gschaider (see also in [54]). Those packages are based on the intuitive and in scientific world widespread programming language python [55] or hook into the OF-code by additional libraries, classes and utilities. The handling with those packages is quite straight-forward and basically does not differ from usual OF handling. However, expanding it requires either good understanding of OF coding language or the knowledge of the python language. In this work, an own concept is pursued, which bases on the scripting of the prompt shell command [56] – this is the original handling method of using OF – and develops a more adjusted functionality for the investigations of mixing technology. The already necessary knowledge of shell-programming is consolidated and standardized for this workspace which is oriented on implementing and expanding the standard OF utilities by functionalities that are specific for this work by own utilities or wrapped OF applications. Automatization of preprocessing, solving and postprocessing as well as the constraint of templated case and study structures are the main demands upon this workspace. Of course, simplified handling and generalized procedures are further aims of it. Moreover, the workspace is meant as a basis not only for this work but also for subsequent investigations. Previously performed simulation and automatization constraints shall serve as exemplary source for future simulation, study and utility development. The acquisition of already performed work and adjustment to new challenges is the core and purpose of successful, fast and consistent development. The workspace to its actual development status can be found attached to this work, see 12.2. The associated User Guide as well as the most important study templates are part of it.

3.3. Objects of investigation

Besides the reference process which is a real and working plant in the chemical industry and therefore of a fixed design, the laboratory investigation can be performed for variable vessel, heater, stirrer and baffle types. It is mostly possible to combine those elements arbitrarily. In this respect, the least combination variety can be done on heater-baffle combinations since baffles usually serve as essential constructive elements for the fixation of the heater. The heater and baffles therefore mostly come as a couple. The number of baffles, however, can be variated without troubles. All presented geometries used in this work are drawn by the CAD software

Blender and exported in the stl-format [57] for later use by OFs meshing tool “snappyHexMesh”.

3.3.1. Agitated vessels

Different vessel design types were used in this work. Topologically, a vessel exists of a cylindrical mantle with a certain diameter to height ratio and different types of bottoms. The most usual types are:

- flat bottom
- beaker glass bottom with rounded edges
- dished bottom
- spherical bottom

of which dished bottom (torispherical head, according to DIN 28011, is meant in the context of this work) is the most widespread. In the laboratory investigations, moreover a beaker glass was used due to its topological similarity with a dished bottom and good suitability for the measurement method. The differences can be seen in Fig. 14

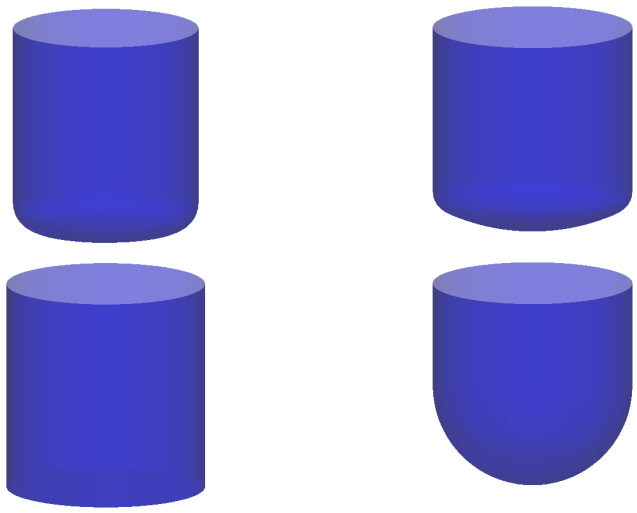

Fig. 14: Used vessel types. On top from left: beaker glass, dished bottom vessels. Below from left: flat and spherical bottom vessels.

3.3.2. Impeller types

Agitators are basically subdivided in three categories: radial pumping impellers, axial pumping impellers and tangential stirrers, whereas the latter are not treated in the scope of this work due to their very specific applicability. Axial and radial pumping impellers (API and RPI, respectively) are realized in a multitude of different designs. The most prominent and investigated in this work are figured in Fig. 15. Further stirrer design can be found in [58]. The strictest representative of APIs is the propeller stirrer. However, due to the lack of practical importance in the area of mixing technology (bad mixing and power characteristics), it is not studied here.

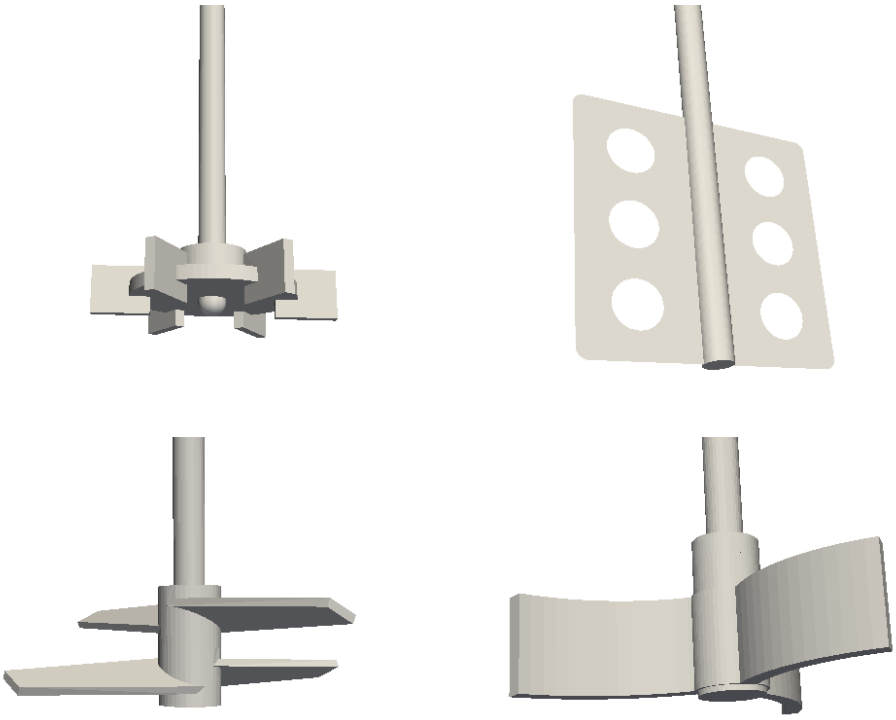

Fig. 15: Used stirrer types. On top from left: Rushton turbine and paddle impeller. Below from left: double staged pitched (narrowed) blade impeller and curved blade impeller.

Each stirrer is connected to the driving unit by a shaft. Depending on the reactor size and the utilized stirrer type, the shaft requires different diameters. In the industrial scale it is usual to use a shaft that reaches from top to bottom and has a two-point bearing. Deflection and wobbling of the rotating element can be suppressed thereby.

3.3.3. Heat exchangers

As mentioned before, there are different classes of heating possibilities in an agitated vessel reactor. However, helical coils pose one of the most important representatives

of inboard heaters [24]. Due to the constructive simplicity and huge heat exchange area, they are highly prominent in industrial use. Often, double coils are used to increase the heat exchange area even more. In practice, dimensioning underlies the very fundamental assumption that heat exchange is increased with growing exchange area in the same manner which has to be scrutinized. Other heaters like tube bundles, plates or tube baffles are disadvantaged by their higher costs and maintenance effort, limitations in the capacity and applicable heat carriers. In this work, single and double helix coils as well as tube baffles are investigated, see Fig. 16. After the identification of the main problems and vulnerabilities of the respective heater, a novel design is proposed that meets the expectations regarding costs, efficiency and flow characteristics (homogeneity, mixing time, etc.).

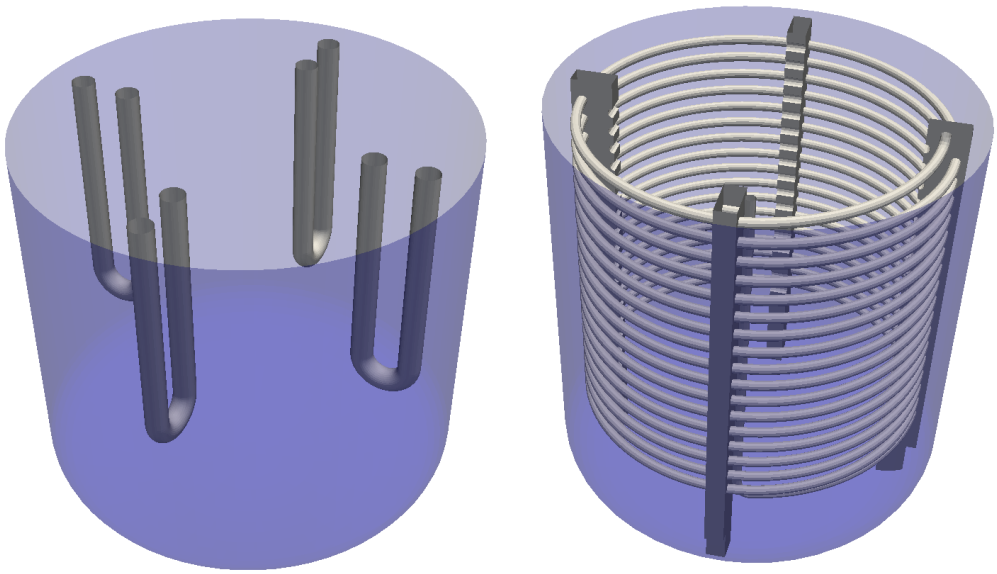

Fig. 16: Used heaters.
From left: tube baffles, helical coil. Double helical coil is shown in Fig. 17

3.3.4. Other internals

Baffles generally serve as fixation basis for coils, but also for suppressing – or at least reducing – the tangential component of the flow. In the case of tube baffles, the heater itself serves as a baffle and forgoes additional internals for this purpose. In the case of the reference reactor, further internals are needed. The gassing is done via a perforated ring underneath the first stirrer stage, see Fig. 17. For technical reasons, the stirrer shaft needs for a shaft guidance at the bottom of the reactor. Additional tubes for temperature and fill level measurement stick into the flow domain, but have comparatively very small diameters and are expected to have negligible influence on

the flow patterns. The entire geometry of the industrial reference reactor is shown in Fig. 17.

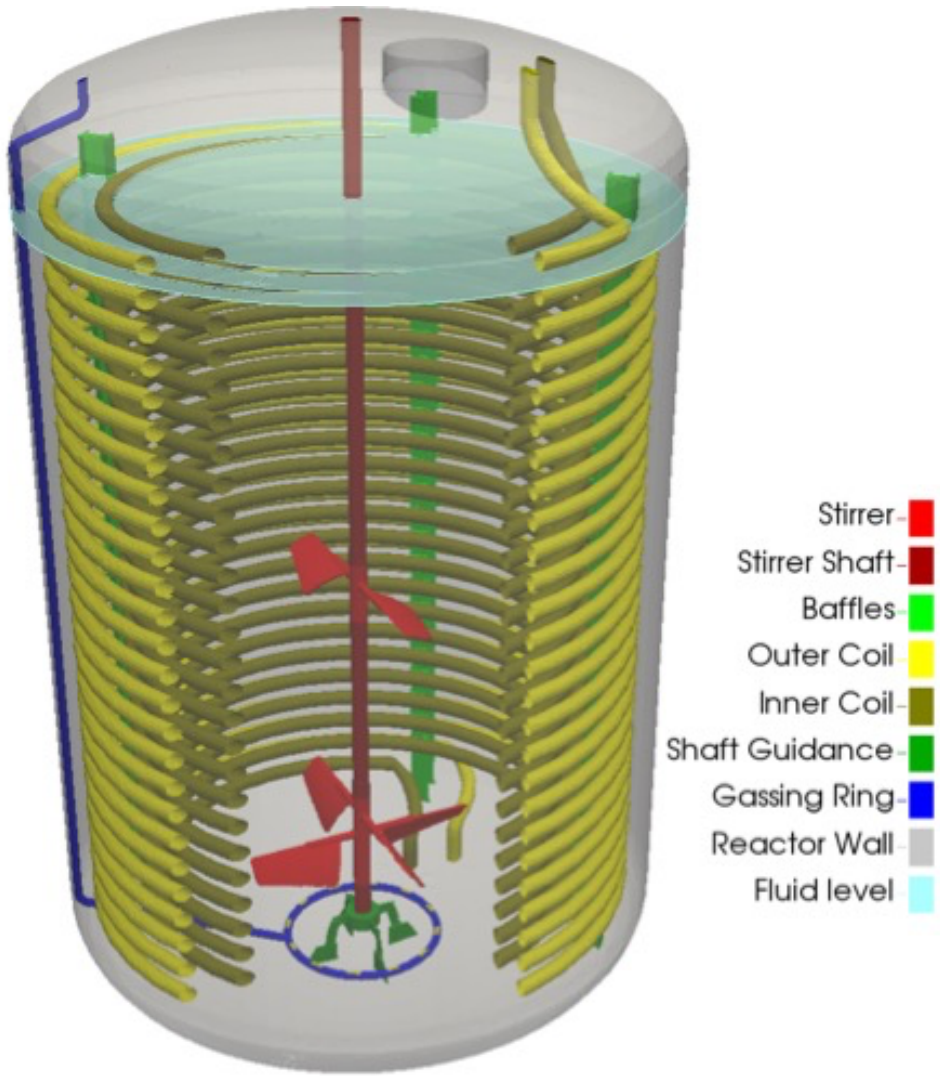

Fig. 17: Reference reactor with all internals.

3.4. Investigated target values

For the evaluation of a process and its comparison or optimization, it is necessary to define target values that can be subjected to an equivalence relation (greater, less and equal). The following target values represent characteristics that are the most important for practical use in the sense of process planning, dimensioning and cost estimation.

3.4.1. Heat transfer

The heat transfer can be investigated by use of the energy equation. Certain boundary conditions allow the implementation of heater and adiabatic surfaces. It is even possible to simulate the total heat transfer through a wall by implementation of two fluids and one solid domain. However, in the scope of this work, only the heat transfer from the surface to the fluid will be investigated. Several solvers for compressible and incompressible cases are implemented in the standard OF version. The buoyancy effect is accounted for by the use of variable density. This can be verified by simulation of the reactor with a frozen stirrer. The chimney effect indicates physical validity of this principle. However, this effect is negligible in the case of highly turbulent flows, since density gradients – which pose the driving forces for buoyancy – are destroyed. The heat transfer principles will be discussed in chapter 6. The main aim of this investigations is to optimize the homogeneity of the whole temperature field in the reactor and augment the process of heating for the reduction of heating time. An appropriate target value for optimization has to be defined then. As well the temperature field as the heat fluxes are used for the discussion of this work.

3.4.2. Mixing time

Besides a well-controlled and homogeneous temperature regulation in the reactor, the other main aim is a fast and homogeneous mixing of substances. Since the reference process used in the scope of this project implies the mixture of two miscible liquids, other aspects of mixing like solid-liquid systems are not observed. Relevant literature like [1], [26], [59] presents the method of determining the mixing time via the observation of the mixing quality by use of a tracer. Like presented in [12], experimental work has been performed on the observed system and can be used for validation, though. An analog method was developed for the postprocessing of CFD results. Further aspects will be discussed in chapter 8.

3.4.3. Energy consumption

Since the aim of this work is to reduce the energy consumption of the stirring process, it also concerns the electrical power consumption. Thereby, the power consumption depends in a high manner from the used stirrer system. Huge work has been done in the investigation of so-called power characteristics [24]. The main

impact is identified in the shape of stirrer blades. In the past, this led to significant reduction of power consumption by stirrer shape optimization. This is also the reason why propeller stirrers have lost their relevance for industrial mixing [2]. The optimization of stirrer shapes is not the subject of this work, though. Rather more, the impact of the positioning of the stirrer stages is discussed here. The power consumption can be understood as the integral energy dissipation all over the domain because the stirrer is the only driving force for the flow movement. Alternatively, the pressure integral along the stirrer can be used for the calculation of the torque and thereby for the power consumption. However, the calculation via energy dissipation guarantees energy conservation and is not vulnerable for e.g. interpolation errors. One has to consider, that in a process where the heat exchange is optimized, the power consumption can rise due to higher energy dissipation. In return, the cost for heating carrier consumption, batch times and product quality can improve significantly. Those opposite effects have to be weighted for the respective process.

4. Implementation of measurement technology

The PIV and LIF technology need optical access to the investigated object, as described in chapter 2.7. In this work, cylindrical vessels are investigated which contain dense internals and make measurements very challenging. This is why all the geometry is built of translucent material. However, even translucent material produces optical distortion due to the differences in the refractive indices of all phases where the light passes from the location of measurement to the camera panel. There are basically three theoretical ways to handle this issue. First is the numerical correction of the distortion. An exact description of the interphase shape is needed for it and light overlapping can inhibit this method. The second method is to align the setup in that way that the light passes orthogonally through all interphases. This is of course only possible for very simple geometries. The third method is to modify the refractive index in a way that it becomes equal to that of the translucent material. This is called refractive index matching (RIM). The complexity of the observed model makes it necessary to combine the both latter methods. Hence, it is not sufficient to fill the reactor model with RIM fluid. The cylindrical shape of it produces a lens effect and distorts the results in this way. The whole reactor is therefore set into an aquarium that is filled with RIM fluid, too. In this way, the scattered light passes through the reactor, the internals and the aquarium without distortion and leaves the aquarium orthogonally to its outer wall. Theoretically, everything underneath the filling level of the aquarium and the reactor remains invisible (no scattering or distortion). In practice, this cannot be achieved perfectly. On the one hand, the internals are not constructed monolithic; on the other hand, bent geometries often have a non-constant refractive index. Slight refraction cannot be avoided, though. However, the presented method allows its suppression mostly. Fig. 18 visualizes the principle on the explained example. For this purpose, a book is positioned behind the aquarium. The reactor is filled up to a higher level than the aquarium. One can see in the upper part, that the internals disappear in the reactor due to the RIM fluid. However, the object behind the reactor appears distorted due to the reactor shape. In the lower part, the reactor itself is hidden by the aquarium environment. Even the book title is clearly readable behind the aquarium, although there is a reactor with internals in between.

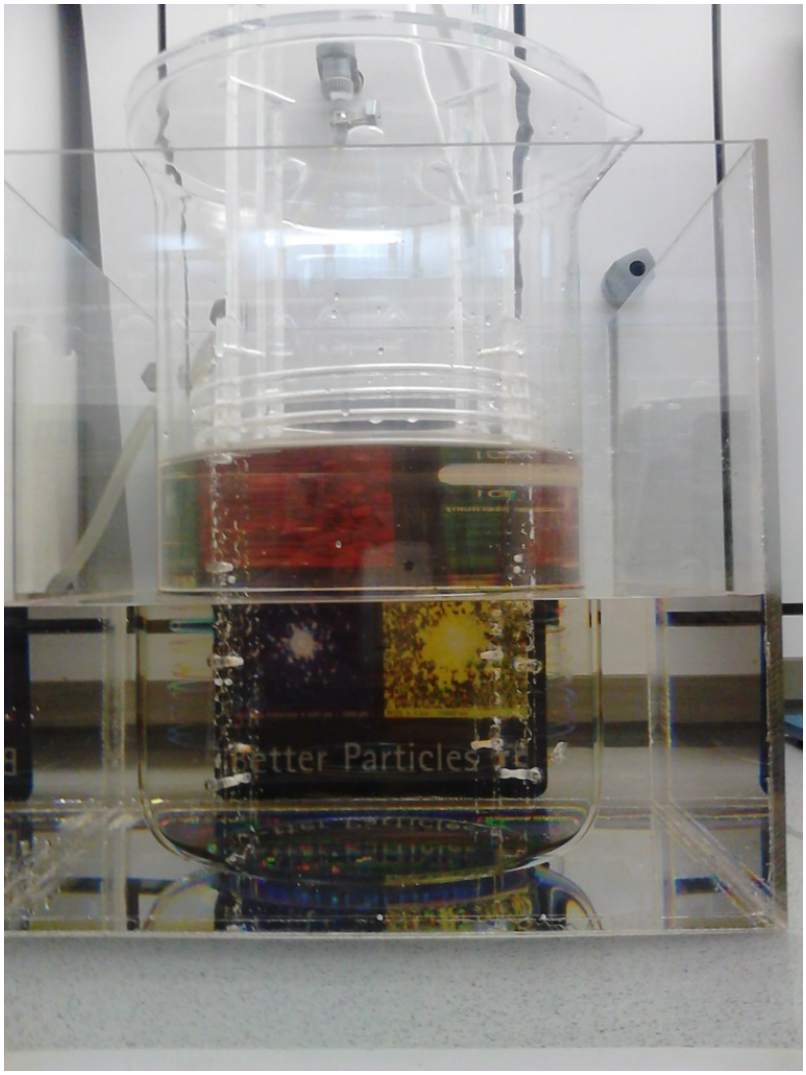

Fig. 18: Principle of a nested RIM system [12]

4.1. A novel setup for manifold optical measurements

The implementation of extended measurement technology requires the use of multiple cameras. The stereo PIV e.g. requires at least two simultaneous shots from different directions. In the case of volumetric PIV, even minimum three cameras from different perspectives are needed. To guarantee an orthogonal surface of the aquarium towards each camera, a special construction has to be invented. Former works implemented aquariums with vertical walls that are orientated towards the camera position. This allows a positioning of several cameras on one horizontal plane. To achieve higher measurement accuracy, the cameras should be positioned from maximally different perspectives, though. A novel shape of the aquarium was developed for this purpose. Fig. 20 and Fig. 21 demonstrate the shape of the novel system. The whole construction contains reproducible adjustment possibilities for the

cameras, the investigated objects (three degrees of freedom positioning inside the aquarium) and even for the stirrer height.

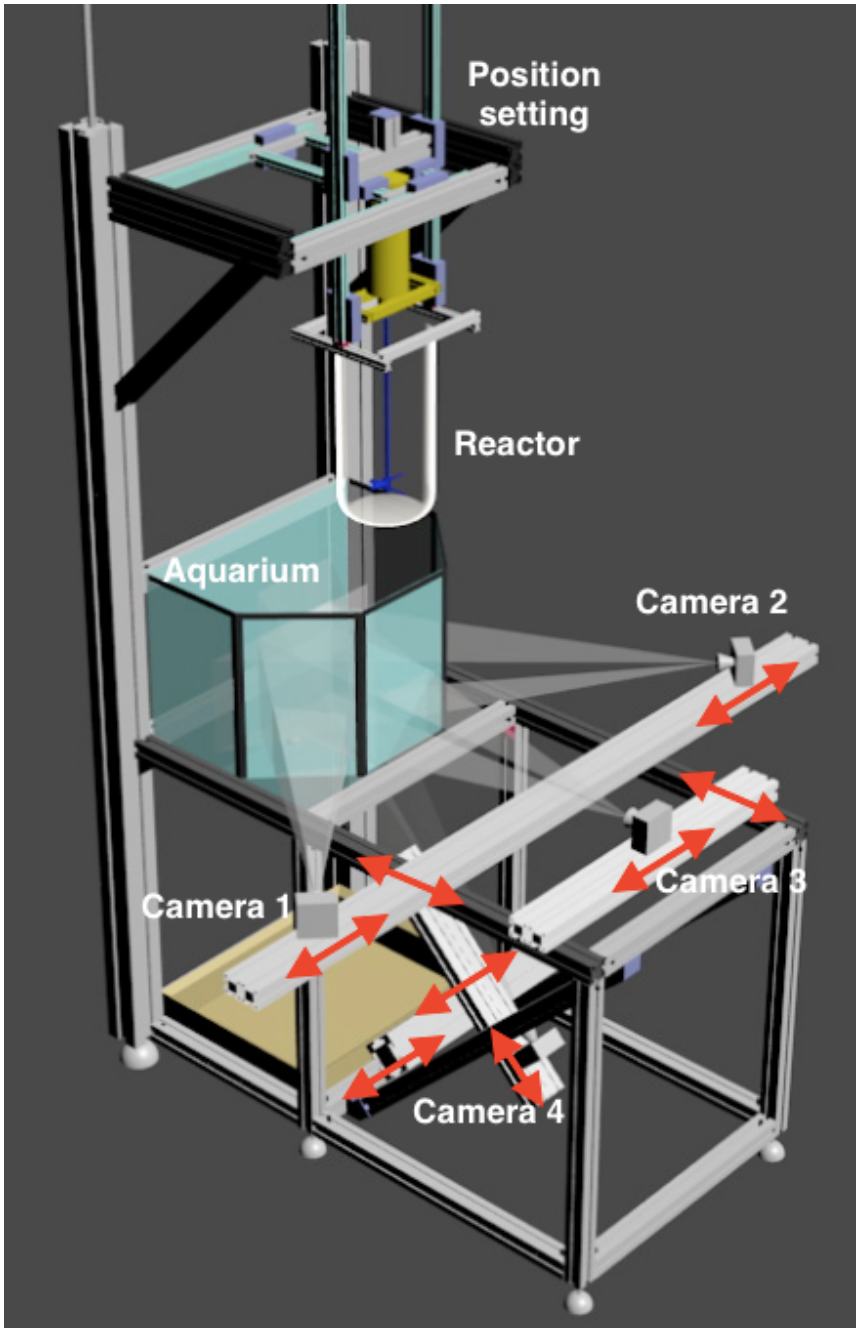

Fig. 19: A novel measurement system for manifold optical observation. Red arrows show the camera degrees of freedom.

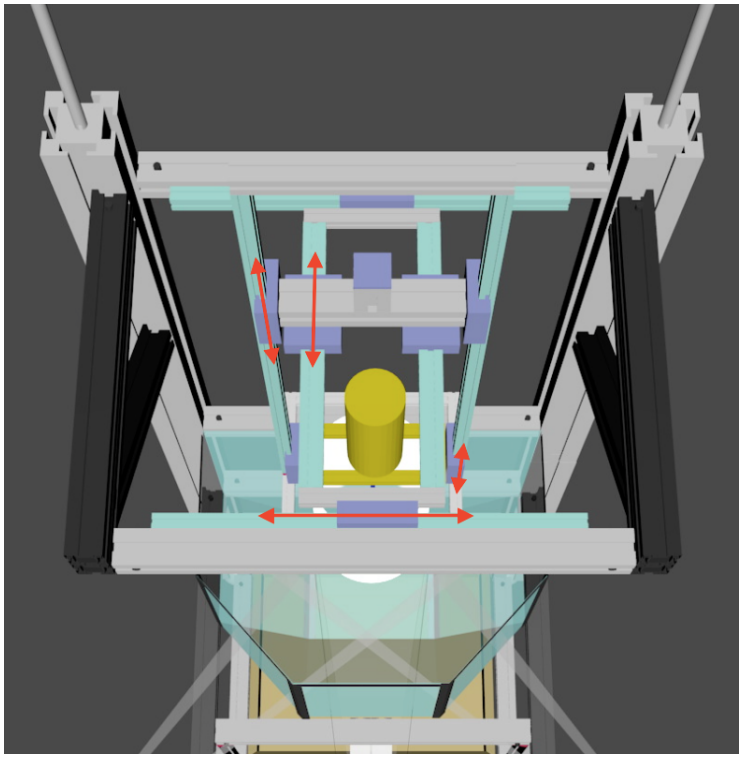

Fig. 20: Left: the object positioning system with 3 degrees of freedom.

Fig. 21: Below: laser sheet through reactor vessel.

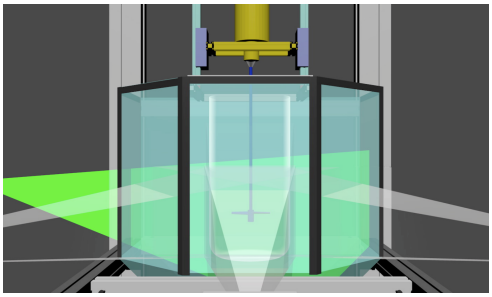

The construction is furthermore built modular, so several elements can be exchanged and used for other investigation work like it is done in [60] and [61] with the same system. It has the capacity to realize all sorts of extended and even combined measurements – e.g. simultaneous PIV/PLIF.

4.2. LIF measurements for mixing time investigations

For the investigation of mixing time, a tracer was used and the concentration was tracked over time. Following the approach described in [2], [26], [59], the mixing quality $M(x)$ is usually defined as the variation coefficient of the local concentration c. This is the ratio between the standard deviation of the concentration $\sigma = \sqrt{\overline{(c-\bar{c})^2}}$ and the mean concentration $\bar{c}$ after the mixing time – i.e. when mixing is already finished. A mixed system is generally considered as mixed, when a mixing quality of $M(x) < 0.05$ is reached. Therefore, a quantity of 10 mL tracer substance is injected in a constantly stirred process. The observed plane is analyzed at several characteristic points. The concentration can be determined by the before performed calibration where a dilution series is measured and correlated with the detected grey scale values. The local mixing quality and mixing time of several points is calculated and

compared. The maximal value is determined as the total mixing time. Of course, this method can only observe the illuminated area of the reactor. It is possible that areas of longer mixing time remain undetected by this method. Assuming axial symmetry of the reactor allows this approach, though. As posed in [59], the mixing time determination strongly depends on the setup and can vary even for comparable models. Within such a study it is very important to assure reproducibility, hence. For example, the injection position can impact on the results, even if it should be the same for constant radial coordinate, since there can be a difference in transport time from the injection spot to the observed plane. It is therefore important for the reproducibility, to maintain the same angular coordinate. However, the radial coordinate has a huge impact not only on the measurement reproducibility but on the mixing time itself. Further details and the results will be discussed in chapter 8.

5. Simulative flow field investigations

In order to perform heat transfer investigations in a stirred tank reactor, it is necessary to obtain results for the flow field. Strictly speaking, the flow field is a basis for the investigation of heat transfer. Since heat can be an influence on the flow field as well, the solution of both, the heat and the flow field can be coupled and has to be implemented in this manner. However, the consideration of this coupling is extremely challenging when additionally, moving geometry elements play a role which is generally the case in mixing technology. The anyway fragile stability of coupled systems is even more vulnerable in the observed cases since the mesh is complex and contains many geometric details which on the one hand provoke disturbances in the flow and on the other hand impede the quality of the finite volumes making them non-orthogonal, skew, distorted or stretched. In the course of this work, stability issues oblige to make simplifications like decoupling of heat transfer and flow field solution. On the other hand, no convenient OF solver can handle moving mesh and heat transfer at a time. The velocity fields are hence separately investigated in this chapter. In the next chapter, a simplified method for heat exchange investigations is presented.

5.1. Development of a flow field simulation structure

In order to make the flow field investigations effective, it is necessary to implement a structure which meets the following requirements:

- fast and stable simulations,
- unified procedures when different stirrers, internals or vessels are used,
- effective memory management.

5.1.1. Mesh generation

On the example of Bliem's work [62], [63], a lab-scale reactor with two baffles and a double helical coil is modelled in the CAD software Blender. The triangulated surfaces, created in this software, are exported in the "stl"-format which is needed for the OF utility "snappyHexMesh". A basic grid has to be generated by the OF utility "blockMesh" which is used then to create a complex mesh that aligns to the modelled

stl-geometry. The principal coarseness of the mesh is based in the first step, however. The exact procedure of mesh generation and its scripting can be found in the appendix of this work (see 12.1.1). An important remark at this point is the special treatment of the cylinder which surrounds the stirrer blades. For the steady state simulation, this cylinder is set to be the MRF zone. Three different stirrers were implemented for this study: the Rushton turbine, the double staged pitched blade impeller and the curved radial pumping impeller with curved vertical blades, see Fig. 22.

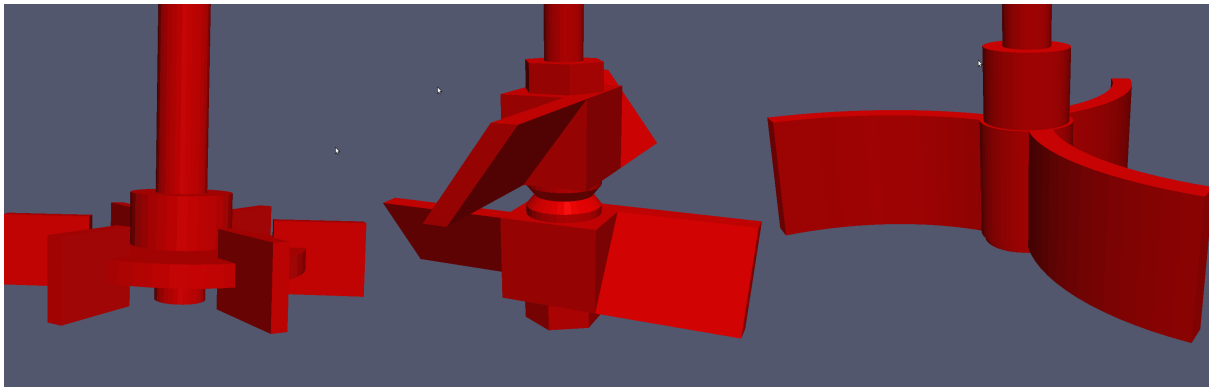

Fig. 22: Rushton turbine, and the double staged pitched blade impeller and the curved radial pumping impeller with curved vertical blades.

The generated meshes were refined close to the geometry boundaries. This is why they had cell numbers between 1.1 and 1.3 million. In [64], further meshes were generated with single helical coils, without coils and even without baffles.

5.1.2. Steady state simulations

Various methods for flow field simulations are considerable. In the least complex method, a stationary process is assumed. This way, only the convergent solution of a stirred state has to be achieved. This method has quite low requirements concerning the memory capacity and the time step difficulty. However, it is quite challenging to conceive convergent simulations when complex internals are used in the reactor which is based in the fact that stirring processes are generally not steady state because of the rotating element in the first place. However, the aim of those simulations is to conceive results that are similar to those obtained in measurements, when averaging them. It is common to use residuum plots for evaluation of convergence. First, in some cases, the residuals do not converge and escalate then.

In other cases, the residuals pass over to a fluctuating but generally stable state. Although this seems converged after certain iterations, it cannot be verified by the respective flow field analysis, as it can be seen in Fig. 23 and Fig. 24.

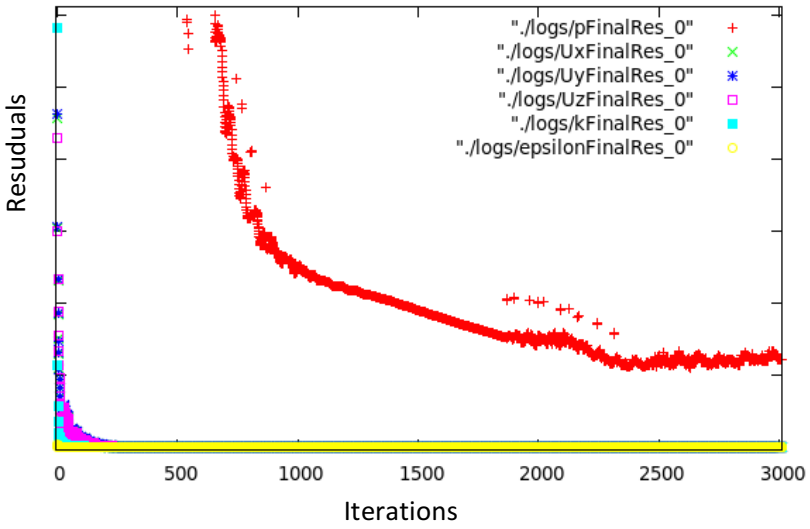

Fig. 23: Residual plot at simulation with strong under-relaxation. Convergence expected after 2,500 iterations.

Fig. 24: Horizontal slice at the center of the fully equipped reactor. Convergence is conceived after 14,000 iterations.

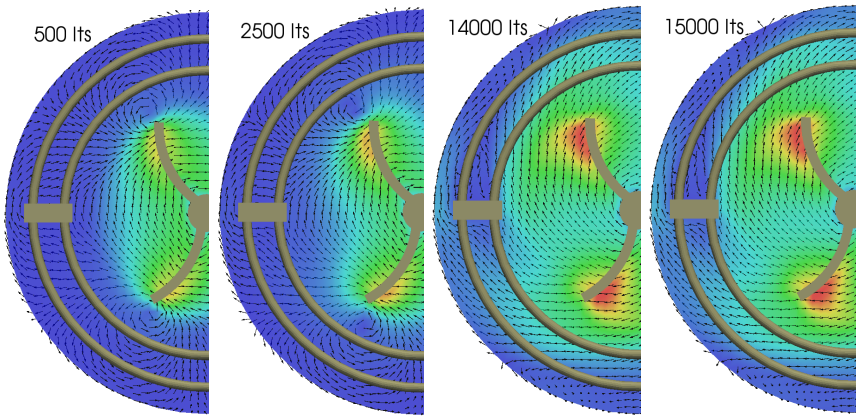

The optical verification is essentially important, hence. Moreover, Fig. 24 reveals another important issue in this kind of simulations. Since the rotor and the stator do not have a relative movement in this setup (MRF principle accounts for rotation miming, see chapter 2.5.1), the horizontal flow field is dependent on its position against each other. To approach this issue, the simulations are repeated with different positions, see Fig. 25. After the simulations have converged, it is necessary to create an average field of them. This, again, posed a challenge since there is no direct straightforward way in OF to generate an averaged field from simulations on different meshes. For this purpose, the fields are all first mapped onto a uniform mesh which is basically a hexahedral block that is cut in the shape of a vessel cylinder. This uniform mesh is used for each mapping. The mapped fields are then

averaged arithmetically by means of a C++ routine that is written exclusively for this uniform mesh and can be found in the appendix of this work (see 12.1.6). The results of the averaging can be comprehended in Fig. 25.

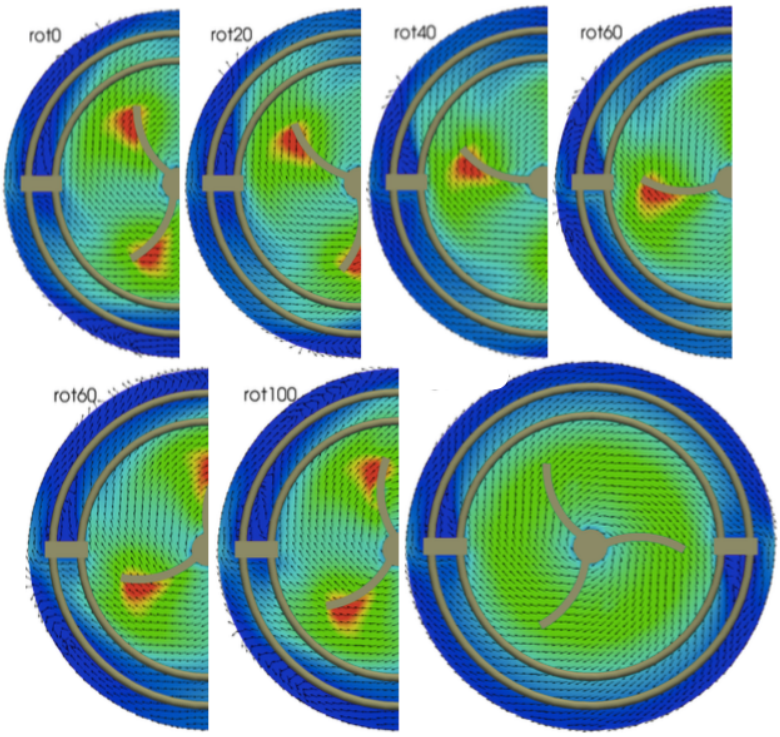

Fig. 25: Steady state simulations with six different positions (rot0-rot100) of the rotor against the stator. Final image is the average field of the six individual simulations. The consideration of more positions does not improve the average field significantly.

The results obtained in the simulation are now compared with the results of Bliem obtained in [63]. In his work, a copper heater was used which inhibits measurements of vertical velocity profiles. However, it is possible to find planes between the heater windings without optical hindrance, see Fig. 26.

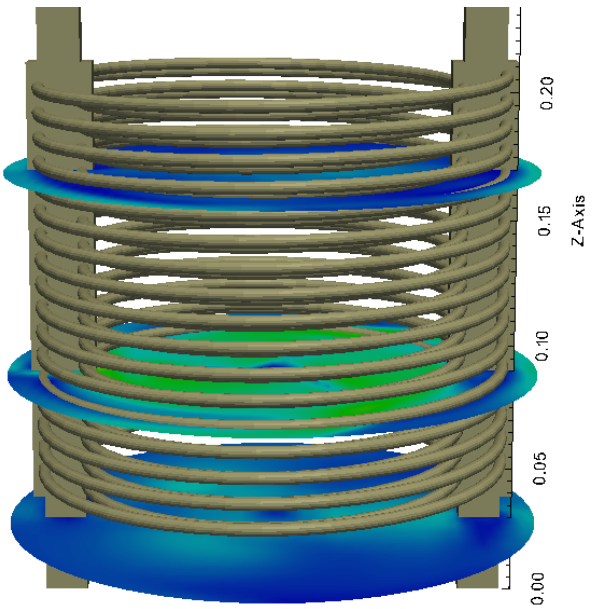

Fig. 26: Horizontal planes chosen for measurements in [63].

In Fig. 29, Fig. 27 and Fig. 28, the results are juxta positioned for the three mentioned stirrer types.

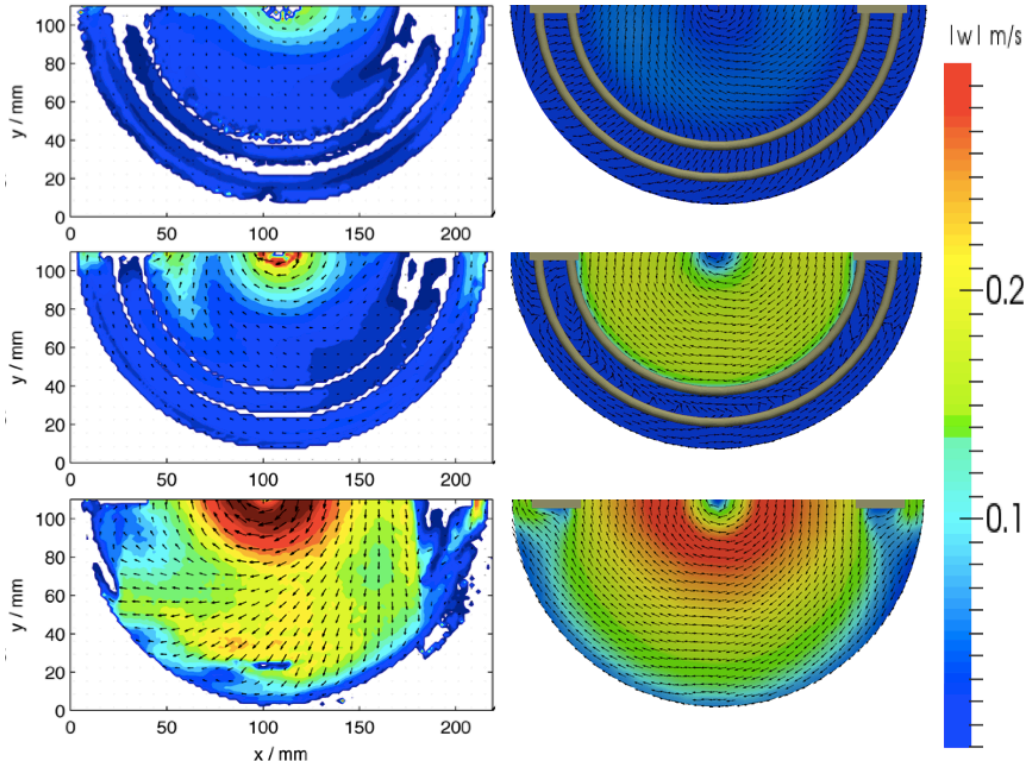

Fig. 27: Comparison of measurement (left) and CFD (right) horizontal velocities produced by a Rushton turbine.

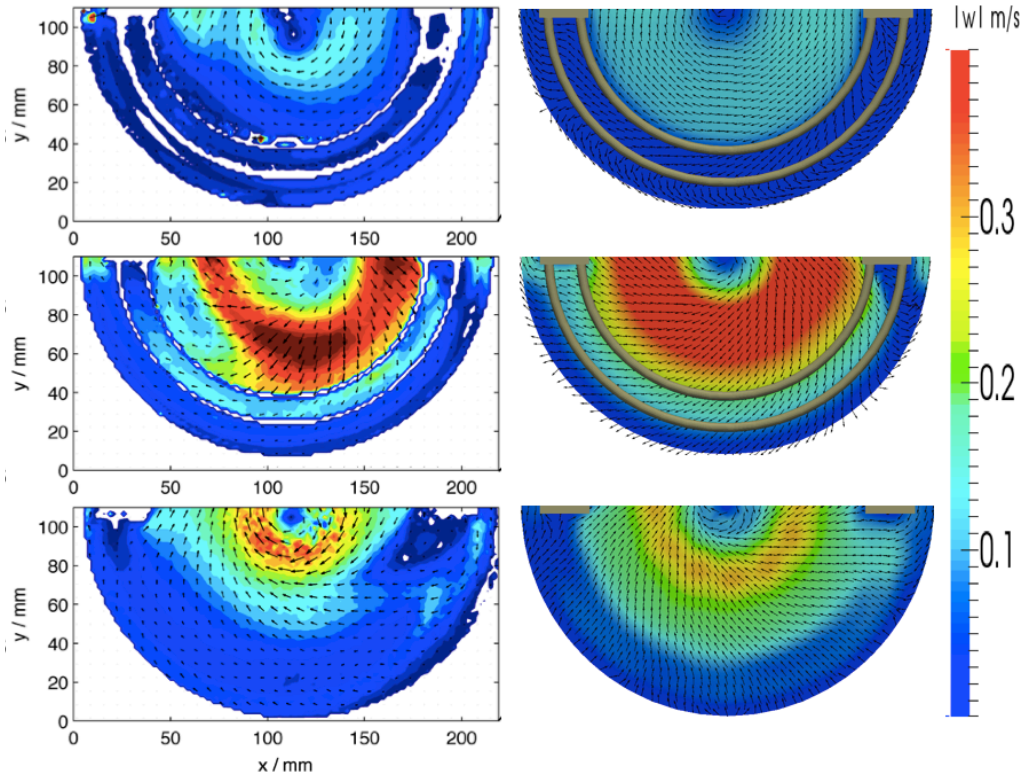

Fig. 28: Comparison of measurement (left) and CFD (right) horizontal velocities produced by a pitched blade axial impeller.

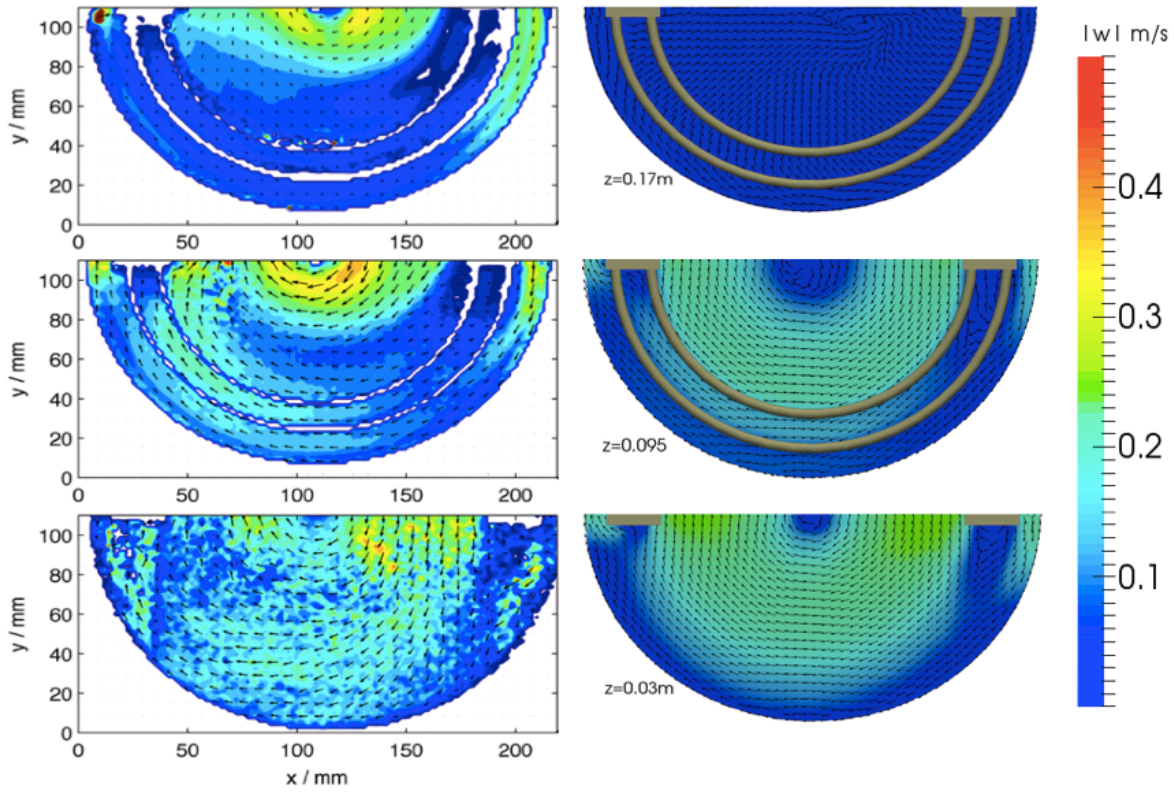

Fig. 29: Comparison of measurement (left) and CFD (right) horizontal velocities produced by a curved blade radial impeller.

For the Rushton turbine, the middle field prediction is strongly higher than the measured field. Instead, the lower and the upper parts are predicted well. On each height, the strong velocity drop the is identified at the heater coils.

The best match between the simulation and the measurement could be found in the case of the pitched blade axial impeller. The velocity intensities as well as the fluid structures were predicted by the simulation with high accordance to the measured reality.

The velocity field of the curved blade impeller is simulated notably lower in the upper part of the reactor. The simulation in the middle part matches the measurements better, the slipstream behind the baffles and the general velocity level, on the other side, is predicted well. The same statement can be made for the lower part of the reactor.

5.1.3. Transient simulations

Although steady state simulations are good for the principal investigation of flow patterns, transient simulations have a greater value since they depict structures

beyond the steady state. The small scale vortex formation that belongs in the area of turbulence is furthermore covered by turbulence modulation. Rather more, the large scale vortices are of much more interest in this case. Vortex shedding at the stirrer blades leads to the effect of hiking vortices that cannot be seen in a steady state simulation but have an immense influence on mixing and heat transfer. For an adequate simulation, the stirrer has to perform the relative rotation against the stator. This is realized by use of AMI patches and a dynamic mesh solver. The rotating area is obviously the before set MRF zone. The static and rotating meshes are divided by the OF utility “mergeOrSplitBaffles”. It has to be considered, that there can occur inaccuracies at the AMI patches, since the mesh is not connected at those point anymore, see chapter 2.5.2. In chapter 5.3.1, the transient flow fields are juxtaposed with measurement data and show a high agreement in their characteristics. The flow field close to the stirrer is then generally strongly cyclic because it is dominated by the prescribed movement of the impeller. Following spatially the discharge stream, the cyclic character of flow movement period become more and more chaotic and unpredictable. In areas where the discharge stream has low influence, a more constant and steady state field evolves. Those areas can even be enclosed by discharge streams, like it is discussed in the following chapters. Those wrapping structures are called cell vortices, there.

5.1.4. Time and memory demand – economical flow field simulation

When the transient simulation is performed from scratch, the fluid is completely resting at the start conditions. The simulation takes long computation time until the flow velocity remains at a relatively constant level. This state is called quasi-stationary. I. e. characteristic flow behavior is constant or periodic. Anyways, the simulation up to this state is expensive concerning the computation time and memory demand. To achieve a more economical solution, the transient simulation can assume the results from a steady state solution and use it as start condition. This Principle is even more improved, when the steady state solution is first used by a transient simulation with MRF (mimed rotating principle). The advantage of a transient simulation with faked rotation is its small memory amount because the mesh remains completely static and has to be stored only once for all time steps. This is both: time and memory demand saving. However, a real rotation is not realized by the MRF and the use of dynamic mesh simulation remains necessary, but

without the need of expensive start-up simulation, then. Nevertheless, start-up simulation with dynamic mesh is needed because this is the only reliable way to simulate shedding vortices. The pure transient quasi-stationary stirring process can be performed by parallel simulation of the mixing process since this additional feature is numerically cheap, see chapter 8.2.

The following procedure is determined for the generic mixer vessel simulation, hence:

- mesh generation
- steady state simulation by use of MRF to convergent state
- transient simulation by use of MRF for 25 stirrer turns
- split mesh into static and rotating part
- transient simulation by use of AMI for 25 stirrer turns (formation of hiking vortices due to shedding vortices)
- transient simulation with parallel mixing time determination, see chapter 8.2.

The structure for this automated process can be found in the appendix of this work (see tutorials of the attached workspace 12.2), including all necessary scripts and comments.

5.2. The industrial precedent: a tank reactor with immersed helical coils and axial pumping impellers

As a representative of the industrial mixing apparatus, the chosen reactor includes possibilities for turbulent stirring by a three staged agitator, gassing by a perforated tube ring as well as heating and cooling by double helical coil tubes. All of those aspects imply certain internals in the vessel which pose influence factors on the mixing characteristics and flow patterns. All the geometries are depicted in detail in Fig. 17. It is known from industrial experience, that even small parts like the stirrer shaft guidance can cause dead zones which for example lead to an accumulation of suspension particles. The reactor is used for a batch wise esterification, where a sequence of process steps is performed subsequently according the protocol. This includes changes of temperature which have to be performed in minimal time.

Moreover, cold liquid is added during the reaction which requires fast heat transfer to maintain the necessary reaction temperature stable. Since the product needs to meet a certain color index, an adsorbent is added to the reaction mixture which tends to resist moistening and therefore retards suspension.

5.2.1. Actual working state of the industrial reactor

The actual working state implies the use of the “Visco-Prop” stirrer by Ekato [58]. The stirrer consists of three stages, where two of them are located in the lower part of the reactor, immediately above the gassing ring and one further stage in the middle of the reactor. The upper stage has a higher angle of inclination, compared to the lower stages. This implies a higher axial discharge direction then the lower stages. Combined with the strong suction effect of the lower stages, the upper stage discharges completely in the axial direction and leads to a total axial profile, although the Visco-Prop stirrer has not exclusively axial characteristics. Fig. 30 shows this profile for the actual operating state.

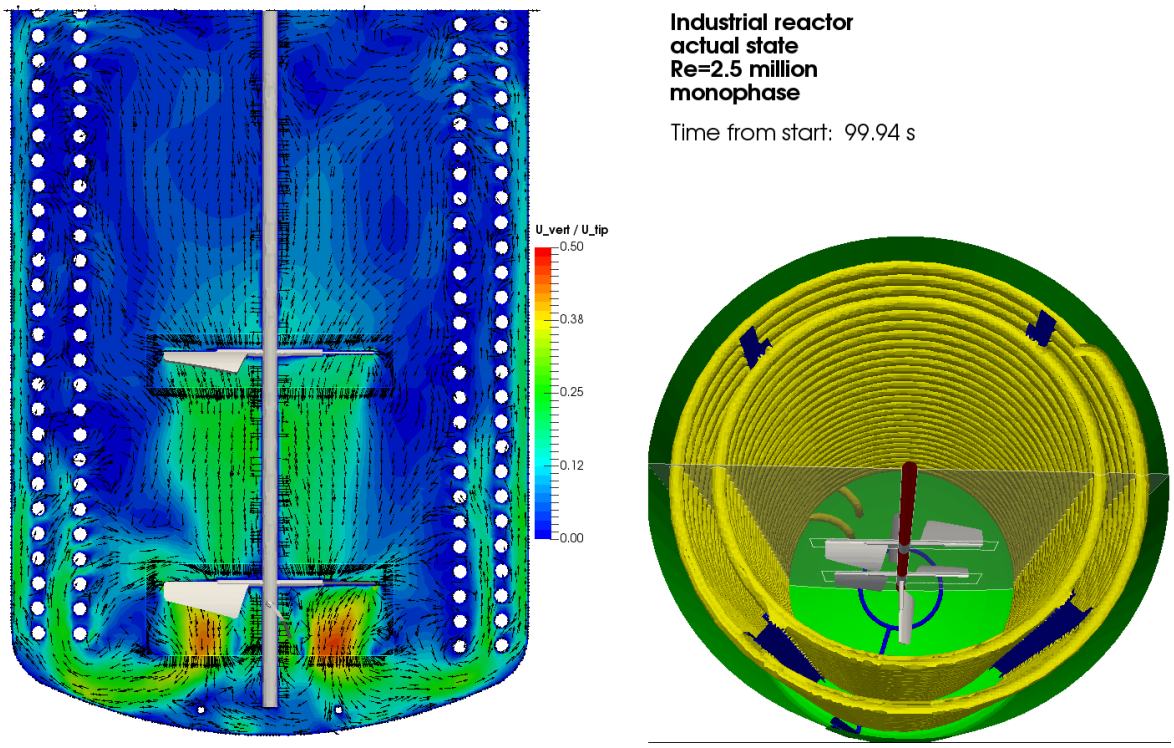

Fig. 30: Velocity profile of the actual state of the industrial process.

It is clearly seen, that the upper stirrer stage acts as an accelerating or charging element for the lower stages which introduce the strict axial flow profile of the reactor.

Basically, this configuration is reasonable from the generic point of view, since it suggests a good vertical flow along the helix coil which is supposed to lay right in the area of the maximum discharge stream, considering the principal flow structure of an axially mixed vessel [1]. However, the analysis of the actual flow field shows that the discharged jet stream mainly passes the coil and runs in the annular gap between the outer coil and the reactor wall. This is why the greatest part of inner helix is not affected by the jet stream in the first place. Moreover, the inner side of the outer coil does not benefit from the jet stream in an adequate amount. Considering the fact, that the local heat is strongly dependent on the incident velocity towards the exchange area, the flow field shows huge waste of heater potential – higher heat transfer can be achieved, if the flow field can be modified in an appropriate way.

The surface of the stirred liquid hardly undergoes movement which can pose a critical issue when charcoal has to be suspended in the process, because it is added in a dry state from above and remains at the surface until it is wet and carried away from the surface by fluid movement. A summarized evaluation reveals that the main problem with the whole process is the expected heat accumulation at heater areas which do not benefit from high fluid velocity and the retarded suspension of the charcoal into the fluid. In practice, it has an impact on the color of the product. The product appears yellow which is not the original color of the substance and indicates an overheating. The charcoal works as an adsorbent and minimizes discoloration. If the main named issues (overheating and delayed charcoal suspension) can be minimized, the product is expected to be improved by two mechanisms. A homogeneous temperature profile would reduce discoloration in the first place; second, if the charcoal is present in the fluid earlier, the adsorption process is supposed to be more effective. In chapter 6.1, the fundamental investigation work showed, that a radial stirrer type leads to higher heat exchange due to direct incident flow. This could be observed even for a single helix coil. Following this perception, the stirrer has to be modified in an adequate way. Since huge and constructive modifications are possible only in rare cases in the industrial active practice due to the enormous economical and administrative effort, the improvement strategy has to be convincing by its low cost and simplicity. The simplest and lowest cost proposal is the reconfiguration of the existing stirrer stages along the stirrer shaft, hence. The next chapter deals with the arrangement of a new stirrer stage configuration in the

process for maximal heater incident flow and simultaneously higher surface movement.

5.2.2. Improved positioning of the stirrer stages in the industrial process

Following the perceptions made in the preliminary study, the stirrer stages have to be organized in a way, where the most part of the heater is exposed to incident flow. Especially the area between the helix coils is challenging to reach by high velocity streams. However, chapter 6.1 shows the principal flow patterns of radial and axial pumping impellers, respectively. The axial pumping impeller generates a mean cellular vortex, that sheers off the boundary layer of the heater tangentially and softly over a comparatively large length whereas the radial impeller thieves directly through the coil and destroys the boundary layer by orthogonally and therefore more effectively but, however, over only a shorter length of the coil. The Visco-Prop stirrer is not exclusively a radial or an axial pumping impeller. It always contains both aspects whereas the concrete characteristics depend on the angle of inclination of the respective stirrer blades. A high inclination obviously leads to rather radial character of the stirrer, whereas a flat arrangement of the stirrer blades implies more axial behavior. In this context, the lower stages of the stirrer are referred to as the radial stages and the upper one as the axial stage. The straightforward solution to have the highest incident flow at the heater is to arrange the stages separately along the stirrer shaft. The challenging question is the concrete configuration of the stage order. The work of Bliem [12] showed, that the arrangement of two stages of the same radial characteristics can lead to an association of the discharge stream. This would mean a stronger incident stream but, however, not solve the problem of local focusing. The target is yet the distribution of the incident flow along the heater. The described effect is counterproductive, hence. Considering this effect, the stage order is straightforward: the radial stages must not be arranged next to each other, hence in the lower and in the upper part of the reactor. The central stage is then the remaining axial pumping impeller. This configuration has to undergo an examination of a vortex formation at the surface, though. Since the vortex is promoted by use of radial impellers and the radial stage is quite high (close to the surface), the probability for unwanted vortex formation is higher than in the original state. Like in the previous chapter, a simulation with the use of the VOF method is performed. As a result, the vortex formation amounts only 5 % of the reactor diameter and can be

neglected, hence. Anyway, the vortex does not reach the upper stirrer stage and is therefore uncritical, see Fig. 31.

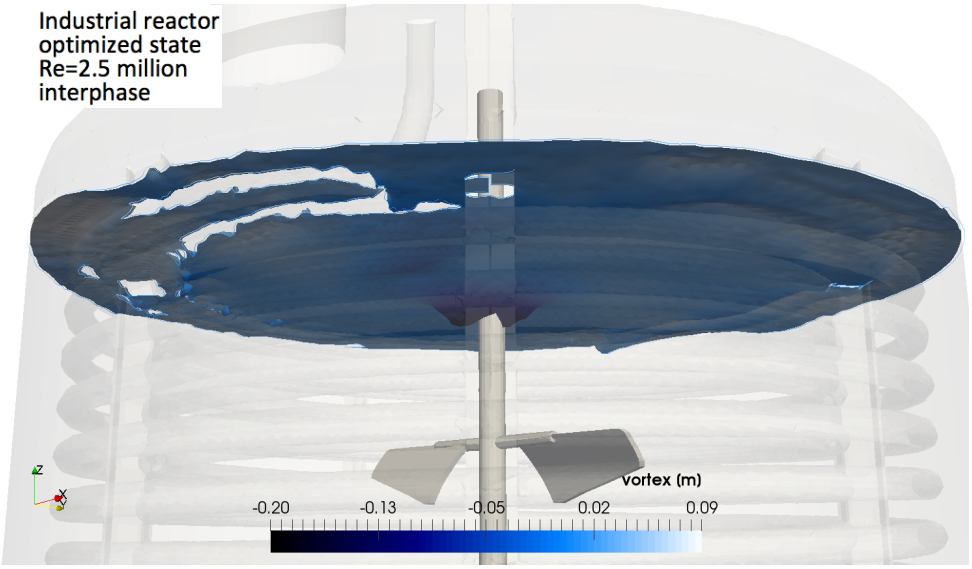

Fig. 31: Vortex formation at the improved stirrer configuration in the industrial process.

This result justifies the use of slip conditions and allows to proceed with single-phase investigations from this point. The resulting flow field is shown in Fig. 32. The above mentioned effect (unification of discharge streams) stays out as expected. The central stage forms a local and mostly circular cell vortex which sheers of the boundary layer of the heater in this area tangentially. The upper and lower parts of the coil undergo incident flow from the residual stirrer stages. The transient view on the flow field shows a remarkable higher unsteadiness than the original process. Better mixing and homogenization characteristics can be expected, hence.

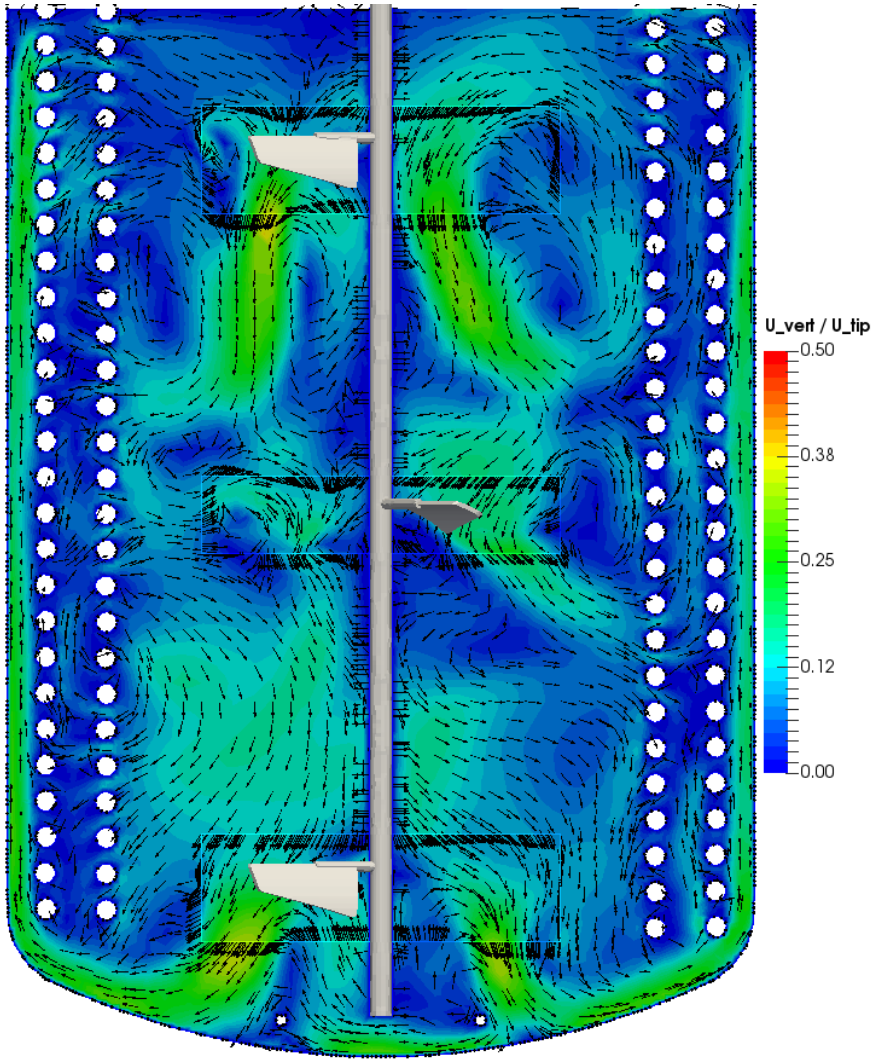

Fig. 32: Velocity profile of the industrial process with improved stirrer configuration.

5.2.3. Comparison of the original and improved state

Whereas the original state shows steady vortices in the area behind the lower stirrer stages, this vortex is formed and destroyed during the stirring process in the improved case. Dead zones and inhomogeneity spots can be reduced this way. The surface part of the reactor undergoes significantly better movement and is expected to have better suspension times which was one of the optimization targets. For a first estimation of velocity level improvement along the coil, the velocity magnitude is plotted in the gap between the helix coils, see Fig. 33. This is an indicator for the flux which thieves through the coil structure and embraces this way the biggest part of the coil pipe.

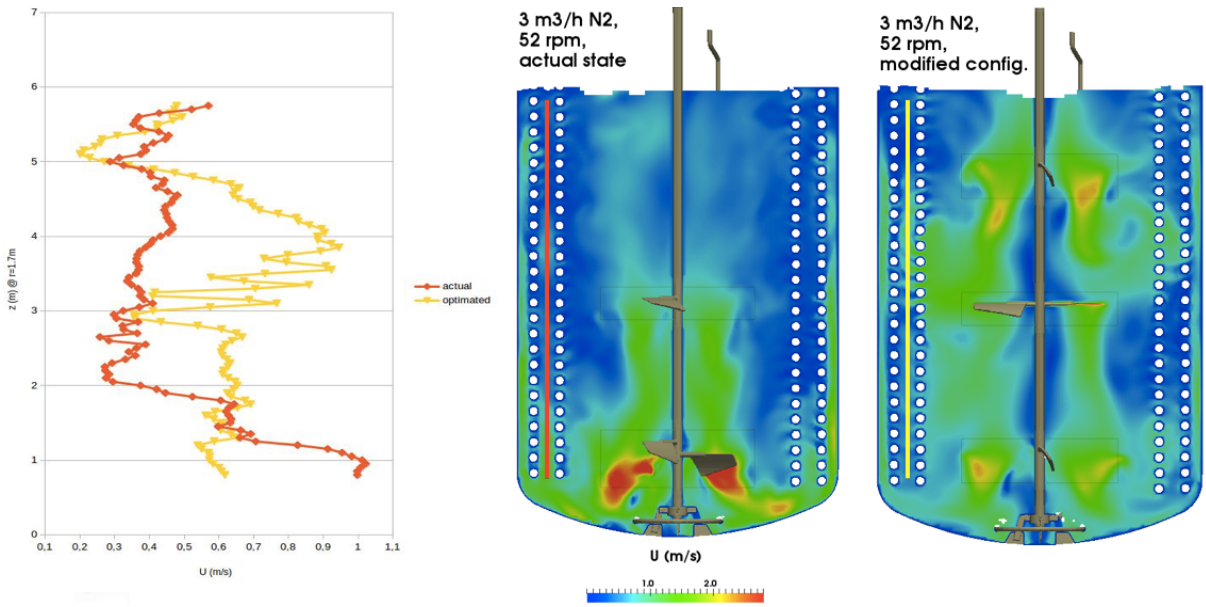

Fig. 33: Velocity magnitude in the annular gap between the heater coils.

The velocity magnitude profile shows a substantial improvement in the modified case. Moreover, a notably jagged curve is observed in the latter case. This is a clear sign, that the flow between the coils thieves through the coils and therefore undergoes interference instead of just passing in the axial direction like it occurs in the chimney effect, see Fig. 66.

The heat transfer is expected to be significantly better and more homogeneous than in the original state, since the whole reactor has a significantly higher velocity level. In order to quantify the improvement regarding the velocity homogeneity, a measure for it has to be defined. A simple velocity minimum to maximum range box (v_{max} - v_{min}) does not help at this point because it gives the same value at each configuration, namely the stirrer tip velocity since the velocity is maximum (v_{max} = v_{tip}) at his spot and minimal at each wall boundary (v_{min} = 0) by definition. Instead, a deeper analysis of the velocity distribution leads to an appropriate measure for homogeneity. Analog to statistical analysis, measures of location and variation can be derived from the velocity distribution plot. To avoid the extreme values (v_{max} and v_{min}) and to ensure a reproducible method, the extreme ends of the distribution are cut off by the 0.1- and the 0.9-quantiles. The box between those quantiles (80%-box) serves as a valid measure of variation since it gives reproducible and valid information about the width of the distribution. In order to make this measure comparable, it has to be normalized by a certain measure of location. The 0.5-quantile is also known as the median value of a distribution and is considered to represent the average level in an appropriate

way. The quotient of those measures is therefore proposed as a measure for relative inhomogeneity. For the application of it, a similar reference reactor is chosen. The differences to the before presented and modified esterification reactor are relatively small and do not require further explanation. The determination of the relative inhomogeneity can be comprehended by Fig. 34.

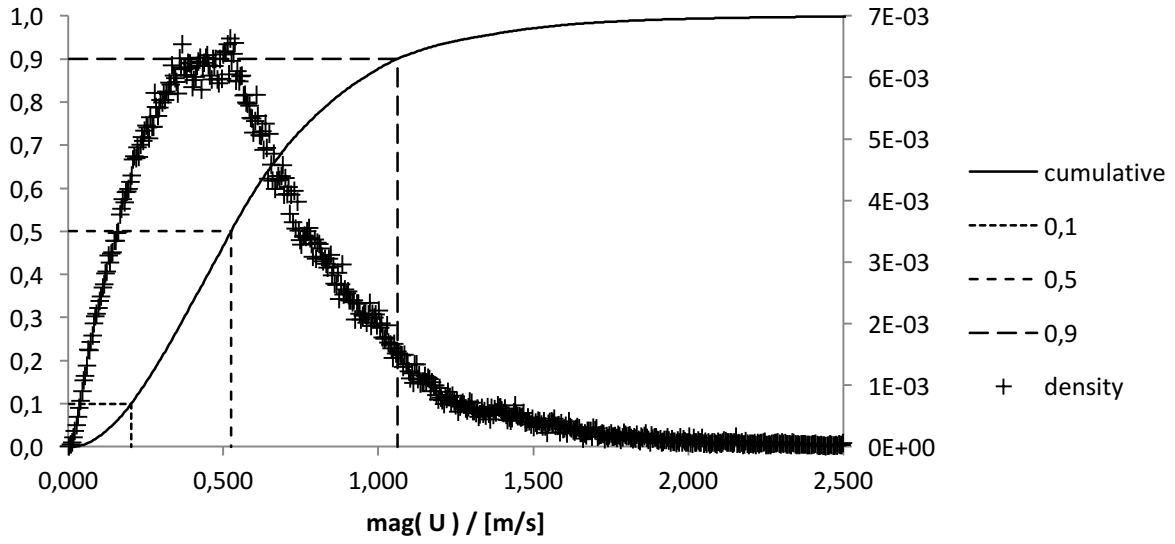

Fig. 34: Exemplary velocity distribution, sum curve and marks (dotted lines) for certain quantiles.

Four different configurations of the stirrer are investigated and can be seen in Fig. 35. The configurations are organized subsequently, i.e. the analysis of one simulation leads to the next configuration and so on. The relative inhomogeneity is determined and compared to the original state. Furthermore, the power consumption is calculated. The results are listed in Table 2. It shows, that the relative inhomogeneity can be reduced by over 30 % at a 73 % higher power consumption.

The main aspect of this work is to achieve better energy efficiency. Since the velocity level is higher in the modified case, the energy consumption for the stirrer is supposed to be higher than in the original case. The energy consumption can be evaluated by the volume integration of the energy dissipation rate ϵ. This can be done easily since it is one of the field values needed for the flow field solution, when a turbulence model is involved. The comparison of the original and modified state shows that the electrical energy consumption rises up to about 50 % with regard to the original state. Absolute power consumption numbers are not given at this point, since they mainly depend of the viscosity of the fluid which for its part depends on the reaction progress and the temperature. Moreover, the effective power consumption

depends on the efficiency of the stirrer driving unit which is specific for the used exemplar and operating condition.

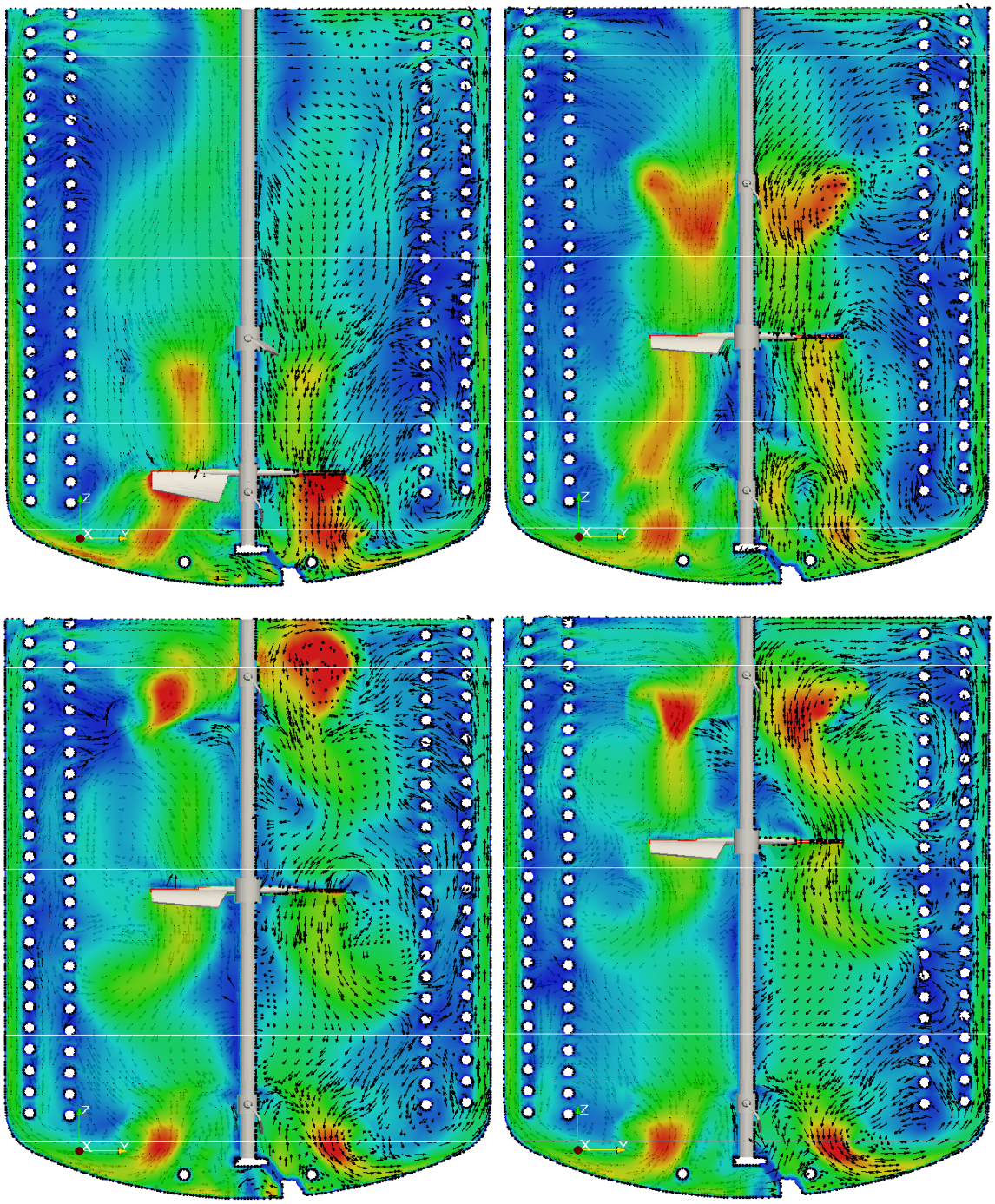

Fig. 35: Theoretical modifications of the stirrer configuration on a second reference reactor. The following configurations are performed subsequently and building up on the findings made after each simulation. Above left: actual state of operation (conv); above right: reorganization of one of the lower stages to a higher position – namely with the same distance to the middle stage (mod1); below left: stretch of the configuration before to achieve better distribution (mod2); below right: shift of the middle stage towards the top due to expected improvement of the velocity profile after the analysis of the configuration before (mod3).

The modification appears to have an opposite effect than it was aimed. However, the higher energy consumption can be accepted regarding the positive effects of the modification which lead to an expectedly better energy balance for the whole process. The heating energy and heating time can be improved by the modification. This leads to shorter production times and better product quality whereby subsequent energy consuming purification treatment can be reduced. This saves not only treatment energy but in the best case also additive chemicals. The discussed results have theoretical character since they are made by CFD investigations. However, the practical application of the modification will lead to further perceptions and prove or dispel the value of the applied CFD methods for industrial purpose without the possibility to validate the flow fields by measurements. However, power consumption, product quality and heating times will give a hint about the value of the performed CFD investigations.

Table 2: Study for augmention of velocity homogeneity in the second reference reactor.

Case	Velocity 0.1-Quantile	Velocity 0.5-Quantile	Velocity 0.9-Quantile	Rel. inhom.	Improvement	P
	m/s	*m/s*	*m/s*	-	*%*	*kW*
conv	0,15	0,46	1,26	2,40	-	1,5
mod1	0,15	0,51	1,16	1,97	17,8	2,9
mod2	0,19	0,50	1,08	1,78	25,7	3,0
mod3	0,20	0,53	1,06	1,64	31,9	2,6

5.3. The laboratory model: a simplification of the industrial precedent

In order to apply the PIV measurements to the stirring process, it is necessary to scale the reactor down to a size that can be handled in laboratory conditions. One has to consider, that special material has to be used for the model and RIM substances are used as fluids which require special treatment and are costly. The size of the laboratory model has therefore to be well deliberated. In this work, a geometrical downscale factor of 20 was chosen. Furthermore, the three-stage stirrer was renounced and one representative stage was used, instead. The reason for it is the interphase behavior. To obtain a turbulent state in the reactor, a certain rotational frequency is needed. In the scale of the laboratory model, it easily leads to strong vortex formation and ruins a stable stirring state. This effect is stronger when multiple

stirrer stages are used. The investigations in this work are restricted to a single stirrer stage, hence.

A further issue in the lab-scale investigation is the residual optical distortion caused by geometries inside the reactor. As described in chapters 2.7 and 4, the internals of the reactor can be made “invisible“ to the measurements. However, little distortions still occur and become serious issues when there is too much of it in the system. As a simplification to the industrial precedent, a single helical coil is used in the lab-scale model, hence.

5.3.1. Axial pumping impeller

As a commonly used example of an axial pumping impeller, an agitator with oblique and tapered blades is used for a representative axial agitation. It has a shape that is comparable to the EKATO Viscoprop and is constructively easy to manufacture. It has good performance characteristics concerning power consumption and mixing, see [12]. The simulations are performed in a vessel with a single helical coil. This is a discrepancy to the industrial reactor and to the simulations and measurements made in chapter 5.1. However, in chapter 5.1, only horizontal investigations could be made since the model consisted of copper coils which posed a problem for optical measurements. In further development, the heater is constructed from Plexiglas which it makes “invisible” for optical measurements thanks to the use of a RIM fluid, see chapter 2.7. The construction of the heater is quite challenging due to instable material and complicated installation handling. Moreover, the “hiding” effect by the RIM principle has its limitations. Anyways, the use of one helical coil shows acceptable measurement results. In Fig. 36, the measurement results are juxta posed to simulation results. The corresponding animation sequence can be found in the electronic appendix of this work, see 12.3. The clip demonstrates in a vivid manner, how vortices shed at the stirrer blades and hike in the annular gap before they dissipate. The similarity between measurement and simulation is seen better in the clip, although.

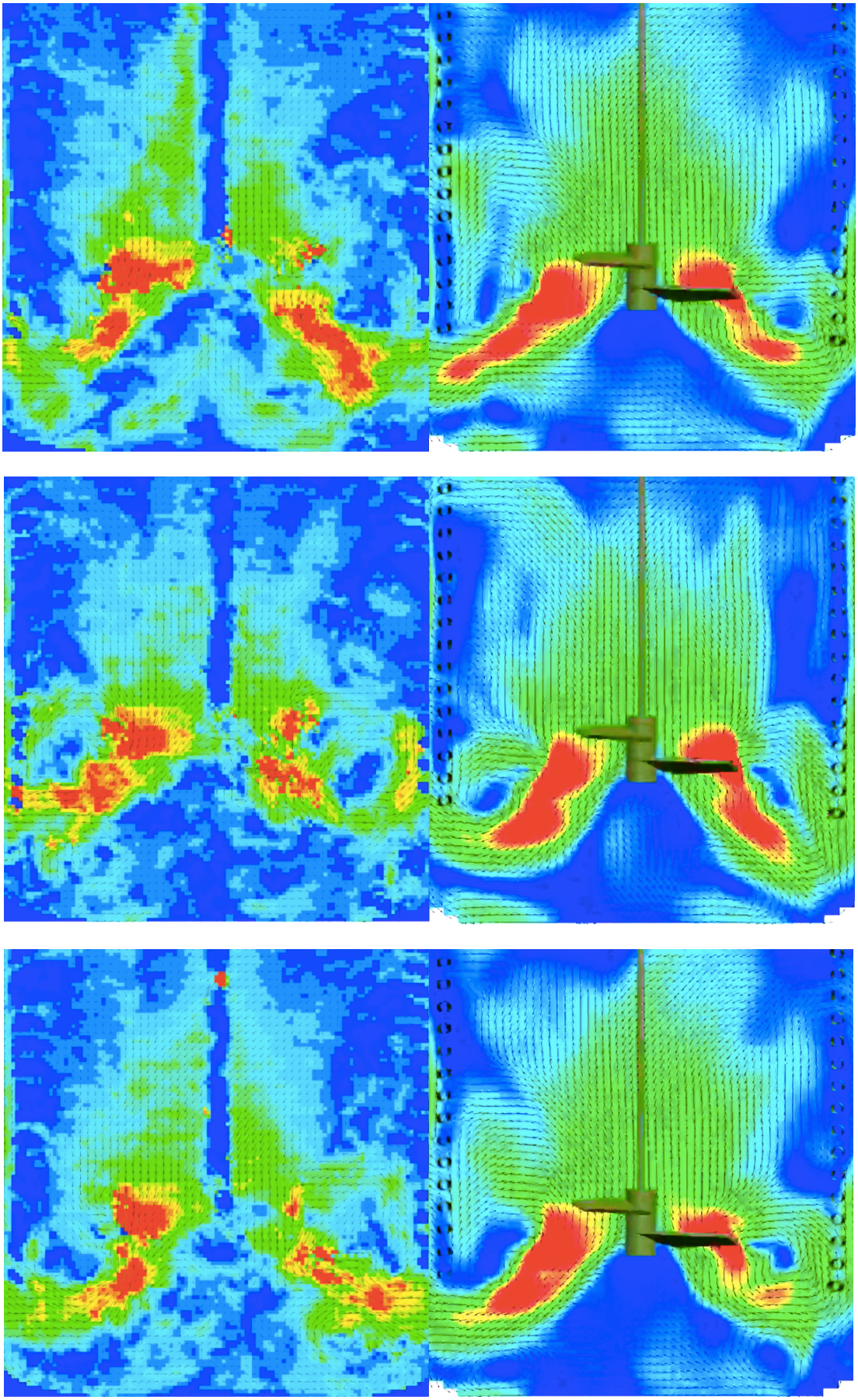

Fig. 36: Comparison of measurement (left) and simulation (right) results for the stirring process in a vessel with a single immersing helical coil and an axial pumping impeller. Three arbitrary shots of transient flow are shown. Hiking vortices are seen in both, the simulation as well as the measurement.

As well in the simulation as in the measurement, a very low velocity level can be observed close to the inner heater side. Despite the use of only one helix, this effect is clearly visible. In periods, shedding vortices arrange strong incident flow on the outside of the coil. The flow pattern forms a large cellular vortex that reaches from the stirrer, runs diagonally towards the lower reactor edges and then turns towards the top. On the top, it turns back to the suction side of the stirrer. The inner side of the coil remains relatively calm. Also the conical sector underneath the stirrer – between the discharge streams – is calm despite its vicinity with the stirrer. Furthermore, a stable vortex can be observed radially next to the stirrer. Although its velocity level is high, it is very stable and is kinetically fed by the stirrer. In the two-dimensional projection, it appears like a circle but is actually a torus that surrounds the stirrer. In contrast to those dead zones on the inner side of the coils which result from the lack of energy in that area, this small torus is a dead zone which is induced by the axial characteristic of the stirrer itself.

5.3.2. Radial pumping impeller

The most typical radial pumping impeller is without doubt the so-called Rushton turbine. It consists of a horizontal disc retainer and blades that are angled vertically and point to the radial direction. The typically six blades are fixed on the disc. The Rushton turbine is a very important representative of radial impellers, since it induces a separation of the flow at its disk. Due to centrifugal forces, the fluid is accelerated in the radial direction and sucked from both sides of the disc. As a result, two main and inversely rotating tori are formed. Those tori are referred to as vortex cells. The principal flow patterns of both, the axial and the radial impellers (vertical slice view) is pictured in Fig. 37.

In the observed case of helical coil use, the coil works like a separation wall and even sharpens the cellular profile. On the one hand, it accelerates the velocity in the annular gap between the coil and the reactor wall but on the other hand, however, lowers the velocity level on the inner side of the coil. This effect rises the probability of a dead zone formation. The high velocity in the annular gap is indeed positive for heat exchange due to a reduced laminar boundary layer but affects the coil only partially and can be destructive in the case of sheer-sensitive organism and enzyme use. Moreover, a tangential vortex underneath the stirrer is formed. This can be observed in the most simulations with the Rushton turbine. It reminds a whirlwind and

entails the risk of dead zone formation like it is known from the tornado center. Generally, the flow pattern is shaped like it is described in the relevant literature like [1]: the discharge stream runs radially towards the reactor wall and then splits in two main cellular vortices, the upper and the lower. A detailed analysis of the velocity field in dependencies of rotation frequencies is given in the collaborating work of Jährling [65] and [66].

Analog simulations have been furthermore performed with a curved radial pumping impeller and a paddle stirrer, see Fig. 38. Basically, the flow patterns have similar patterns which are very typical for radial stirrer types. The curved radial impeller consists of three blades. The temporal behavior, hence is different from e.g. the Rushton turbine. Whereas the Rushton turbine produces a relatively constant and highly energetic jet stream, the curved impeller produces larger hiking vortices due to the huge gap between its blades and the significantly higher surface of the blades. The flow field is less steady, hence. This impedes more chaotic movement in the fluid which can be advantageous concerning dead zone formation, mixing and hot spots.

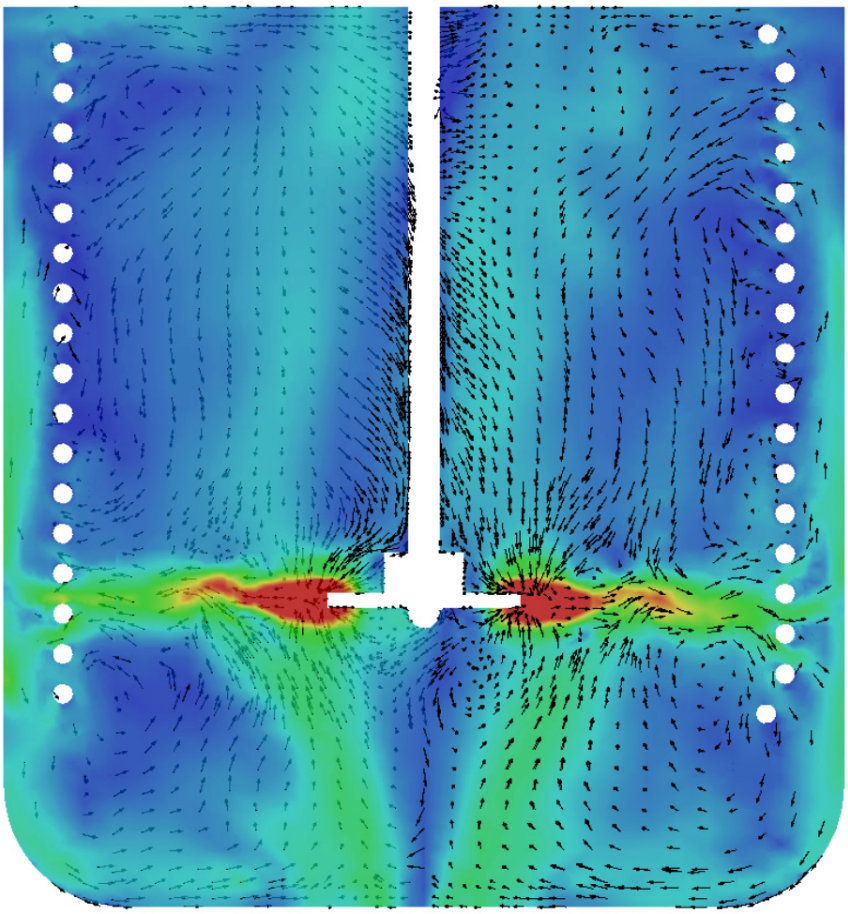

Fig. 37: Radial flow pattern, caused by a Rushton turbine. Axial slice representation.

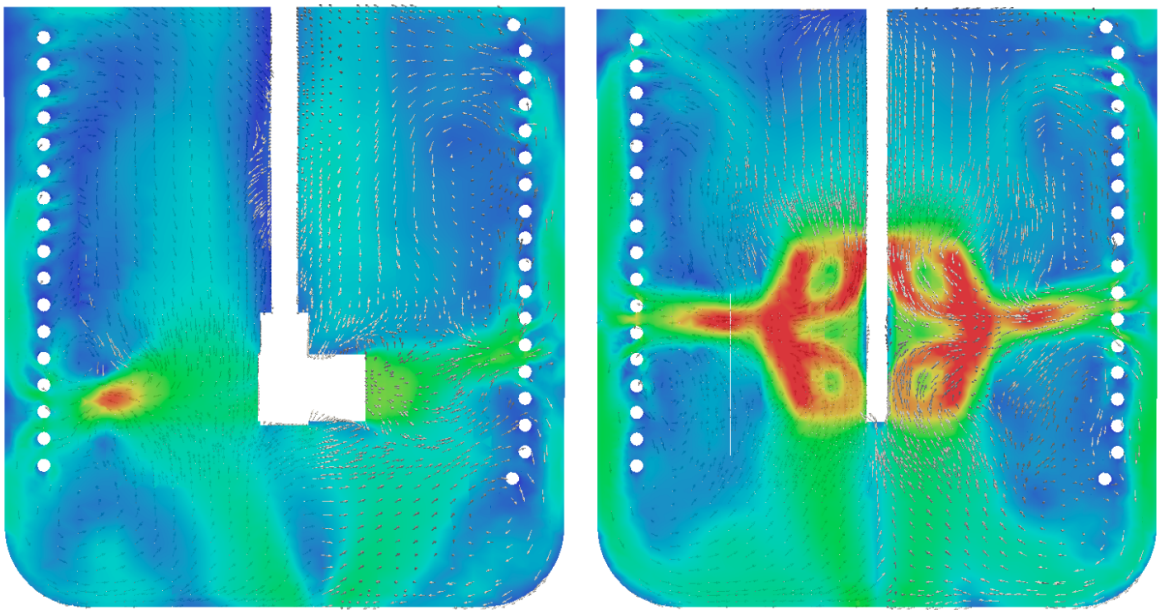

Fig. 38: Flow patterns of the curved radial pumping impeller and the paddle stirrer.

The paddle stirrer has comparatively wide blades, which are the triple or more the width of other radial stirrers. The use of this kind of stirrer is obvious – a great blade surface promises a high pulse transmission to the fluid. Of course this high surface is notable in the flow resistance and the resulting high power amount. On the other side, the wide blade could be advantageous for the heat transfer if larger areas of the heater coils can undergo the high velocity and direct discharge flow. However, this effect cannot be observed in the simulation. Rather, the discharge stream narrows to a thin jet that barely has the thickness of that of the curved impeller which is three times thinner than the paddle. Moreover, the flow field is highly periodic. The chaotic character which can be observed at the curved impeller and partially at the Rushton turbine is not present here. Formations like cellular vortices are more stable in this case which has negative influence on dead zone and hot spot formation.

5.4. Use of alternative heater elements

In order to consider alternative heating possibilities due to the huge issues in the case of helical coils, tube baffles are implemented and investigated. The work of Jährling extensively treats the use of different alternative heaters in stirred reactor vessels [65]. In this work, tube baffles are used as a representative for vertically installed heater elements. The huge advantage of tube baffles is their function as both, heater and baffles without separating the flow in different segments like it

happens with helical coils. Tube baffles have low complexity and are therefore economical. On the other side, tube baffles provide a small surface. They can only be used for processes with low heat exchange demand, hence. The heating media enters the tubes downwards and leaves them upwards. This fact makes them useless for steam heating since condensed water would accumulate at the baffle bottom.

Fig. 39 shows the simulation results for three different types of reactor vessel bottom. The first of them – the flat bottom – is mostly used in laboratory investigation environment but has little application in industrial reality, however. The second – the dished bottom – is the most used type in the industry thanks to its stability and constructive feasibility. The last – the half sphere bottom – is used for special applications only. Its construction requires very special know-how and is expensive, hence. However, the spherical shape is optimal for pressure distribution and has the best area per volume ratio.

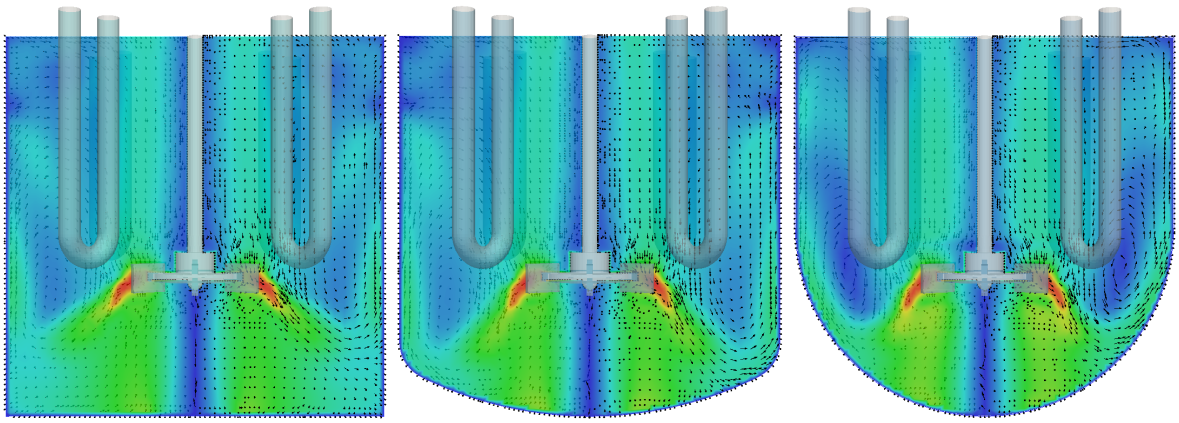

Fig. 39: Use of tube baffles for velocity field investigation in three different types of reactor bottoms. Re=16000; strictly uniform distributed and radial configuration of tube baffles; bottom clearance=1/3H. More details about further configuration options are excessively treated in the work of Jährling [65].

The velocity field of the three simulations is very similar concerning its principal characteristics. Each of the flow patterns shows a discrepancy to the expected. Despite a Rushton turbine is used, the discharge stream is not radial but axial. The only element that reminds the characteristics of a radial impeller is the whirlwind underneath the stirrer. Axial impellers tend to have a conical structure at this point. This reason for this discrepancy is based in the tube baffles which are responsible for the following effect. It is based in the Bernoulli principle. The baffles suppress the

tangential component in the upper part of the reactor. The lower part, therefore, rotates faster. The difference in velocities produces a difference in the pressure according to Bernoulli's law. This effect pulls the discharge stream even more towards the high velocity section. In Fig. 40, the so-called stream tracer filter shows the path of fluid that passes through a tube baffle and then is inclined towards the lower part of the reactor. The pressure drop in the slipstream of the baffles is visualized by the contour filter in Fig. 41.

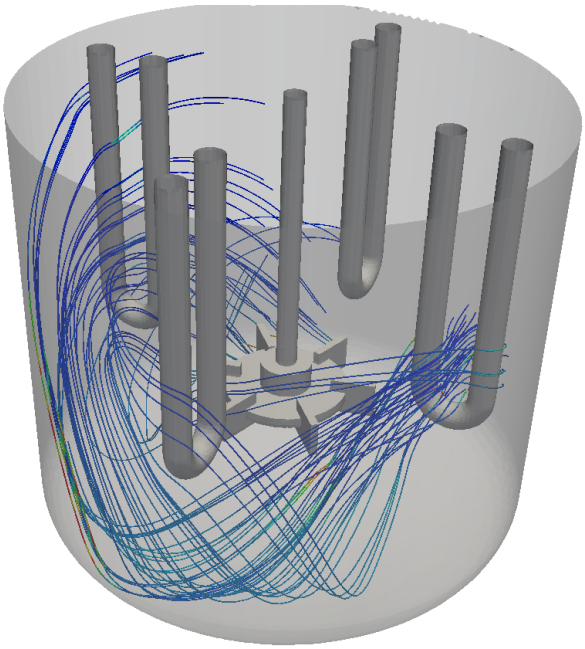

Fig. 40: Fluid path through the reactor with tube baffles and a Rushton turbine.

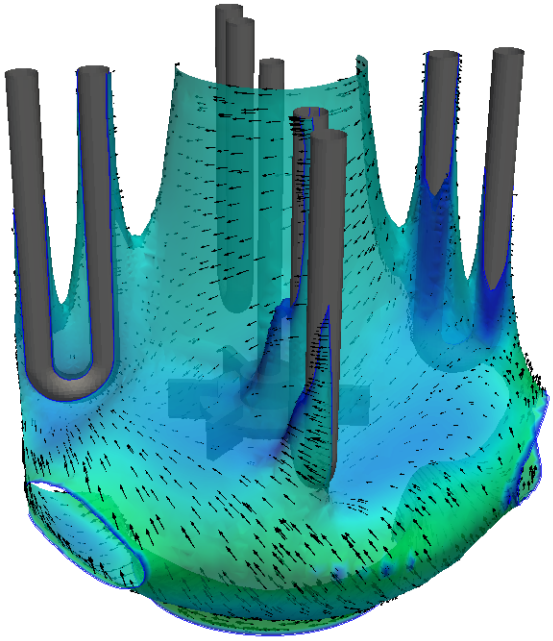

Fig. 41: Pressure contour in a reactor equipped with tube baffles.

Despite the commonly established assumption that the main flow pattern is generally induced and conducted by the stirrer, the use of tube baffles shows that static internals can affect the flow pattern in a fundamental way. The bottom type, in this special case, does not have a significant influence on the flow pattern. However, Jährling showed in [65] that flow patterns differ notably when spherical bottom reactors are used. The tightening structure impedes the use of baffles in that area. As a consequence, the tangential component cannot be suppressed effectively in that section and the Bernoulli effect becomes relevant. Beyond constructive and economic reasons, the dished bottom is generally recommended for mixing processes. The flat bottom, of course, provides the most volume off all three types.

However, the lower edge is predestinated for dead zone formation. Cellular vortices tend to have smooth curves and the corners remain comparatively calm, therefore. The dished bottom, on the other side, wipes those problem zones away. The spherical bottom does it in an even more radical way but takes away much reactor volume.

The described results are confirmed by measurements via stereo-PIV, see Fig. 42. The visualization has to be made differently from the normal. The reason is based in the fact that the laser plane had to be positioned with an offset from the stirrer shaft and therefore does not intersect the axis. Thus, some losses in accuracy and symmetry have to be accepted. Moreover, internals are hidden from detection by use of RIM fluid. Hence, the postprocessing omits the fading-out of non-fluid elements and interpolates those sections by surrounding field values. The stirrer is therefore not seen in the measurement visualization but is located at the same height as in the simulation. The comparison confirms the anomaly in the flow pattern, although it is less strong. The whirl underneath the stirrer is by the factor 2 tighter in the measurement then predicted by the simulation. Beyond that, the results match with high precision. The velocity level is equal and the baffles are visible in the slipstream. The velocity is distributed homogeneously in the reactor.

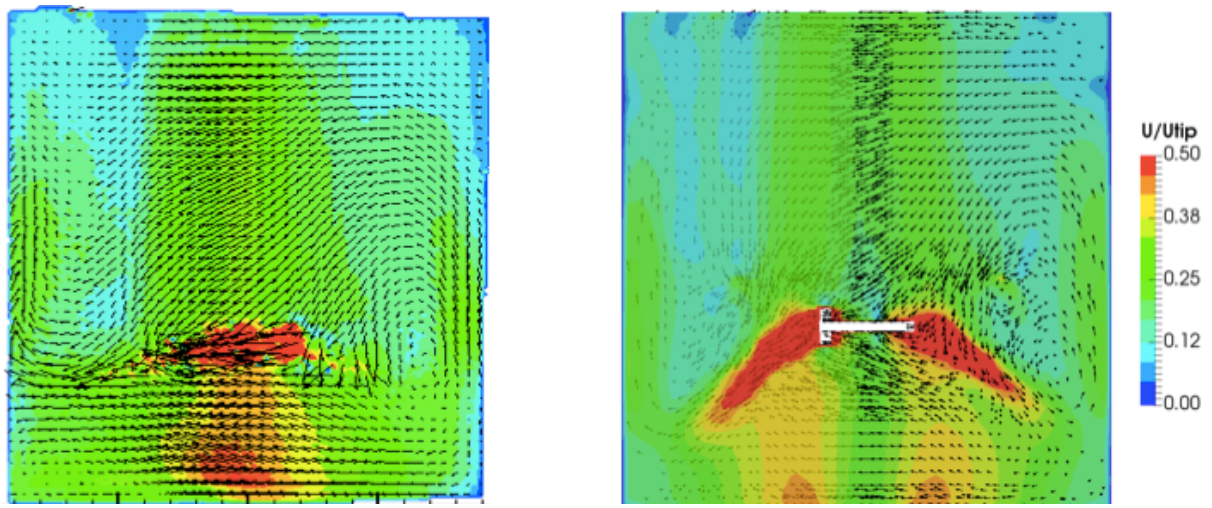

Fig. 42: Comparison of stereo-PIV (left) and CFD (right) results for stirring with a Rushton turbine and the use of four tube baffles. Re=16000; straight and equidistant configuration of four tube baffles; bottom clearance=1/3H.

6. Heat transfer investigations

The contents of this chapter have the highest relevance for the industrial optimization; however, the here discussed results cannot be validated in an appropriate way. In the scope of this work, an alternative strategy is used, hence. The value accuracy is not demanded since it cannot be validated by experiments. Rather more, studies are performed to detect tendencies and sensitivities to certain parameter changes. Since the implementation of a full complex model including moving geometries, turbulence models and heat transfer is not feasible due to stability and computability issues, simplified models were implemented and proved valid for the velocity fields. The simplified models allow fast and stable computation and serve as a useful tool for further heater development.

6.1. Influence of the impeller's bottom clearance on the heat transfer

In the industrial practice, low influence can be made on an existing design of an apparatus. Heat exchangers cannot be exchanged or modified without more ado. However, the position of the stirring stage can sometimes be modified by comparatively low mechanical effort, since the stirrer stages are fixed on the agitator shaft by screws or similar detachable joints. For a given reactor design, the stirrer stage position – called bottom clearance – is a good optimization opportunity. As the helical coil is a commonly used heat exchanger and moreover the one used in the reference process, the influence of bottom clearance is investigated for it. The here discussed results are summarized and published in [67].

6.1.1. Investigated model

For the preliminary study, a lab scale reactor model was used, since the results should be comparable to possible laboratory experimental results. In [62], Bliem showed that the tangential flow component is relatively low close to the helical coil in a setup with four baffles. The radial and axial components prevail, hence. Considering this to be a preliminary study, this circumstance leads to a simplification of the CFD model. Instead of a three-dimensional simulation, only the radial and axial flow components are observed, neglecting the tangential flow. In addition, axial symmetry is assumed and the cylindrical reactor is diminished to a vertical slice or –

spoken in CFD jargon – to single cell layer mesh. Such a simplification makes it impossible to implement the agitator as a rotation unit, since it has solely tangential movement, which in this model is completely excluded. A more abstract view on the agitator is needed, hence. From the mechanical perspective, the stirrer serves as a pumping unit that sucks fluid on one side and discharges it to another side. In the case of a radial pumping impeller, the discharge is strictly radial, the rest of its geometry can be considered as suction area. The stirrer now can be implemented as a black box pumping unit without any real, i.e. transient, movement but with a fixed discharge condition. The resulting geometry model is shown in Fig. 43. The constructive parameters like reactor, heater and stirrer dimensioning are acquired from the standard design recommendations in [1], [2], [25].

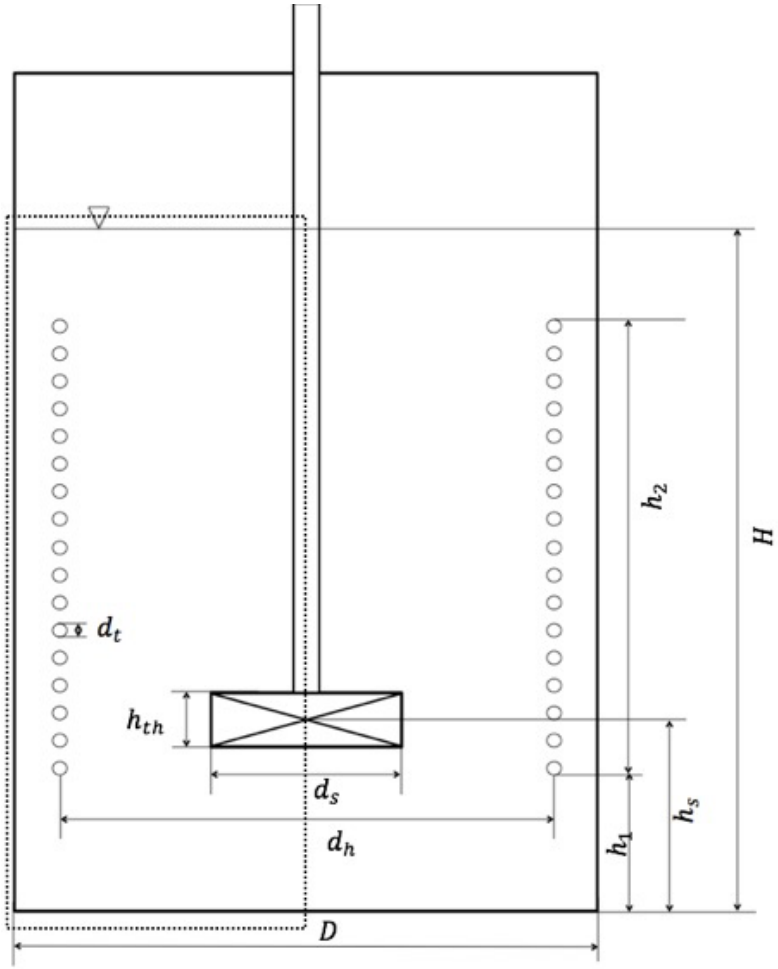

Fig. 43: Model geometry of the 2D abstraction of a cylindrical reactor with a helical coil.

$D = 0.85\ H$

$d_t = 1/42\ D$

$b = 0.1\ D$

$N = 17$ windings

$d_s = 1/3\ D$

$d_h = 0.85\ D$

$h_1 = 0.2\ H$

$h_2 = (2N - 1)\ d_t$

In industrial applications, steam is a common heating medium. Due to latent heat, the temperature along the coil is assumed to be rather constant. A fixed value can be implemented for the heater boundary condition, though. The vertical pumping black box (PBB) boundary is set to a constant radial flux velocity since it is orthogonal to the radial direction. The rest of the PBB is set to free input/output condition. Since the

tangential component is low, the vortex formation at the fluid interphase is neglected. This was also confirmed by experiments for the relevant rotational frequencies. The upper boundary can therefore be implemented with slip condition, whereas the rest of the geometry takes standard wall boundary conditions. This model abstraction also works with an axial pumping impeller, when the discharge is defined to be at the lower boundary of the PBB. The generated mesh is shown in Fig. 44.

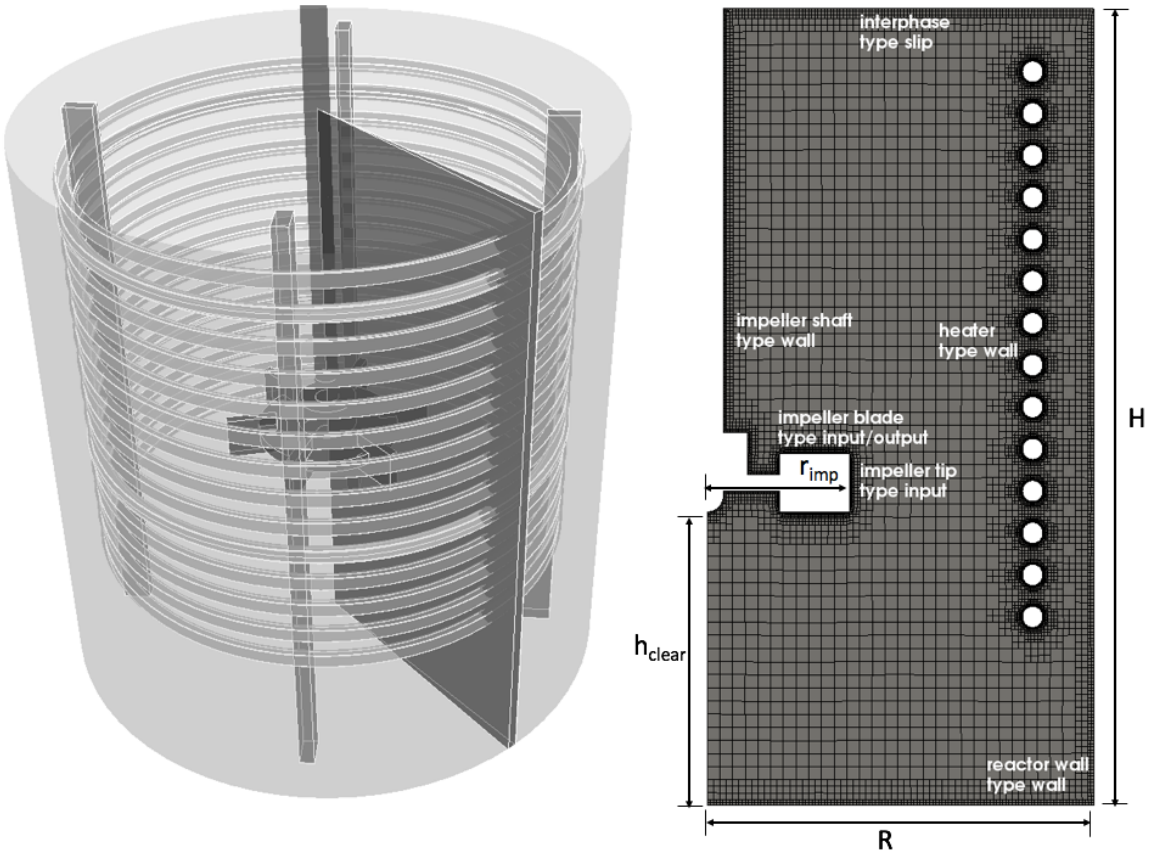

Fig. 44: Resulting mesh of the pseudo 2D-abstraction, generated for a Rushton turbine. Details about cell number and fineness are listed and discussed further on.

6.1.2. Simulation setup

For this basic and preliminary study, additional simplifying assumptions are made. Since the heat transfer distribution along the heating coil and the temperature distribution inside the reactor are the subjects of interest, a steady state model was made up. In a batch process, on the other hand, heat transfer and temperature profiles are not stationary, because the process ends up in a homogeneous temperature field without heat flux, when the it becomes stationary. To maintain a stationary heat flux, the pumping unit is implemented as a perfect heat exchanger,

that has a discharge of a constant, cool temperature. Practically, a cool fixed temperature boundary condition (293 K) is set to the discharge patch and a hot one (333 K) to the heater coil patch. This way, a constant temperature difference is implemented and ensures a temperature distribution for the stationary observation. The OF solver “buoyantBoussinesqSimpleFoam” was used for this simulation study. The discharge velocity is set to the details about the numerical schemes and linear solver adjustments can be reviewed in the appendix, see 12.1.5.

6.1.3. Flow field of the two-dimensional abstraction

The velocity field of a stationary simulation of the described model is in good agreement with the measured data, obtained from PIV measurements. Fig. 45 shows a comparative measurement and simulation flow field for a bottom clearance of 0.36 relative to the reactor height or the filling level, respectively.

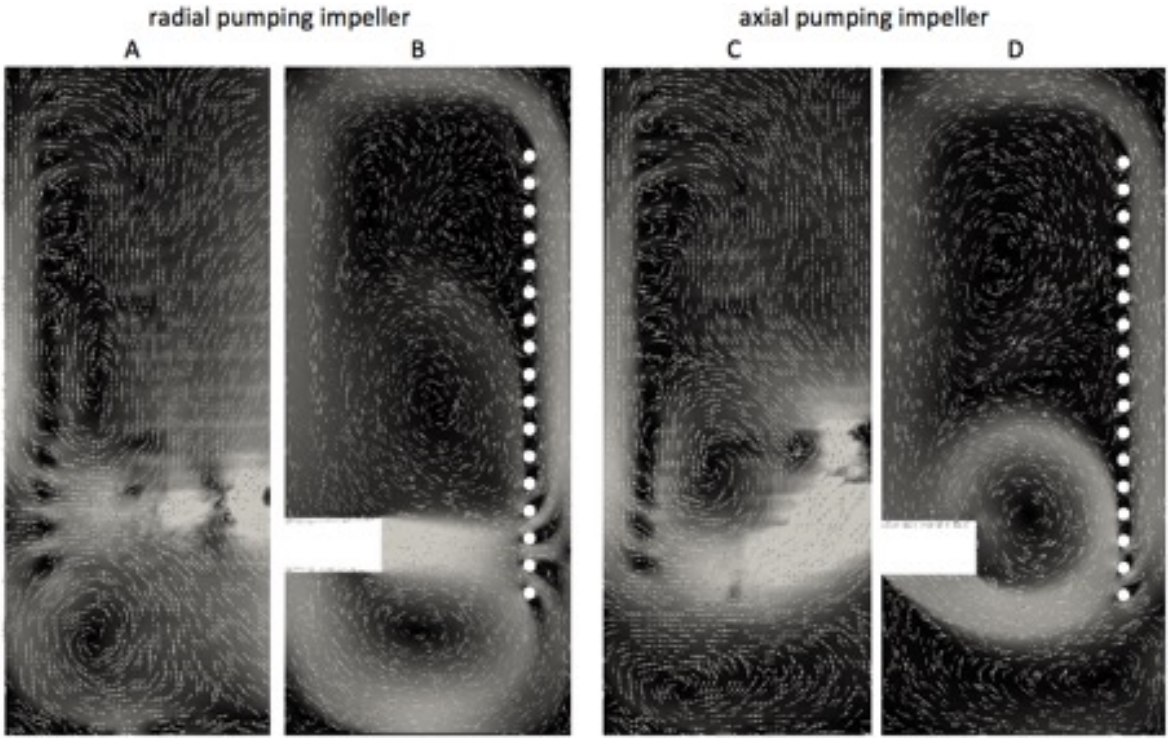

Fig. 45: Flow field comparison of PIV measurements (A, C) and abstracted CFD simulation (B, D) data. Due to visualization variances and neglecting of less important details, the images can appear slightly shifted. However, the setup was consistent between the measurements and simulations.

In the scope of a preliminary study, the simulation corresponds sufficiently well to the measurement regarding the flow field. This is found for both, the radial as well as the

axial cases. The same cellular vortex formations can be found around, above and underneath the PBB. Even the sub cycles and flow short circuits appear in simulations and measurements. For both cases, the flow field is on a comparatively high level in the area of the annular gap but, however rather low at the inner side of the heating coil.

In the case of the radial pumping impeller, the discharge jet stream runs strictly radial towards the wall, sieves through the coil and then splits into two main cellular vortices, which run along the coil and then return to the PBB after performing a maximal circle. Little sub circles are formed in the area between the inner side of the coil, the PBB and the main cellular vortex. The disadvantage of cellular and sub vortices is of course the center, where low velocities entail bad mixing and low transport.

In the case of the axial pumping impeller, the discharge jet stream has to be adjusted with more care. Due to the used impeller – that is not strictly axial – the discharge is not strictly in the direction of the reactor axis. Measurements confirm this statement. Of course, it has to be accounted for when setting up the fixed discharge velocity vector as a boundary condition. The best results are achieved, when the discharge vector points to the lower corner of the reactor. The axial pumping unit shows fundamentally different characteristics, compared to the radial pumping impeller. In contrast to the radial case, the jet stream does not split into an upper and lower cellular vortex but into an outer and an inner vortex. The inner vortex shape is rather circular and has a diameter in the extent of the stirrer radius. A significant part of the jet stream flux sieves through the coil helix and forms a vortex loop, that runs in the annular gap to the top of the reactor, precedes along the interphase to the center and comes back to the agitator close to the shaft. Again, a huge part of the coil is not well touched by high velocities, namely the inner side of the helix, where the velocity level is quite low. Secondary vortices are formed inside and outside the main cellular vortices but have significantly lower flow levels and suggest bad mixing characteristics. A strong deviation between the axial and the radial cases is in the lower area of the reactor. Meanwhile in the radial case, the lower and the upper vortices seem symmetric regarding their topology, in the axial case the sub cycle in the very low part of the reactor seems completely detached from the rest of the main flow. It even circulated in the opposite direction. Material accumulation and dead zones are expected here, though.

The discussed characteristics of the vertical flow patterns are found in both, the simulation as well as in the measurement approach. The good agreement serves as a basis for the model validity. The heat flux results cannot be transferred from the simulation to the real case, since huge simplifications and abstractions were made. However, when it comes to the pure influence of the bottom clearance on the heat flux, the absolute values play a subordinate role. The tendency within the used model is of greater importance since it shows general interdependencies, including relative improvements that can be estimated this way. The absolute values are expected to deviate from the measured data anyway, since effects of baffle slipstreams, residual tangential velocities etc. are neglected in the simulation. The principal validity of the model abstraction regarding the radial and axial velocity profile, however, encourages to proceed with the two-dimensional abstraction for heat transfer investigations. The compelling argument for the use of the simplified model is its low calculation cost and memory demand. Any study can be performed in a deeper and more detailed manner exploiting the resources optimally. After deriving the main statements from the study, the investigations with less simplifications can be performed on a more focused range.

6.1.4. Temperature field of the two-dimensional abstraction

The temperature at the stirrer discharge patch is set to be at a constant temperature value of 20°C, whereas the wall temperature of the heater coils is set to a constant value of 60°C. The agitator acts as a perfect thermostat which guarantees the temperature drop between heater and discharged fluid even for a stationary case. This cannot be realized in experimental setup but is an essential precondition for the usefulness of the abstracted model. Moreover, a constant temperature on the whole coil is hard to facilitate in the laboratory scale. The exchange area of the coil is comparatively high with regard to the reactor volume. Under laboratory conditions, the heat transition occurs in a minor part of the coil and the heat carrier loses its capacity for the residual heater fraction. This issue can be theoretically circumvented by the use of steam heating, since latent heat guarantees constant heat carrier temperature. However, laboratory experiments show that the emerging condensate clogs the relatively thin coil pipe and makes it impossible for the steam to reach long way parts of the coil. Hence, the concept of coil heating appears to be limited to bigger scale applications but turns out to be a waste of heater area in this small

laboratory scale. However, for the analysis of the main characteristics of velocity profiles and turbulence, the laboratory model – as a geometrical downscale from industrial applications – has its full value. The measurement approach of heat exchange in this model is described in [68], but will not be treated here due to the lack of setup comparability.

In the described simulation setup, multiple effects of temperature distribution can occur. One has to distinguish between areas that lay in the direct downstream of the heater and those in sub circles. The detailed discussion is better comprehensible on the example of a concrete simulation in Fig. 46. A radial pumping impeller was chosen for the description.

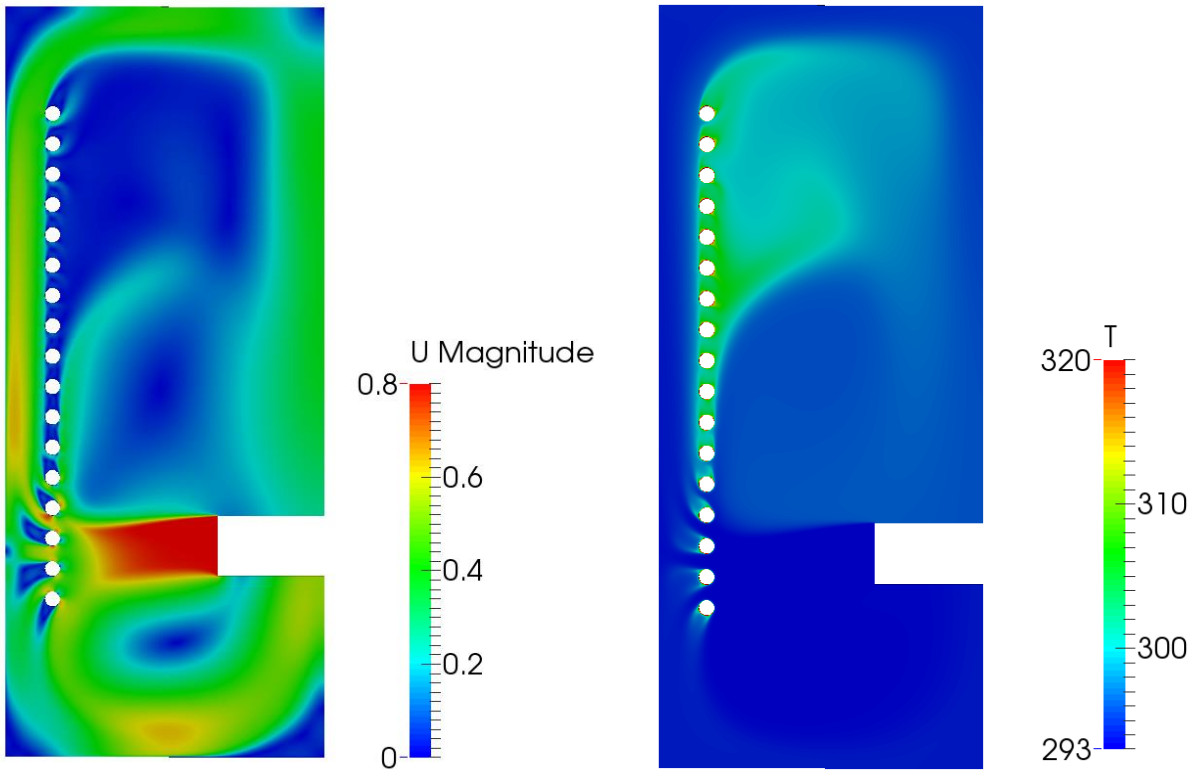

Fig. 46: Comparative visualization of velocity and temperature fields for a coupled heat transfer simulation. Radial pumping impeller is installed at a relative bottom clearance of 0.36. The stirrer discharge velocity corresponds to fully turbulent mixing at Re ~ 20000.

It is clearly visible, that the hottest spots emerge on the inner side of the heating coil, especially there, where the dead zone is expected to be, when observing the velocity field. This area is on the one hand a direct downstream domain of the heater but has a very low velocity level on the other hand. Hence, the heat accumulates in the downstream area. This leads to formation of so-called hotspots. On the outer side of

the coil, the velocity level is high and capable of transporting the exchanged heat very fast by convection. In this section, the temperature is very low, since the convection drives the fluid back to the agitator quite fast, where it is cooled down artificially by the boundary conditions. The pattern of the upper cellular vortex is even seen in the temperature profile. The upper sub circle is also well visible, but has a significantly lower temperature than the hotspot. On the one hand, the sub circle is not a direct downstream area of the heater and does not accumulate heat in the same amount. On the other hand, it has tangential contact area with the heater, but seems to exchange the so gained heat with its surrounding main cell vortex. Of course, it still is assumed to be a dead zone for material transport, but appears to be least prone for hotspots. This discrepancy is explainable by different sources of heat and material. The heat source is the coil – and the agitator in this case – whereas the material source can be the whole reactor domain (chemical reaction) or a certain spot (dosing point). The described hotspot cannot be seen in the lower part of the reactor for the observed case. This can be described by the absence of direct downstream sections with low velocity level. The only downstream part of the coil belongs to the lower cellular vortex and has a high velocity and short residence time, though (here, residence time is meant as material dwell time from agitator discharge to the suctioned return to it). The enclosed sub circle has a low temperature since it hardly has contact to the heat exchange area. A dead zone is expected here, although.

6.1.5. Homogeneity of the temperature field

The temperature range in the domain reaches from minimum to maximum by simulation setup (vicinity of preset boundary conditions). When the term homogeneity is mooted, the pure minimum to maximum range is therefore not suitable. Cases with obviously different degrees of homogeneity would then have similar ranges – even before the simulation is run. An appropriate measure has to be implemented for homogeneity. A more auspicious approach is the inspection of the temperature distribution, e.g. via temperature histograms. However, the tails of the distributions show high peaks which undermine the sense of a homogeneity measure. On the other hand, those peaks are expectable when analyzing the simulation setup and the heat transport phenomena. Even in a very homogeneous case with a narrow distribution, the very close sections to the heater (thermal boundary layer) have high

temperatures. This matter of fact results in the right peak at the tail of the temperature distribution. The other way around the discharge jet stream of course carries cold temperature until the first contact with the heater surface. Any histogram will have this peak at the left tail of the distribution. In order to exclude those effects, it is useful to cut off this part of the histogram. Since those effects originate in certain areas of the domain, it is appropriate to cut off the data in a manner that this area is excluded from the histogram. After the analysis of certain cases, a cutoff of 5 % hottest and coolest area each appears to be suitable. The temperature range of the resulting data is now representative for the distribution width.

6.1.6. Impact of the stirrer frequency on the heat exchange

The characteristic equation (2.9) puts the Nusselt number as a function of the Reynolds number. The change of the rotation frequency impacts on the heat flux in the way $n^{c_{Re}} \sim \dot{Q}$ by the connection of equations (2.5), (2.6) and (2.9). The slope of a logarithmic plot of the total heat flux against the rotation frequency is the value of c_{Re}, hence. The simplified simulation setup does not allow a straightforward utilization of the rotation frequency since there is no actual rotator in the simulation. Instead, a radial stirrer tip velocity is used, which should be linear to the rotation frequency and therefore valid for the logarithmic plot. The results are shown in Fig. 47. The study was performed for a relative bottom clearance of standardly used 0.36. Different bottom clearances are identified by the acronyms χ1: *z/H*=0.24; χ2: *z/H*=0.36; χ3: *z/H*=0.49; χ4: *z/H*=0.61.

The slope is determined by linear regression and appears to be 0.9. This result contradicts the information given in the literature [69], where the exponent in the characteristic equation (2.9) is specified with 0.67; thus the influence of stirrer velocity has a stronger influence on the heat transfer than posed in the literature. Experimental work has to be done on this to find out whether this discrepancy originates in the simplifications of the model or if there is a need to scrutinize the literature values. However, the experimental validation of this work presents huge difficulties as described before.

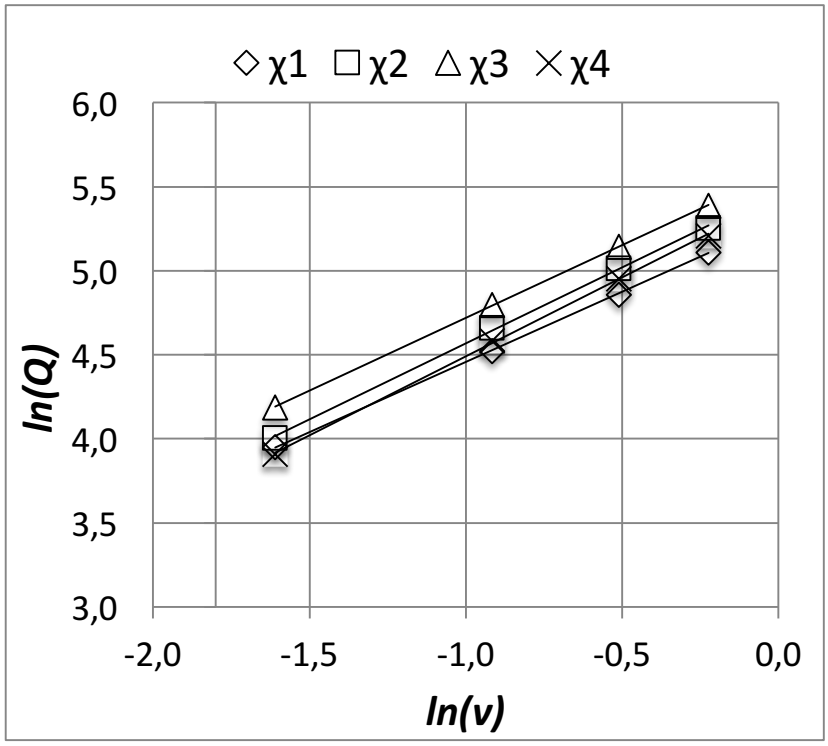

Fig. 47: Logarithmic plot of total heat flux *Q* against the stirrer tip radial velocity *v*.

6.1.7. Local and total heat exchange

In order to evaluate the influence of the stirrer position on the heat exchange characteristics, the heat fluxes at each coil winding was plotted and normalized to the total heat flux. The results are shown in Fig. 48. Especially in the case of the radial pumping impeller, the heat flux distribution along the coil appears flatter and thus more homogeneous, when the stirrer is positioned at the half height of the reactor. This can also be verified by the visualization in Fig. 49. The temperature fields for the central installation height is significantly more homogeneous than in the residual cases. Especially very hot zones can be avoided or reduced this way. When temperature sensitive substances are used in the process, this circumstance deserves special attention.

Observing an industrial process, the described effects of overheating at hotspots can remain hidden, if the temperature sensor is located in a less problematic spot. Although the automated temperature control may be restricted to a certain value, such hotspots would violate the process specification and moreover remain

undetected. The consequences can be side reactions, product damage, material and energy waste, abrasion and device damage.

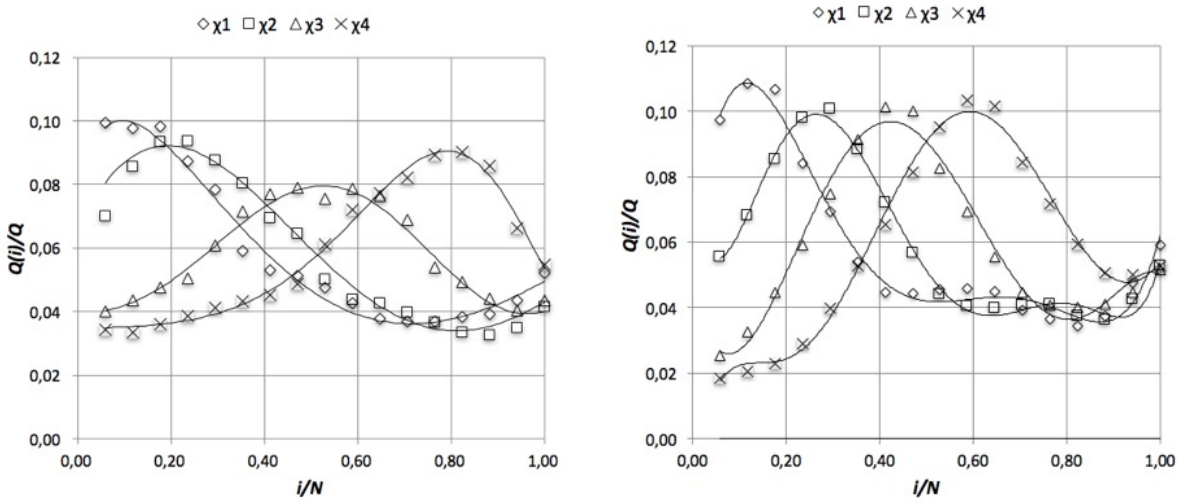

Fig. 48: Normalized local heat flux (for each coil winding *i*) at different bottom clearances. Results obtained from investigations with the 2D-abstraction model. Left: use of generic radial pumping impeller; right: use of generic axial pumping impeller.

Beside the local heat flux distribution considerations, the bottom clearance of the stirrer has an influence in the total heat flux, see Fig. 50. Several observations can be made, here. First of all, the heat fluxes for radial pumping impellers appear to be up to 100 % higher than for axial pumping impellers. This poses a strong argument for radial impellers since the heat flux is decisive for heating time and dimensioning, thus the investment in the heater and the whole process. The of the stirrer position, on the other hand, is less seen in the case of an axial impeller. However, for the radial impeller, the central installation shows the best results, again.

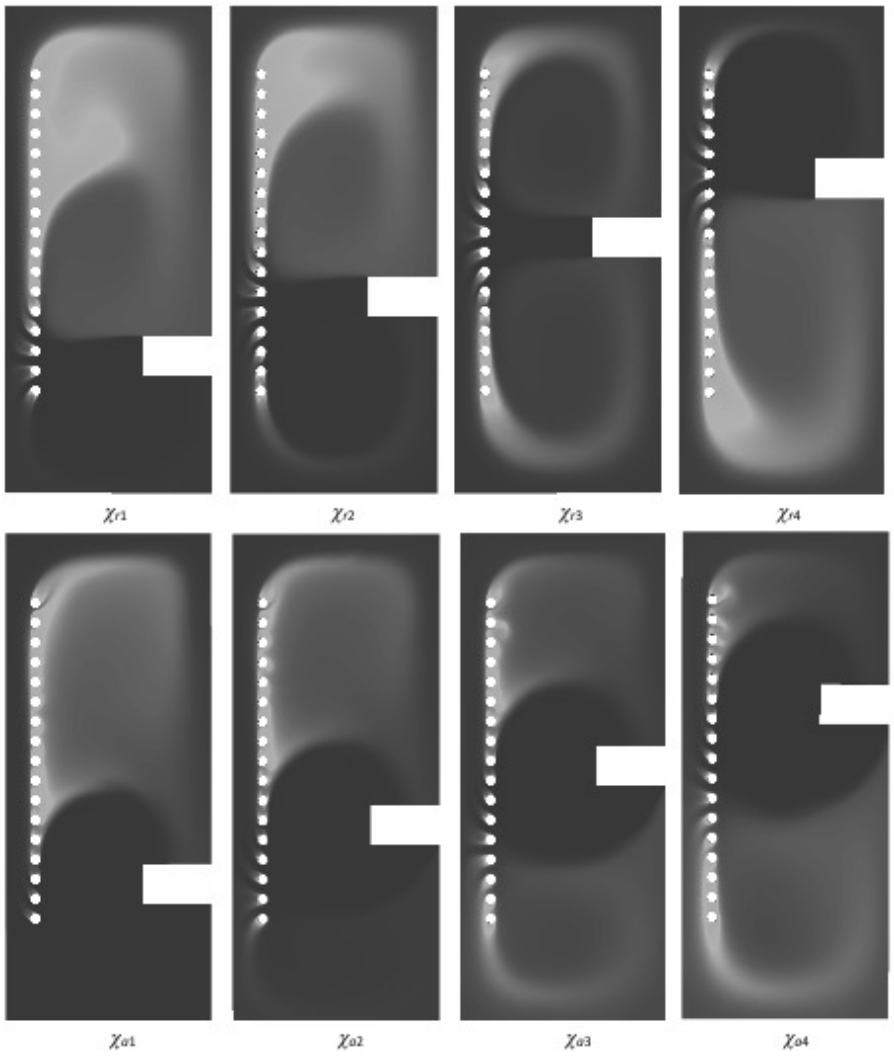

Fig. 49: Temperature fields for different bottom clearances of the stirring unit. Above: use of a generic radial pumping impeller; below: use of a generic axial pumping impeller. Results obtained from the 2D-abstraction model.

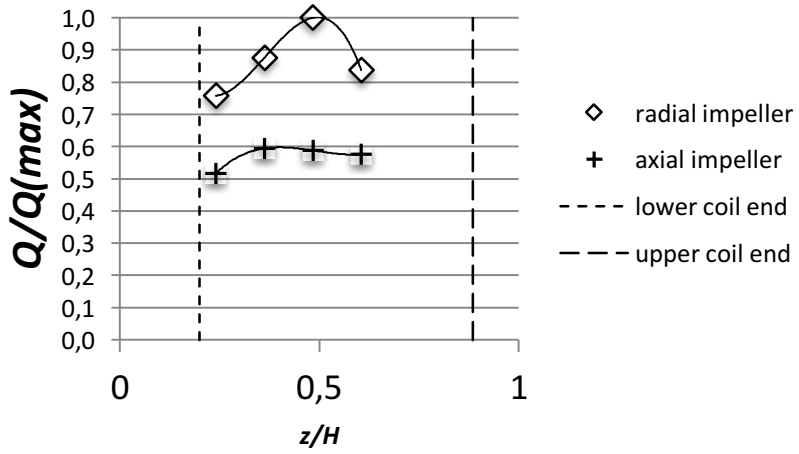

Fig. 50: Total heat fluxes for different bottom clearances of the stirrer. Study performed for radial as well as axial pumping impellers.

6.1.8. Practical conclusions

Originating from the findings of the investigations performed on the basis of this model, some recommendations can be formulated:

- if helical coils are used in the reactor, radial pumping impellers are to be preferred over axial impellers due to up to twice higher total heat flux
- the total heat flux is significantly better for a central installation in the case of a radial impeller
- the bottom clearance also has a strong influence on the local heat flux and thus on the temperature distribution inside the reactor. A central installation shows the least formation of hot zones
- the temperature in the reactor can easily exceed the permitted value and remain undetected due to unequal distribution of temperature (overheated zones) and false spotting or insufficient number of detectors. Huge care has to be taken at this point.

6.2. Development of an iterative algorithm for the optimal heater design

The development of an alternative to the industrially widespread heat exchangers is supposed to consider the known issues and integrate the minimization of negative effects in the development process itself. The principal topology of a helical coil heater is used for the development of a novel heater. As a circle shaped pipe provides a huge exchange area and is constructively simple and very little susceptible for corrosion solution, it is used as a starting point for the development of the heater. From the beginning, it is obvious that the vertical and radial components of the flow are of most interest since they are responsible for the incident flow towards the heater surface and minimize the boundary layer, hence. To convert the pumping energy of the stirrer maximally into radial and vertical flow, it is appropriate to suppress the tangential component by use of baffles. Those can be used as fixation elements for the heater, too. Therefore, a secondary condition at the development of the heater is to take into account the practical and constructive feasibility and possibility for fixation on the girder baffles.

6.2.1. Idea and principle concept of the development

As discussed before, two main aspects are relevant for the local and total heat flux. On the one hand, each internal inside a stirred vessel influences the flow pattern. The coiled structure of a helix, for example, functions like a perforated, cylindrical baffle (not to be confused with the baffles for suppression of the tangential flow component). It guides the main jet streams inside or outside the coil along vertical axis in one or various cellular vortex loops. As a result, the jet streams get passed by the heater without exchanging the heat in the optimal way. This shows the main problem of the second aspect – the local heat transfer limitation. The local heat transfer is a function of several factors, like described in [23]. Although there can be found tabulated values for mean heat transfer coefficients, equation (2.4) shows an incident influence of the thickness of the thermal boundary layer on it. The thickness of the thermal is directly dependent on the laminar boundary layer thickness via the Prandtl number, see also chapter 2.2.3. Obviously, the aim of influencing the flow field is to diminish the laminar boundary layer. A general approach is to rise the turbulence in the process. Actually, from an engineer's point of view, this means an augmentation of the stirring power. This approach is primitive and straightforward; however, it does not solve the issues mentioned before. A more sophisticated way of using the available kinetic energy is sought for. The diminishing of the laminar boundary layer can be achieved by rising the velocity in the vicinity of the wall and by directing the main flow stream from parallel to orthogonal towards the wall. The latter effect is basically achieved by suppression of the tangential flow component with baffles. The augmentation of the velocity is again associated with the augmentation of the stirring power. However, the available kinetic power can be used in a more optimal way by positioning the heat exchange area to certain spots, where the flow stream is maximal. The positioning itself, of course, influences the total flow field. It is therefore not appropriate to follow this concept for the heater as a whole. it is rather obvious to make the development an iterative adjustment, where the flow field gets influenced little by little due to more and more heater coil windings. After the implementation of a further coil winding, of course, the resulting flow pattern can change in a way where the previously positioned coil windings are not spotted optimally anymore. This effect must not be ignored; however, the main changes of the flow pattern occur downstream of a barrier like a new heater coil winding. Hence, the iterative process should start positioning the first winding in the very strong jet

stream of the stirrer and spot further windings always in the downstream area of the already existent heater surface.

6.2.2. Simulation setup for use for the heater design development

In the style of chapter 6.1, a simplified simulation setup is chosen. The method has been improved, however. Again, a single layer mesh was used under the assumption of a negligible influence of the tangential flow component. The difference consists in the shape of the cell layer. In chapter 6.1, a normal pseudo two-dimensional simulation was performed. This leads to a clear deviation from the three-dimensional simulation, since the fluxes are calculated without consideration of the narrowing of the slice towards the center axis. This is accounted for in the improved method. Since the two-dimensional abstraction has to implement a three-dimensional cell layer anyway, this layer is made in a wedge shape. The non-physical approximation is replaced by a verified method, hence. An exemplary check of the results, presented in chapter 6.1 showed little improvement by the corrected method regarding the heat flux. The coil windings had the same radius and the same exchange area, though. This is probably not the case, when the windings can be placed randomly. The spot-dependent coil area of each winding has a crucial influence on the results and is to be considered, hence. The wedge method accounts for it, however.

The biggest part of the work in setting up the simulation is the appropriate generation of the mesh. Basically, there are mostly rectangular edges between the pumping unit, the reactor walls and the surface. A block structured mesh is therefore a good choice. However, the implementation of circular representation of the coil windings impedes strict use of block structured mesh generators. In 6.1, the windings were positioned above each other and therefore could be implemented block wise without distorting the Cartesian structure of the mesh. Considering a free positioning in this study, the block generation will not be possible with manageable effort. The OF in-house mesh generator snappyHexMesh is used for the implementation, hence. The working principle of this generator is to take a block structured mesh (base grid) and modify it in the environment of a defined geometry. This geometry can be represented by a geometry file like “stl” or by generic geometrical structures like cylinder, cone, box, plane, sphere, etc. The application then finds the intersected cells of the base grid by the geometries. Those cells are split and the vertices

relocated towards the geometry surface. The faces of the relevant faces become aligned to the geometry thereby. If points become very close in this procedure, they are melt to avoid too small face areas. Non-hexagonal and distorted cells become very probable at this stage. As the cells are split in this step, the neighboring (not split cells) have to split their adjoining face, too. Without changing the cell shape, they become non-hexagonal, though. As one side of the geometry lays inside the flow domain and the opposite is not relevant, those cells are erased. Before the split and reduced mesh is called “castellated mesh”, because its jagged structure reminds of a castle wall. The subsequent face alignment to the geometry surfaces is called snapping. In an optional third step, it is possible to push away the cells from the geometry surface and insert additional cell layers in the resulting gap. This is done to achieve cells, which are orthogonal to the geometry surface. Especially in the case where diffusion plays a crucial role, the cells orthogonality is very important, because non-orthogonality is the main factor for so-called numerical diffusion – an overestimation of diffusive effects that origins in numerical errors and not in the physical description but is mathematically of the same shape, though [16]. The rest of the mesh becomes squeezed by this procedure and is therefore to be used with care. However, for heat transfer problems, the use of additional cell layers is highly recommended. The splitting step entails the problem, that a one-layer grid obtains several layers at this point, since splitting is always performed in all three Cartesian directions. Although those cells generally do not undermine the simulation, the total cell number is unnecessarily high. A further OF application can be used to face this problem. Via the “extrudeMesh” application, it is possible to take only the front and back side of a mesh (both must have the same number of points and faces and the faces must be topologically equal). The cells between the back and front are erased and one single layer is made by connection of single opposite back and front face couple. It is also possible to adjust the distance between the front and the back and to subdivide the generated cell layer in several layers. The mesh quality then is significantly higher in comparison to the original snappyHexMesh grid. It is further possible to adjust the angle between the front and back patches. This is how wedge mesh generation is performed. By use of subdivision, a strict axisymmetric mesh can be generated this way. Special care has to be taken when a wedge mesh is implemented because one side patch of the geometry becomes squeezed to an edge. The relevant cells are not changed topologically, i.e. the respective faces are not erased, have an area of zero, though. This leads to a computation fatal error,

because face areas are used during the interpolation step in the solution. Division by zero leads to direct abort of the solution. The faces can be erased by additional use of the utility “collapseEdges”. All relevant steps and dictionary files for the generation of the mesh are attached to this work, see 12.1.5.

6.2.3. Development of the algorithm

For an ideally large downstream way towards the vessel wall, it is reasonable to spot the first coil as close as possible to the stirrer. One has to consider the decreasing exchange area, when the winding has a smaller radius. As a good starting point, the first winding is set at half distance from stirrer tip to the wall. A further question is related with the distance between the separate coils. Of course, the distance has to be short for maximal exploitation of available space. On the other hand, too close positioning leads to the effect that a winding lays to close in the slipstream of the upwind winding. This would provoke the opposite effect of the actual development aim. As a general rule, the pipe diameter is used as minimal distance between the windings, as it is also recommended for normal helical coils in [1], [21]. The simulation is first performed according to the setup, but at this stage without coils. This is important for obtaining the position of the maximal flow velocity of the stirrer discharge. The discharge flow will be referred to as jet stream. The spot for the first coil winding is found by plotting the velocity magnitude along a vertical line that goes at the half distance from stirrer tip to the reactor wall. Fig. 51 demonstrates this procedure.

After the positioning of the first coil, the jet stream is expectedly split into two jet streams; hence, two domains of the downstream area can be used for further development of the heater design. Therefore, in the next step, two further coil windings will be placed at once. For the exact positioning of the windings, it is necessary to know the maximal jet stream velocity position at the distance of one pipe diameter. For this purpose, the velocity is plotted at a curved line which maintains the implied distance to the present windings. Practically, circles are drawn around the present coils and the non-intersecting part of it in the downstream area is used as this plotting curve, as demonstrated in Fig. 52.

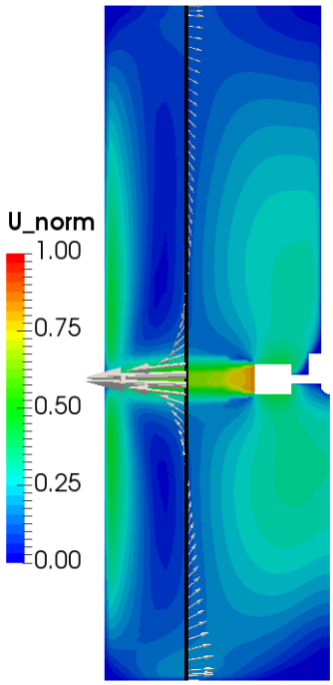

Fig. 51: Determination of the maximal jet stream velocity for positioning the first coil.

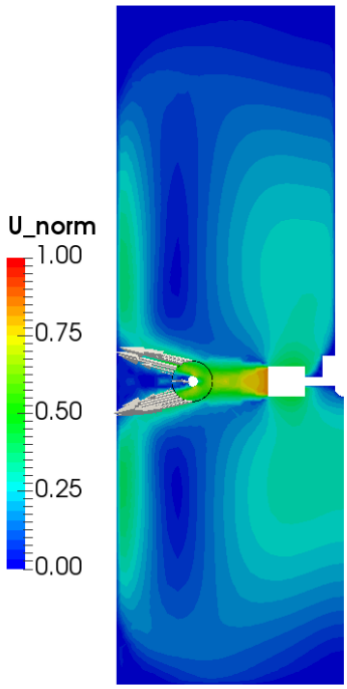

Fig. 52: Determination of the maximal jet stream velocities in the downstream area.

The straightforward assumption is that the previously generated two jet streams will be split into four by the next two coils. However, this effect is levered out by the fact that two of the jet streams units to one, namely those which are between the new two coils. The total number of jet streams is therefore three instead of four, see Fig. 53.

The positions for the next three coil windings is forwardly done like in the step before: a non-intersecting offset of the coils diameter is drawn in the downstream area and the three local maxima determined by plotting the velocity magnitude. However, the strongest of them is the central jet stream. Its thickness and intensity is similar to the jet streams of the previous step. Two further procedures are conceivable. Either – the positioning of three coils, each in the local maximum on the velocity magnitude plot around the three coils or – positioning of the next coil in the strongest jet stream. Latter is being preferred since homogeneous heat transport is desired and the central jet stream can be interpreted as an extension to the previous iteration considering its intensity (shown by comparison of Fig. 53 and Fig. 54). However, Fig. 54 demonstrates the importance of additional consideration of the temperature field beyond only the velocity field. In the downstream area of the first coil, the fluids heat is not yet dissipated and encounters the new coil with augmented temperature.

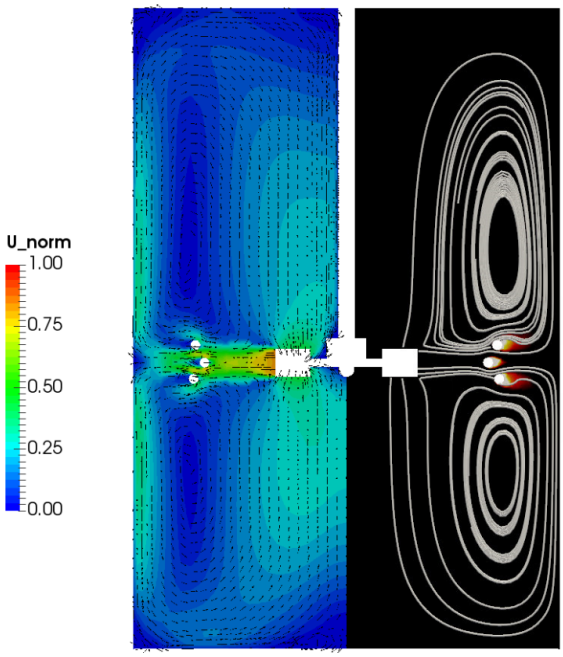

Fig. 53: Unification of close jet streams. The number of jet steams is thus reduced.

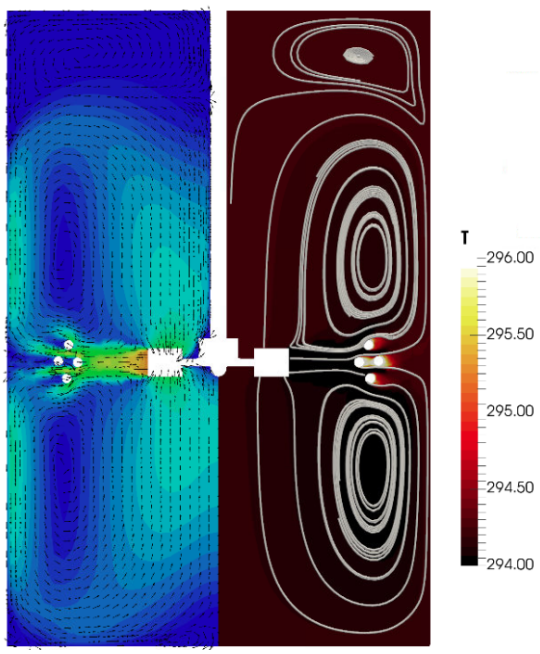

Fig. 54: Fourth coil as an extension of the previous iteration.

As a result, the heat exchange is dimmed according to equation (2.5) because the temperature difference is not maximal. To resolve this issue, the jet stream is permitted a longer trail for heat dissipation, i.e. the new coil is positioned with larger distance in the jet stream maximum (Fig. 55). In this step, the described effects lead to the formation of in total four similar jet streams. Moreover, a dead zone can be identified in the upper region of the reactor. This indicates that the height of the reactor is too large for this type of heat exchanger and stirrer system, i.e. the recirculation takes place in a limited area around the stirrer. In this case, a lower reactor height is recommended or the use of further stirrer-heater stages. First option will be performed in further on in this chapter, the second is applied theoretically to the industrial reactor where the reactor geometry is given anyway. As a final step in the actual development, four further coils are added in the jet streams which resulted from the previous four coils. The result can be seen in Fig. 56. The next coil would have to be positioned in the strongest jet stream in the center. However, the distance to the wall would be too small. Further development is aborted at this point.

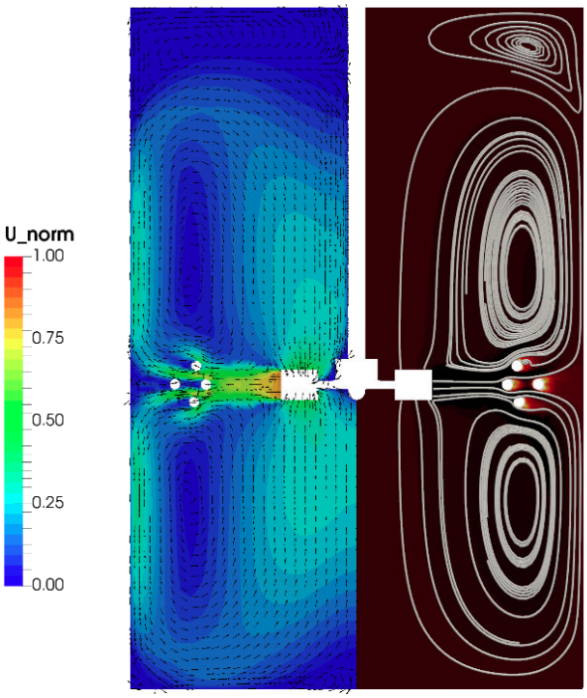

Fig. 55: Displacement of the fourth coil for better heat exchange.

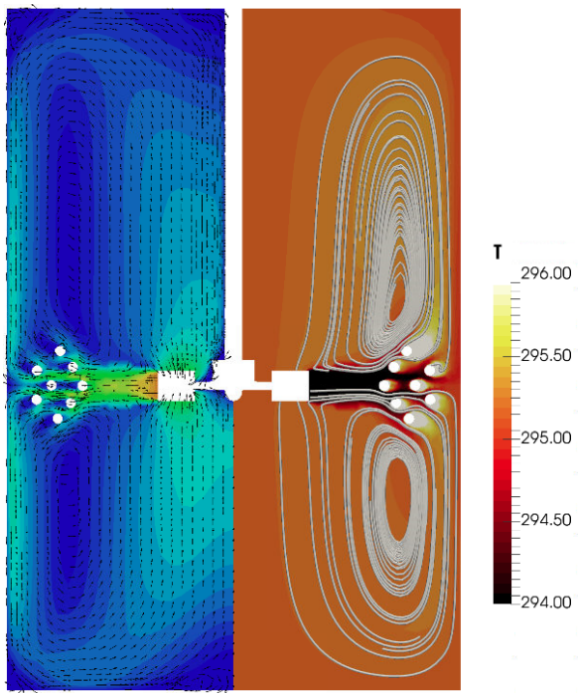

Fig. 56: Addition of further four coils to the total number of eight.

Furthermore, the usage of downstream fluid for heat exchange is not ideal, since it is preheated by the upstream coil windings and diminished in its temperature difference and therefore in its exchange driving force.

The validation of each of those iterations poses an immense expense and undermines the sense and benefits of such an abstraction. Hence, the quality of the results has to be verified by means of numerical aspects. In order to verify the consistency of the results, the results have to be proved on finer meshes, like it is described in chapter 2.6.3. Fig. 57 shows a series of simulations performed for the same case but different mesh finesses. The maximum cell edge length x_{max} was halved four times. It is clearly visible, that the mesh is consistent at a cell length of 1.25 mm. To approach the maximally possible cell length, 1.67 mm is also tested and considered consistent. However, the cell length of 1.25 mm is recommended for further application of the method for secure consistency.

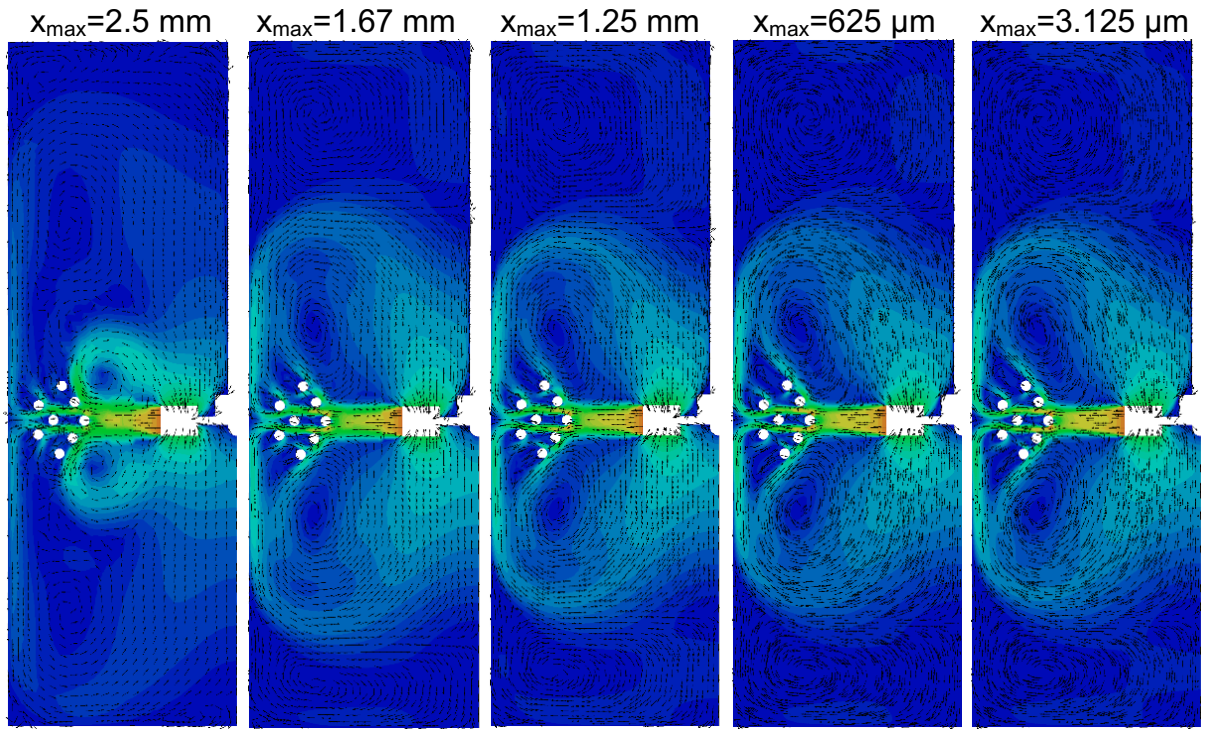

Fig. 57: Mesh consistency study of the novel heater in the 2D-abstraction.

The constructive feasibility is made as final and cogent reason for the termination of the algorithm at this stage. At the actual state, one can imagine the heater as a skewed double helix of fife coil windings at the inner and three at the outer helix. Following the constructive principle of the double helix heater, where the coils are fixed on both sides of the girder baffles, this method can be maintained if modifications on the girders are allowed. Fig. 58 shows a proposed tree-dimensional model of a constructive realization of the novel heater.

The comparison shows that there is a high accordance in the two- and three-dimensional models concerning the flow patterns. The before used boundary definition of the stirrer with inlet and outlet patches is not necessary here because the stirrer rotation is actually performed instead of being replaced by a pumping black box like in the two-dimensional abstraction model. Consequently, the stirrer does not permit a fixed discharge temperature. Thus, the heat transfer principle could not be transferred to the three-dimensional model since the artificial perfect cooling is not possible in this case.

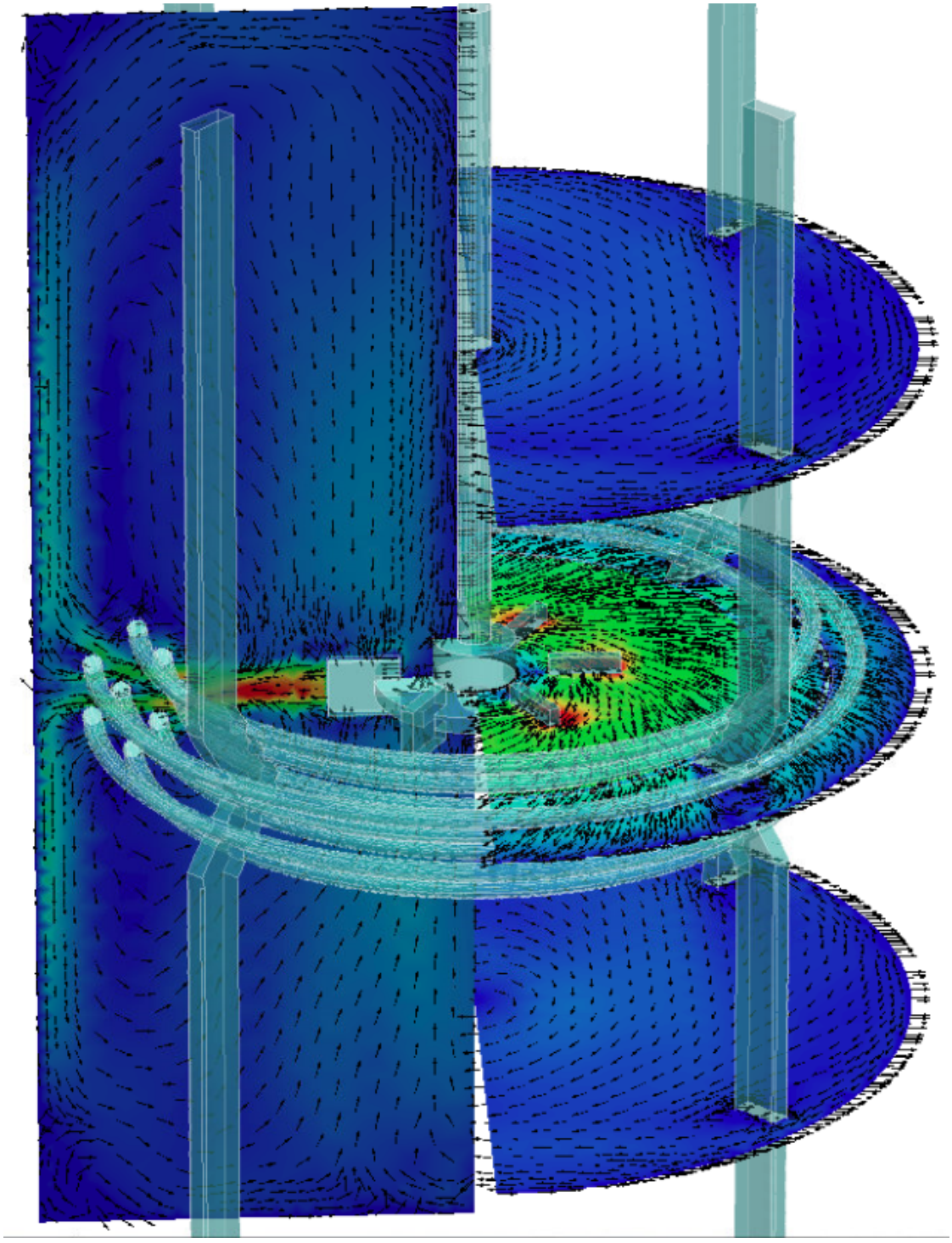

Fig. 58: Three-dimensional model of the developed heater in a reactor vessel.

The development is repeated for a reactor with a diameter to height ratio of one. The development is shown at a glance in Fig. 59. In this new approach, a different strategy has been chosen after the first three coils. Instead of direct inserting the next coil in the strongest jet stream, the previous coils are moved to achieve equal intensities in all three jet streams, see 2nd and 3rd iteration in Fig. 59 (counting mode

described there). This procedure opens the jet streams and redirects the high velocity flow from a tending radial to a more axial type. This is of course desired since the radial way towards the reactor wall is limited whereas the way up and down offer more space for heater development. Now, three coils can be set in the jet streams. For more control, this step is divided into two parts. First, the central coil is set and the remaining two coils in the following step, see iterations 4 and 5. However, an analogous procedure is not reasonable in the next step, since it would push the flow towards the wall. The next two coils are placed into the strongest jet streams, thus. In this step, the number of coils of the previous development is already reached. However, the flow field shows potential for further coils which are set, of course, in the downstream spots of velocity maxima. The development is aborted at this point, because further coils would either violate the constructive feasibility or the distance to the wall.

The designed heater is validated by three-dimensional simulation in the first step. Despite the flow patterns appear slightly different in Fig. 59 and Fig. 60, the velocity field matches very well at a more detailed analysis. The field around the heater shows similar characteristics. The sizes of the cellular vortices appear smaller in the abstracted model which can have multiple reasons, e.g. the rotational component. However, this does not change the characteristics of the flow pattern. The two-dimensional abstraction is considered verified for the development in the scope of CFD, hence. That means, that the mathematical and physical model match for the abstraction and the complex simulation.

In the second step, the consistency of the mesh has to be proofed. In Fig. 57, the consistency for the abstraction could be safely reached for the here used maximal cell size of 1.25 mm. The three-dimensional model is tested on two meshes – with maximal cell lengths of 50 mm and 25 mm, see Fig. 60.

The flow patterns match perfectly for both, the coarse and the fine mesh. The velocity level seems to differ slightly in some areas. However, the differences are small and occur in areas which are not critical for the purpose of the work. Despite the coloring suggests differences between both cases, they are marginal. The color scale at the side confirms it. The use of the coarse mesh does not pose a disadvantage, hence. On the other hand, the meshes differ in the cell numbers immensely. Both, the memory as well as the computation demand rise by times due to the halving of the

cell edge length, see Table 3. The study is performed for the economic steady state case.

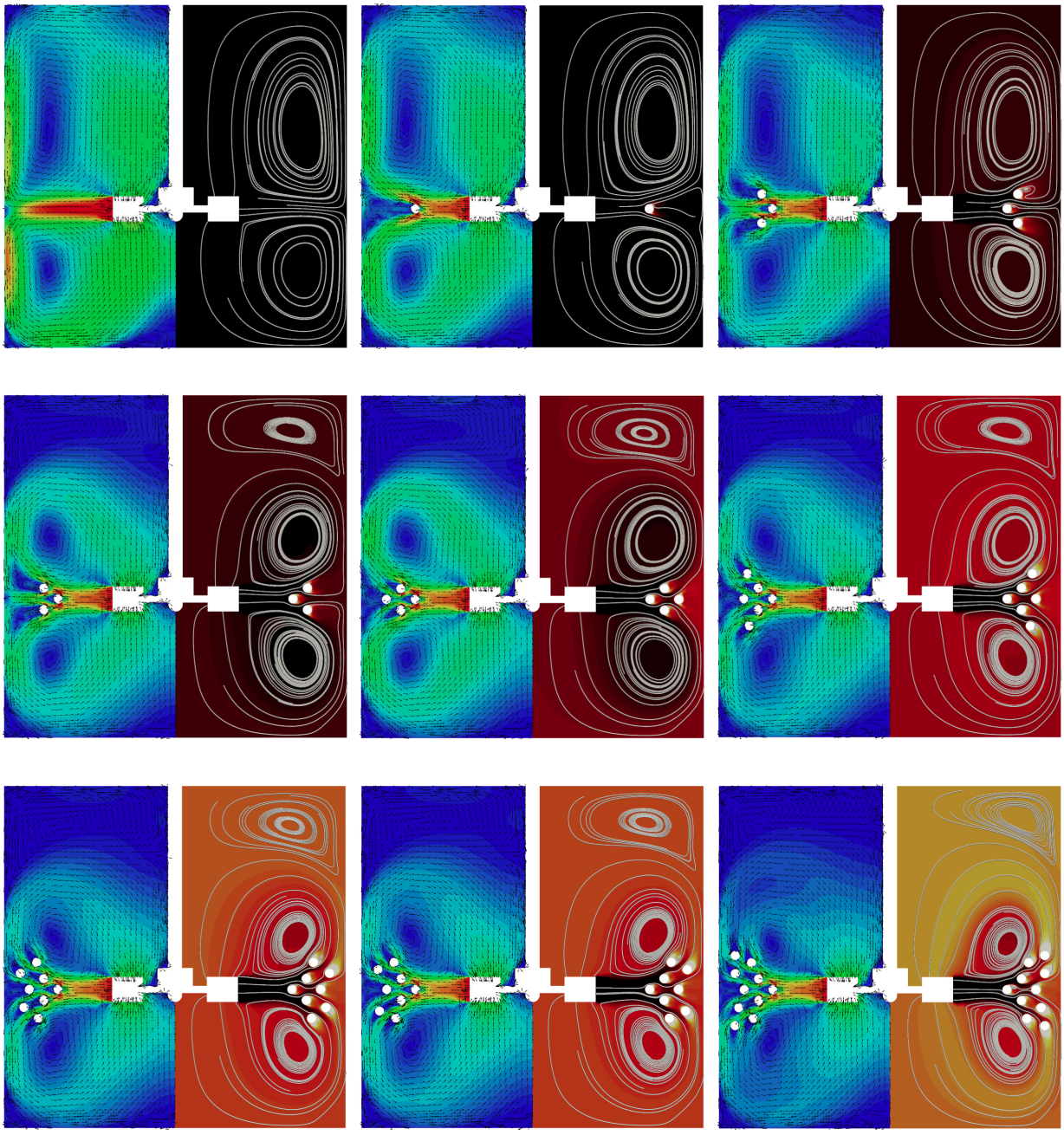

Fig. 59: Overview of the heater development iterations. Iterations are counted beginning with 0 and from left to right, by lines.

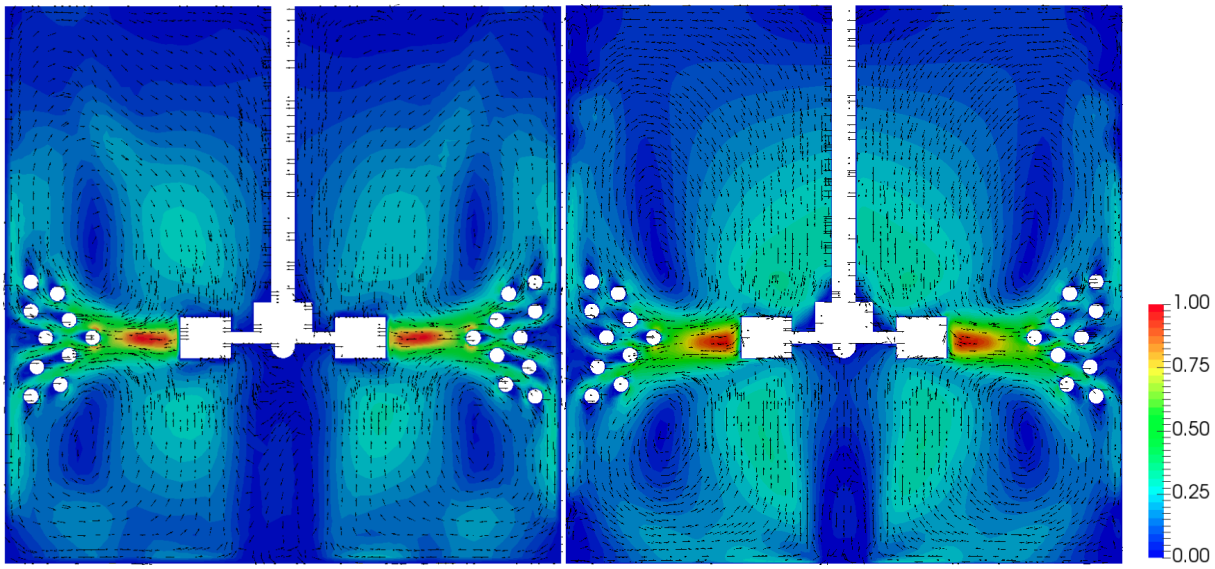

Fig. 60: Mesh consistency study for a three-dimensional simulation of the novel heater design. Maximal cell lengths of 50 mm (left) and 25 mm (right).

The comparison shows high differences in all aspects, the cell numbers, the convergence velocity, the required computation time and the memory amount. Considering the similarity of the results for both cases, the cell edge length of 5 cm is considered acceptable.

Table 3: Comparison of different mesh fineness concerning computational and memory demand.

Cell length *mm*	Cell number -	Iterations -	Time used *s*	Memory dem. *MB*
25	1,431,902	2000	1500	400
50	3,145,242	3000	5000	940

In the third step of validation, the results of the three-dimensional simulation are compared to those of the measurement. Like in chapter 5.4, the horizontal flow cannot be measured perfectly in the center. The symmetry seen in Fig. 60 cannot be observed in Fig. 61 where measurement and simulation results for the novel heater design are juxta positioned. Some differences are seen close to the stirrer shaft. Despite the simulation has an implementation for its rotation, the shaft has lower influence on the velocity field than in the measurements. One reason for it might be the shaking of the stirrer shaft during the measurement which is not covered by the simulation. In the lower part of the reactor, the whirl can be observed in both, in the simulation as well as in the measurement. Further regions are as well predicted with

high precision. Especially the area around the heater matches very well and strengthens the conclusions of the work as well as its confidence level.

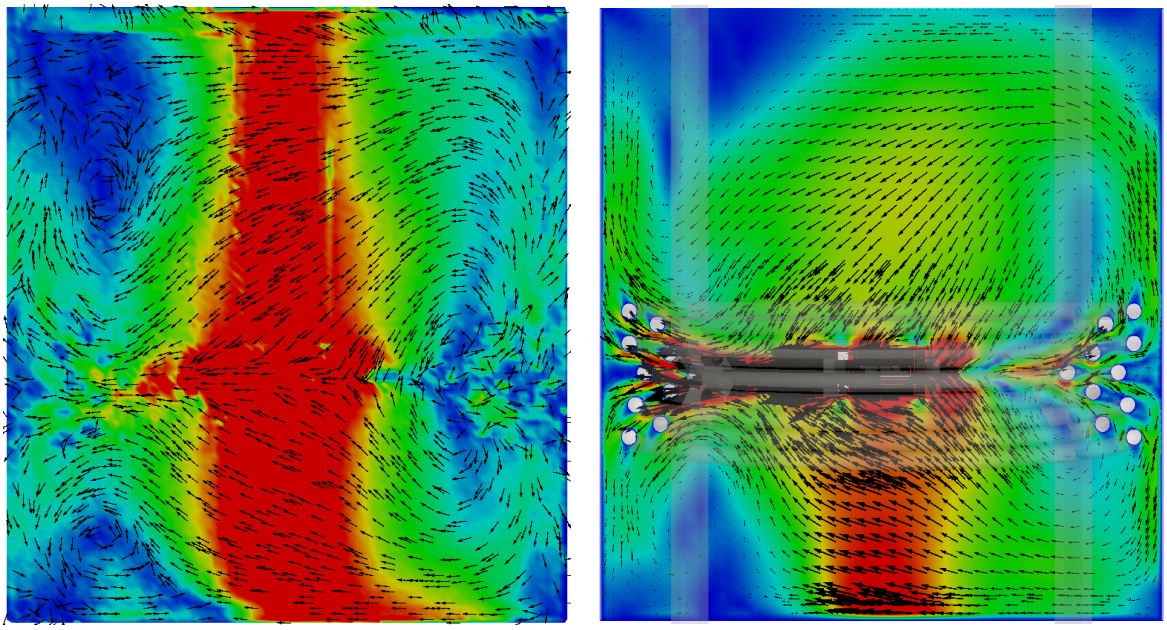

Fig. 61: Comparison of measured (left) and simulated (right) flow fields for the novel heater.

6.2.4. Comparison of the novel heater to conventional helical coil heaters

In order to evaluate the improvement of the novel heater against the classical construction design, comparative studies have been made. In this manner, as well the total heat exchange as the homogeneity of the temperature field are determined for both cases. In the case of the convenient design, different numbers and configurations of coil windings were used. This enables to estimate a coil length equivalent for the novel design concerning the total heat exchange. The temperature homogeneity of the convenient design is not competitive, since it was determined as one of the main issues in the first place and is used for optimization in the novel heater design. A selection of performed simulations can be found in Fig. 62.

In this context, it is essential to evaluate both variants by measurable values. The first and obvious approach is to compare the total heat exchange numbers for all simulated cases. Fig. 63 shows clearly that there is a linear increase of the heat exchange in the case of the novel heater design with increasing exchange area, i.e with increasing coil windings or iterations, respectively. Up to a certain number of windings in a classical double helix, this trend equals – which is reasonable since the

structure of the coils is quite similar to that of the novel heater in the early development stage, see Fig. 62. However, the increase flattens rapidly. To achieve the same heat flux as the developed heater, almost twice of the exchange area is needed when using a conventional double heating.

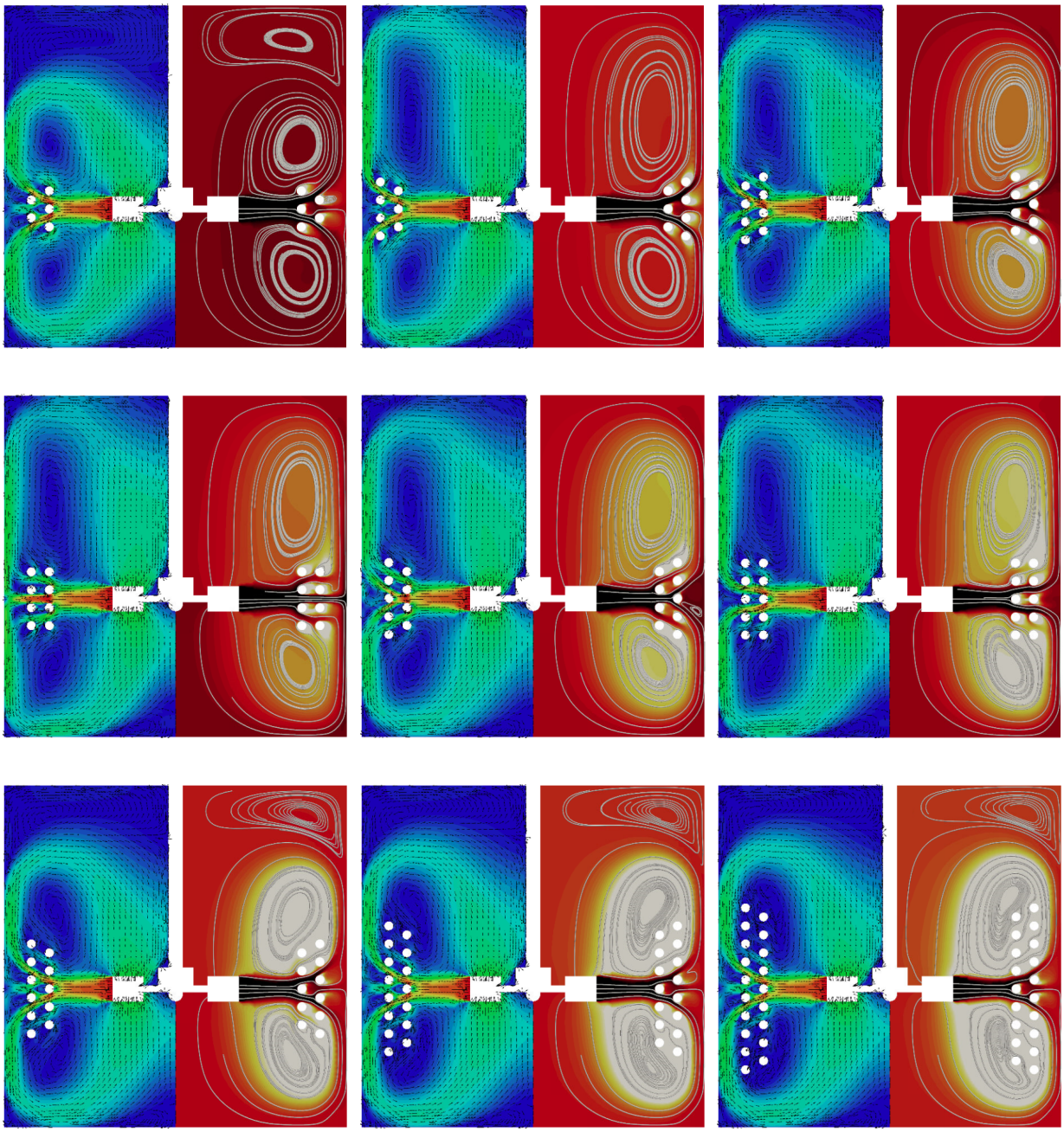

Fig. 62: Different configurations and numbers of coil windings in a convenient double helix heater.

Besides, the improvement of the total heat exchange, the homogeneity was posed as a main factor in the development of a novel heater. In chapter 6.1.5, a certain temperature box was presented, which expresses the temperature range in 90 % of

the observed volume. The cut-off is necessary due to the cold discharge stream and the very close areas around the heat exchanger. Otherwise, every simulation would give the same temperature range due to the model implementation. Fig. 64 demonstrates the procedure of finding the box. Vertical dotted and dashed lines demark the temperatures of the 5 % and the 95 % quantile, respectively. The distance between those marks is the temperature box. Obviously, the temperature box $\Delta_{90}T$ cannot be a measure itself, since it rises with augmenting number of coil windings and therefore with augmenting total heat exchange $\dot{Q}$. Therefore, the relative inhomogeneity I_{rel} is implemented:

$$I_{rel} = \frac{\Delta_{90}T}{\dot{Q}} \tag{2.28}$$

Fig. 65 plots the relative inhomogeneities for all observed cases. The inhomogeneities of the conventional heater coil produce partially very high temperature inhomogeneities whereas those of the developed novel heater never exceed a maximum which is half of the average I_{rel} of the observed conventional cases.

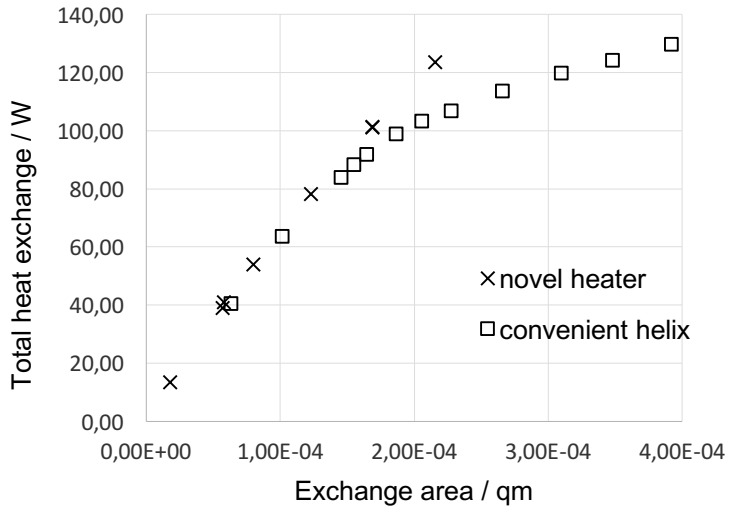

Fig. 63: Comparison of the total heat flux for classical and novel heater coil design.

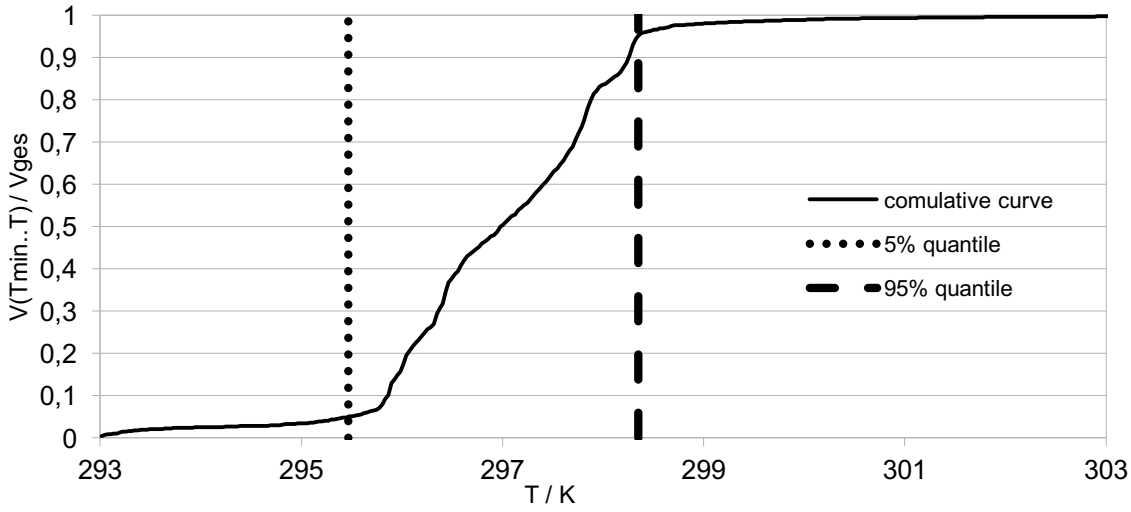

Fig. 64: Typical cumulative plot of the temperature distribution in the observed volume

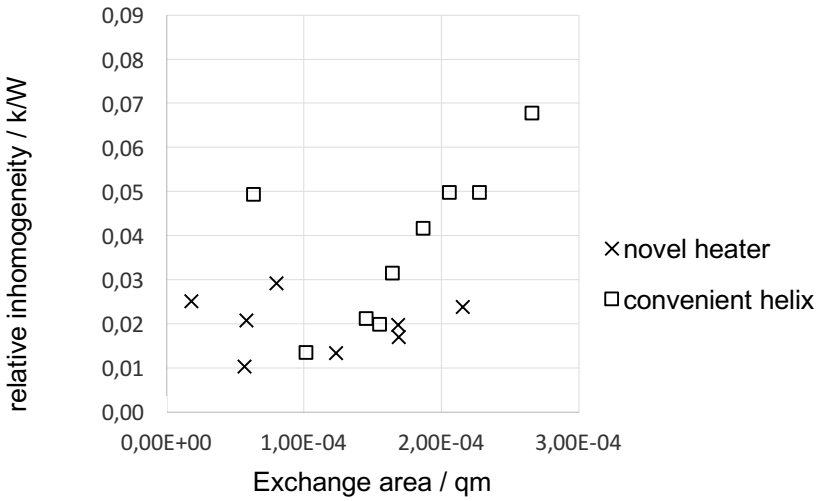

Fig. 65: Relative inhomogeneities for the novel and the conventional heater coil

6.3. Application to the industrial process

The industrial side of stirring technology often implies issues that are not present in the laboratory scale of investigations. Especially, when simplifications or changes in the operating modus are made, unexpected and unforeseen side effects can occur. Therefore, it is very important to perform simulation investigations not only in the laboratory where the results can be verified to a certain stage, but also in the industrial scale, although the simulation results remain without direct measurement

verification. Engineers usually have to rely on principal findings in the laboratory. However, if the lab scale investigations show a good agreement in simulations and measurements, the confidence in the simulation results of industrial scale is significantly higher.

6.3.1. Acceptable simplifications for the simulation of the industrial process

The industrial process is investigated without the possibility of validation by means of measurement technique. Hence, it is highly important to take into account as many geometrical and physical details as possible. However, the computational capacity has to be considered, too.

From the physical point of view, the process is heated and mixed, a charcoal suspension is integrated and there is a liquid gas interphase. Moreover, a reaction takes place which can lead to a shift as well in the transport properties (viscosity and density), as in the heat development.

From the geometrical point of view, there are additional internal features, compared to the laboratory model. Of course, the fixation clamps are to be neglected due to their small size. However, the stirrer shaft guidance has a significant influence on the axial vortex on the bottom of the vessel. The geometry of the guidance has the shape of little baffles and is capable of producing small dead zones which have an influence on mixing time and homogeneity. These effects must not be neglected, hence. Moreover, a gassing ring is implemented which lays in the jet stream area of the lower stirrer stages and expectedly leads to a remarkable influence on the energy dissipation in this area. This can diminish the heat transfer in the downstream area and is considered in the mesh generation, though.

Physical and thermal simplifications have to be discussed in detail and require additional detail investigation. Of course, it is highly challenging to reconcile the complex and partially unstructured mesh with transient solution, heat transfer, particle tracing, multiphase fluids and chemical reaction. Since the chemical reaction is slow and thermally neutral in this case (esterification reaction), it is not observed and not taken into account in the scope of this work. Laboratory experiments [70] showed, that the used charcoal amounts do not influence the rheological properties of the used chemicals and the suspension can be simplified by normal single-phase

fluid, hence. The implementation of particles is therefore unnecessary. All of the used educts and products are mixable and can pose a single liquid phase. This has an interphase with the overlaying gas phase. If a vortex is formed at this surface, further investigations have to be performed in the mode of two-phase simulations. However, if there cannot be observed a remarkable vortex formation, a simple implementation of a planar surface with slip conditions will be adequate. For each operating mode (namely stirrer configuration and rotation frequency), this has to be checked. This simplification has therefore to be reviewed at the actual state and at further improved states. A critical point is the buoyancy effect at the double helix coil heater. To estimate the amount of this effect, a simulation is performed with a switched off stirrer. A temperature difference of 100 K is implemented in the start conditions between the fluid and the heater. A chimney effect is expected between the coil helixes and a drop off in the central part of the reactor and possibly in the annular gap between the heater and the reactor wall. Fig. 66 shows the temporal progress of the fluid movement after heating start in a resting state. The chimney effect is clearly visible and appears as expected between the coils. The drop off takes place in the annular gap and the central part of the reactor. However, the effect grinds to a halt after a comparably short period of time. At this point, the average temperature is far from the desired level. For reasons of general comparability, the velocity is normalized to the freefall velocity at the middle of the reactor (1/2*H*) which a mass element reaches when it is dropped from the surface. This normalization is justified by the fact that buoyancy is induced by gravity *g*:

$$U_{norm} = \frac{U}{\sqrt{gH}} \tag{2.29}$$

A stirred process is always normalized to the velocity at the tip of the stirrer which is generally supposed to be the maximal velocity in the reactor. According to the velocity fields shown in the next chapters, the buoyancy effect is expected to have a very small part in the total velocity profile. Moreover, the chimney effect is further diminished by the stirring, since the necessary density gradient is disturbed by the mixing effect of the stirrer. The simplification, where buoyancy is neglected is justified, hence. Taking all these simplifications into account, the flow field investigation can be performed by a dynamic solver for turbulent single-phase cases without heat transfer. This makes this investigation feasible by means of standard OF-tools without manipulation in the source code.

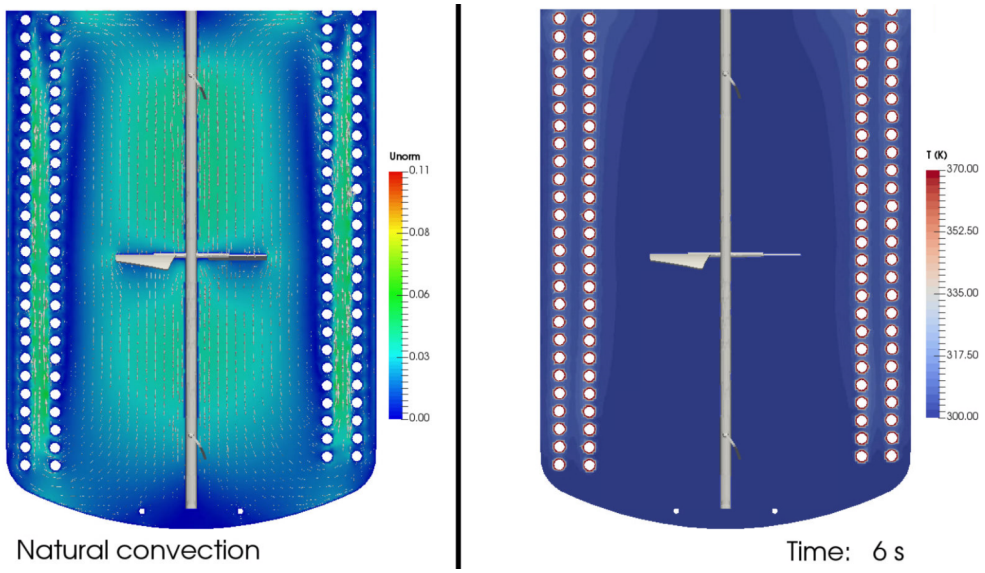

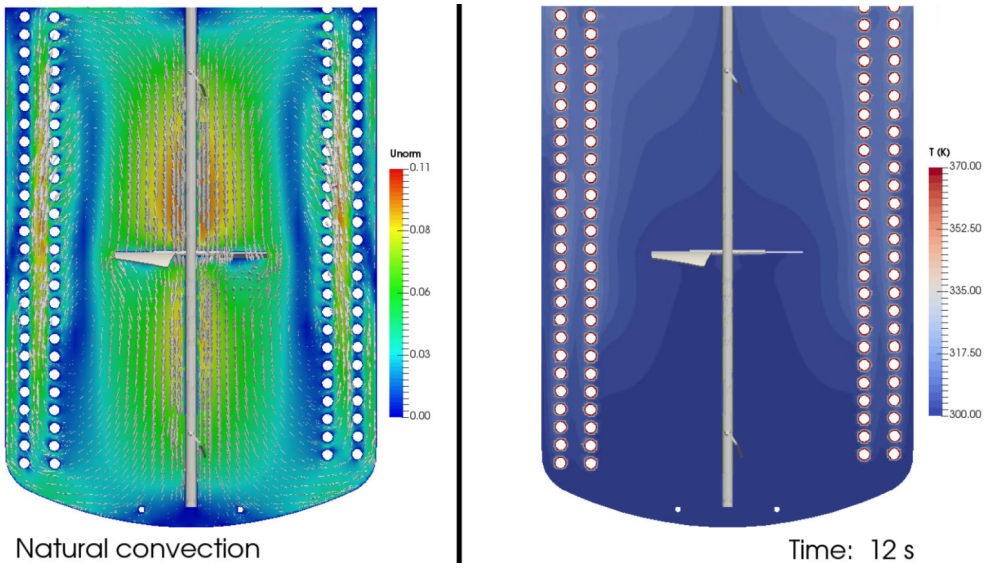

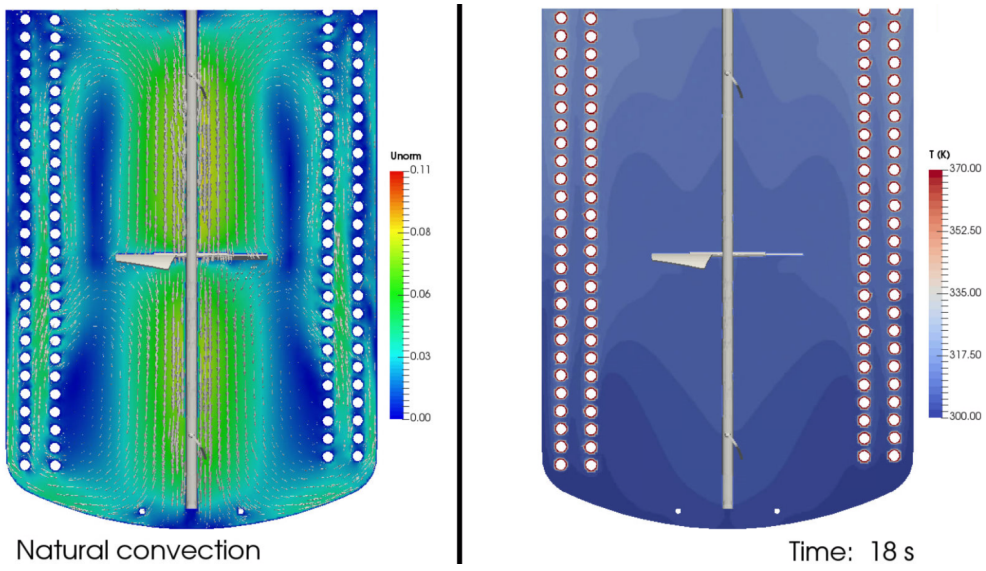

Fig. 66: Buoyancy effect of the heated reactor without stirring.

6.3.2. Application of the novel heater design to the industrial reactor

The before treated modification of the reactor facilitates a good improvement concerning heat transfer and mixing time. The three stages of the stirrer are a good starting point for an appropriate mixing and fast and effective heat transfer. However, further improvement can be achieved if a constructive modification at the heater element is allowed. The application of the novel developed heater in three stages is a straightforward principle of optimizing the industrial reactor to the maximum.

However, the investigation model by means of the vertical slice abstraction was used in a setup of very low complexity, so far. In the industrial reactor, multiple aspects have to be considered:

- The stirrer is neither strictly radial nor axial. The direction of the discharge stream has to be adopted, hence.
- The discharge is not at the very stirrer tip but along the whole stirrer blades. Linear increasing discharge velocity has to be implemented as boundary condition.
- Multiple stirrer stages are present. Each has to be treated individually.

In order to apply the abstraction model to the industrial case, it is necessary to validate it with the velocity fields of normal three-dimensional simulations. The results are shown in Fig. 67 and Fig. 68. In order to achieve the correct discharge of the pumping black box, previously performed three-dimensional simulations are looked up, see chapter 5.2. Special care had to be taken at implementing the boundary conditions since it is varying over the length of the stirrer blade. In this examination, the total heat flux could be improved by over 40 % in this model but has to be taken with care since the abstraction model does not allow direct conclusion to the reality. Neither does it allow statements about the effective heating time since it is designed for steady state simulations. However, an improvement is clearly visible also in the homogeneity of the temperature field. The relative inhomogeneity differs by the factor of two. As it can be seen in Fig. 67 and Fig. 68, the model describes the velocity fields appropriately, although there can be recognized some deviations. Considering the strong simplifications in the model and the complexity of its archetype, the results are satisfying enough to examine it for the development of the novel heater with multiple stirrer stages.

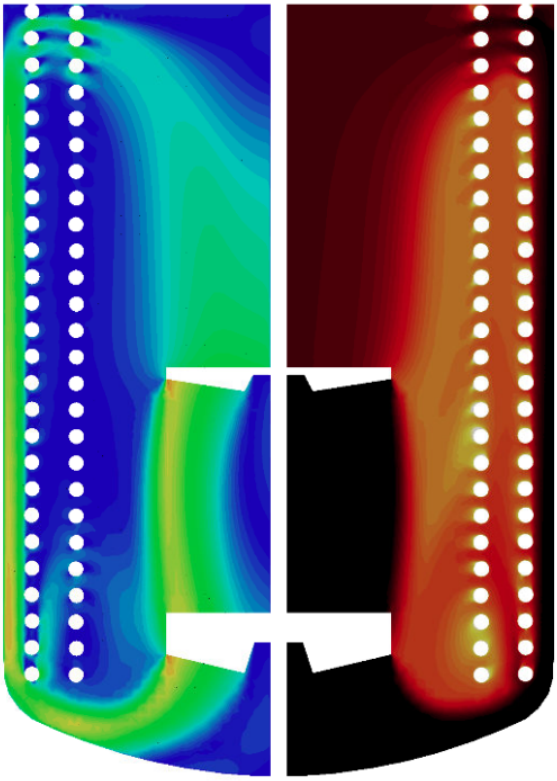

Fig. 67: Pseudo 2D abstraction of the industrial process in the principal state

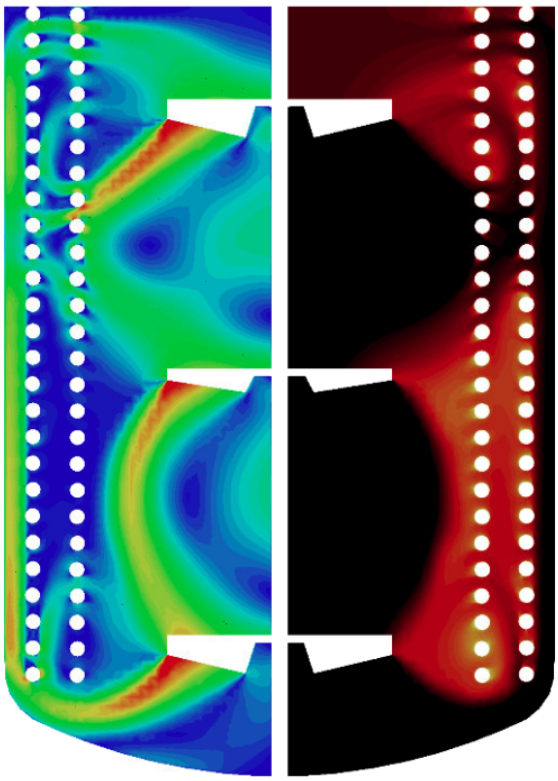

Fig. 68: Pseudo 2D abstraction of the industrial process in the optimized state

In the next step, the aim is to apply the novel heater development principle to the industrial reactor. This work is completely theoretical, since there is no way to evaluate the process in the reality in contrast to the stirrer position work, because latter can be evaluated in the industry after the changes. The construction and implementation of the novel heater is not feasible due to logistical and financial issues, however. Fig. 69 shows the development for three stages of a radial stirrer. In opposite to the previous state, radial pumping impellers are chosen here for variate reasons. First, former investigations have shown that radial stirrers have a principally better influence on the heat exchange when coils are used as heaters. Second, the definition of boundary conditions is easier or even possible when radial pumping impellers are used. Axial pumping impellers, despite to their name, never have a strictly axial profile as can be seen on the example of the EKATO Viscoprop. Therefore, it is hard to predict the discharge direction of such stirrers, especially when multiple stages are used. The interaction with other internals like baffles and heaters impedes a reliable prediction even more. The stirrer stages are positioned equidistantly along the stirrer shaft. In Fig. 69, only six from almost thirty selected

iteration steps of the development are shown. Due to the system of three stirrer stages, the interaction and cross influence between the individual jet streams is strong and to be handled with huge care. It is also obvious that the upper and lower cellular vortices are declined as if they are pushed away by the central one. In the last iteration, the heater pack appears to be asymmetric, which comes unexpected. However, this is the result of the described development method and violates the aimed requirements concerning homogeneity if there is added a further coil for symmetry.

The coil winding positioning has to adopt to this circumstances, hence. The development is aborted after each stage has seven coil windings. By addition of each coil, the system becomes even more unstable and the interactions are hard to handle. An intuitive displacing of the winding is necessary and does not yet allow a formalized description of the algorithm. However, at this point of development, total heat exchange is 18 % higher (compared to the simulation in Fig. 67) and the heater surface is only 35 % of the original case, pursuant to the abstraction model which has no claim of validity.

The validation of the abstraction model fails at the transformation of it to the three-dimensional model, like it is demonstrated in Fig. 70. Manifold reasons might be responsible for it. First of all, the before validated lab-scale model had only one stage and no influence of the pattern above and underneath of itself. Second, the flow field undermines the tangential component which can have big influence at the use of radial impellers and when the reactor equipment does not suppress it in an adequate amount. Furthermore, multiple sections of different tangential velocity levels can have additional influence, like discussed in chapter 5.4. Further work and investigation has to be invested for a valid model and a working development principle, when multiple stages of radial impellers are used.

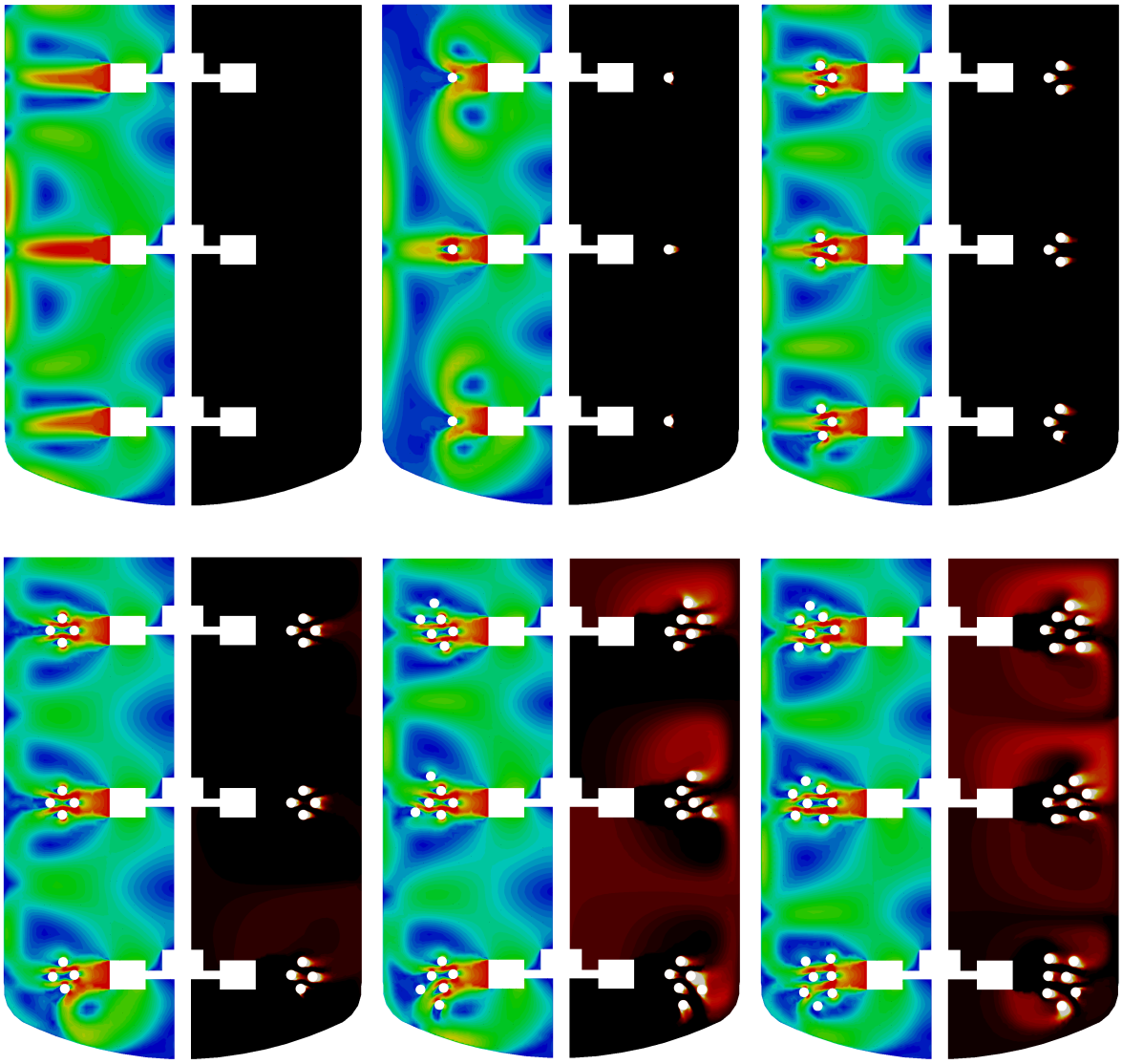

Fig. 69: Development of the novel heater for multiple stirrer stages. Re~2.5 Mio; three equidistantly distributed Rushton turbines in an industrial reactor with a dished bottom. Results obtained from a 2D-abstraction model – preliminary study.

This investigation is just a first approach to a topic that is almost entirely passed over by literature. Descriptions of multiple stages are rare in literature and call for further effort. Authors like [69] touch this subject incidentally. Multiple stirrer stage systems still lack for satisfactory models and descriptions.

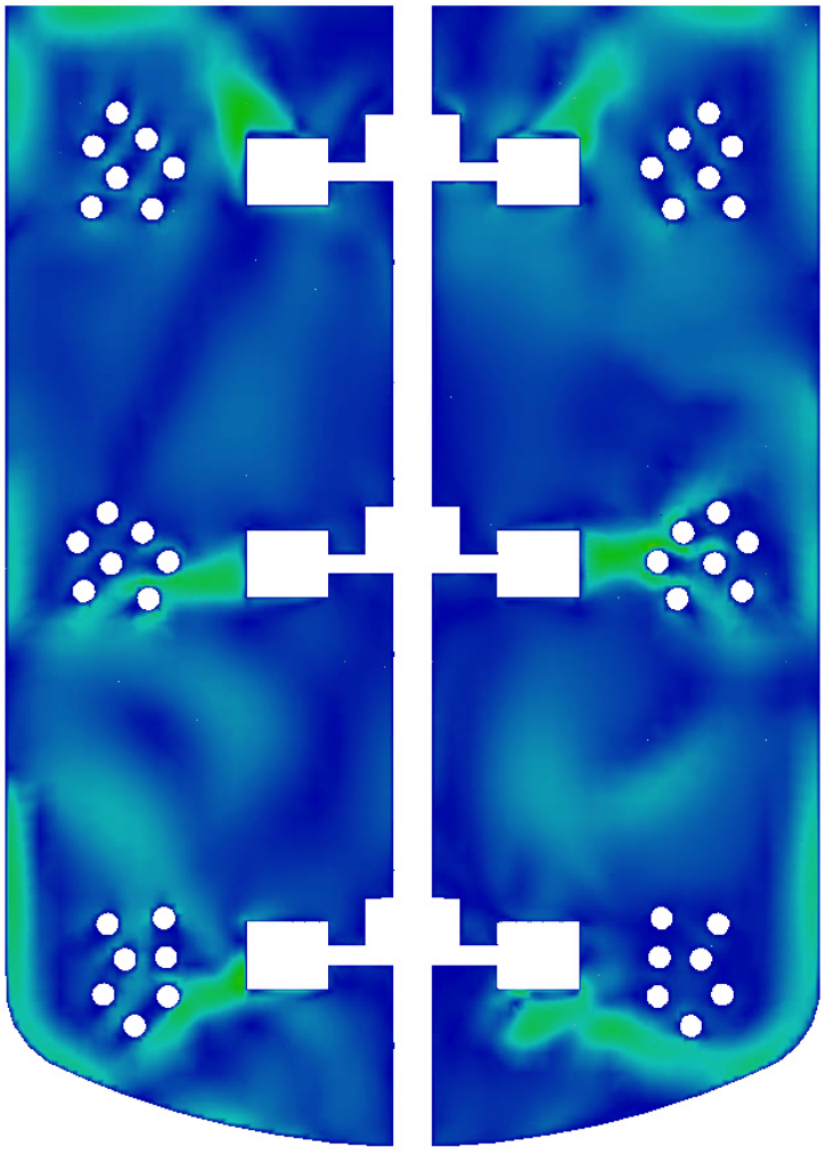

Fig. 70: Failed transformation of the design developed in the abstraction model to a three-dimensional simulation.

7. Energy consumption

The consumption of electric power in a stirred process is characterized by the *Ne* number, like it is described in chapter 2.1.4. In practice, the power consumption is measured by the torque that the stirrer has in the process. Of course, this can be also implemented equally in CFD analysis. However, pressure would have to be extrapolated to the surfaces of the stirrer and then integrated over the whole surface of the stirrer where the extrapolation step implies interpolation errors.

7.1. Simulative approach to power consumption

An alternative method is possible in CFD analysis. Since the energy dissipation ϵ is solved for in the scope of turbulence modelling, this can be used for the calculation of the power inserted into the fluid in the reactor. A dimension analysis shows, that the volume integral of energy dissipation is the power, divided by density. Equation (2.2) then reads:

$$Ne = \frac{\int \epsilon \, \mathrm{d}V}{n^3 d^5} \tag{2.30}$$

The integrated energy dissipation can be calculated in the postprocessing via the filter “integrate variables”. Table 4 lists the simulated cases and the corresponding Reynolds and Newton numbers.

Table 4: Listing of simulated cases including the Newton and Reynolds numbers

Stirrer	**Heater**	**rpm**	**P**	**d**	**n**	**Re**	**Ne**
-	-	*1/min*	*W*	*m*	*1/s*	*1E04*	-
Rushton turb.	single helix	200	7,4E-02	0,070	3,33	1,63	1,18
Rushton turb.	novel heater	400	1,2E+00	0,070	6,67	3,27	2,47
Rushton turb.	tube baffles	200	9,0E-02	0,070	3,33	1,63	1,45
Curved imp.	single helix	100	6,5E-02	0,095	1,67	1,50	1,82
Pitched imp.	single helix	200	3,2E-02	0,095	3,33	3,01	0,11
Paddle	single helix	200	1,2E-01	0,070	3,33	1,63	1,95
ViscoProp	double helix	52	1,9E+03	1,700	0,87	250,00	0,21
ViscoProp	double helix	52	3,0E+03	1,700	0,87	250,00	0,32

The results for the simulations of the lab-scale cases give Newton numbers that are slightly but not by magnitudes lower than expected (e.g. compared to Fig. 3).

However, the Newton number for the pitched blade axial pumping impeller is clearly lower than for other stirrers.

In the industrial reactor, the energy consumption rises by about 50 % as a consequence of stirrer configuration modification. This seems like the opposite result of the desired aim. On the other hand, the modification lead to a significant improvement of the whole batch process. Heating and cooling can be performed in shorter time periods. The consumption of heating utility (60 bar steam) is significantly lower, since overheating is prevented. The improved heat exchange allows dosing of additional cold substance during the process without a drop-off of the temperature which makes the process more flexible and allows 12 % larger batches and 6.5 % shorter batch times. Furthermore, the product quality could be improved due to less hot spot formation [71], [72]. The improvements lead to higher space time yield which entails lower energy consumption in the first place. The aim of efficiency enhancement is hereby successfully reached.

8. Mixing time investigations

One of the main aims in stirring technology is the fast mixing of substances and thermodynamic states. A qualification value for the effectiveness of mixing is the mixing time, as mentioned in the theoretical part. This chapter deals with the measurement determination of mixing time and the development and application of a method to determine the mixing time by use of CFD.

8.1. Measurement approach

Like described in chapter 4.2, the mixing time is determined by means of the so-called mixing quality. This is a measure that decreases with the progress of the mixing process. A more intuitive measure is the degree of mixture. In [2], Kraume defines it as the difference of concentration deviations and the end concentration, normalized by the end concentration. This leads to a straightforward principle of determination of the mixing time. The usage of LIF technology allows a noninvasive determination of concentration values over a wide space in the observed object. Assuming the fact that the tracer will be homogeneously mixed after a long time period, the concentration will have reached its end status at each point of the reactor. This concentration can be evaluated by the start concentration, diluted to the reactor volume. In the case that the local actual exact concentration is of importance, the measurements have to be calibrated by a dilution series. Since the signal intensity obeys the Lambert-Beer law in a certain concentration range, it can be correlated linearly to the concentration in those limits. For the mixing time investigations, the exact local concentration is tracked over time and converges to the end concentration which is known by the injection dose, see Fig. 71. This way, the costly calibration work can be skipped and the whole concentration curve normalized to the end intensity, since it is proportional to the end concentration. As Fig. 71 shows, even in a single measurement, the end concentrations differ when comparing different probe locations. Either one has to suppose permanent dead zones or to accept that the signal strength can vary despite accurate calibrations. First option is not valid however, since a full blending is observed in praxis. Skipping the concentration calculation and normalizing the curves to the end signal strength leads to the same results without the need of expensive calibrations.

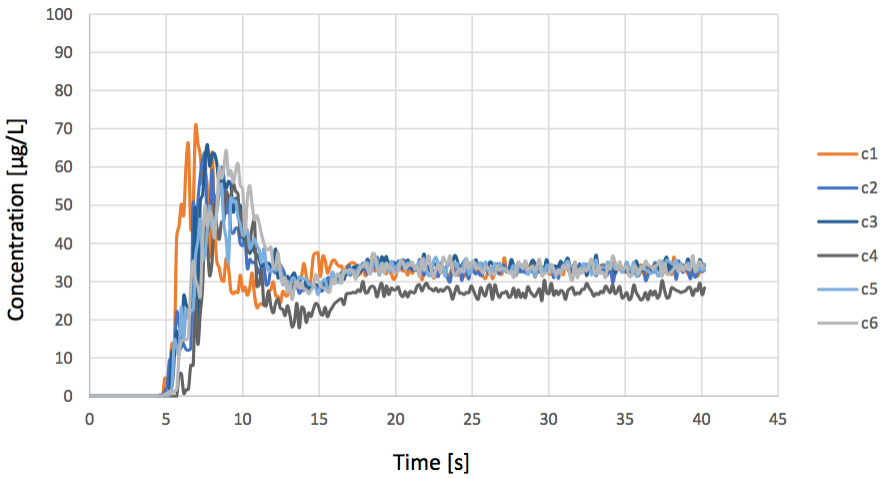

Fig. 71: Typical concentration deviations at variable measurement spots [73].

8.2. Development of a method for simulation of mixing times

In the simulative approach, variate methods are conceivable. Among others, the OF-solver “twoLiquidMixingFoam” gives a promising base for developing a method on its code. In stirring processes, the dynamic mesh library has to be added to it, though. J. Vollmer covered this approach in his work [74]. However, different difficulties were faced in his work. Among others, the complexity of the solver leads to unsatisfying mesh convergence order of 1.3, see Fig. 72. With huge computational effort, some valid simulations could be performed, but with strong instabilities, however.

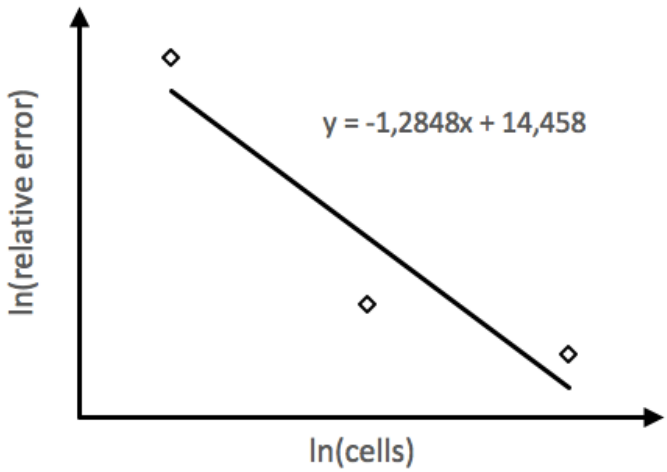

Fig. 72: Mesh convergence order of the method used by Volkmer [74].

In this work, another simulative approach was chosen for the determination of mixing times. Since the trace substance was solved in the same substance like the surrounding fluid, no real mixing of two phases was present. Rather, a classical mass transport is observed in the reactor domain. The straightforward solution is the use of

an existing and stable solver and modification of it by a transport equation. Obviously, the tracer does not influence other fields like velocity or pressure which are solved by the solver. Thus, no coupling is needed in the solution algorithm and the solved velocity fields can be used for the computation of the concentration field as just an additional step in the time step loop. The pressure-velocity coupling algorithm remains untouched by this procedure. The scalar transport of the transformed concentration ψ can be described by the Reynolds theorem, like everything else in the NSE system, see chapter 2.3. This method is called passive (no coupling) scalar transport and reads:

$$\frac{\partial}{\partial t}\psi = \nabla \cdot (\Gamma \nabla \psi) - \nabla \cdot (\boldsymbol{u}\psi) \tag{2.31}$$

where Γ is the diffusion coefficient. The implementation of the passive scalar transport in a standard OF solver code is well described in many online tutorials and relevant OF literature like [54].

Like in the practical investigation approach, the tracer is added to the reactor when it already is stirring in a quasi-stationary state. Therefore, such a solution is achieved by the standard procedure described in 5. In the measurements, the tracer is injected via a pipette at predefined interphase spots, namely close to the stirrer shaft (centric) and in the annular gap (eccentric). In both cases, the tracer is dropped from onto the interphase within a short time period, i.e. all at once. This produces a jet that forms something like a thin column of tracer before it is carried away by the flow. However due to the small amount of tracer, it does not notably influence the total flow pattern of the reactor. In the simulation, this is realized by just set the mentioned column domain to $\psi = 1$ and the rest of the reactor to $\psi = 0$. In Fig. 73, the tracer is pictured with green color. The figure shows the progress in a mixing process. The depicted slice cutout goes through the baffles and produces vertical gaps, though. This slice is generally used, since the eccentric injection was between the reactor wall and a baffle.

In [73], Hirtsiefer used six characteristic points in the vertical slice to track the tracer concentration over time. Although this spots were chosen representatively, it still does not exclude the possibility of some undetected dead zones which are still not

mixed. The used LIF measurements, of course, only permit the observation in a slice of the reactor. In the simulation, on the other hand, the whole three-dimensional resolution has to be done, a priory. This circumstance offers the possibility of the implementation of a more accurate method.

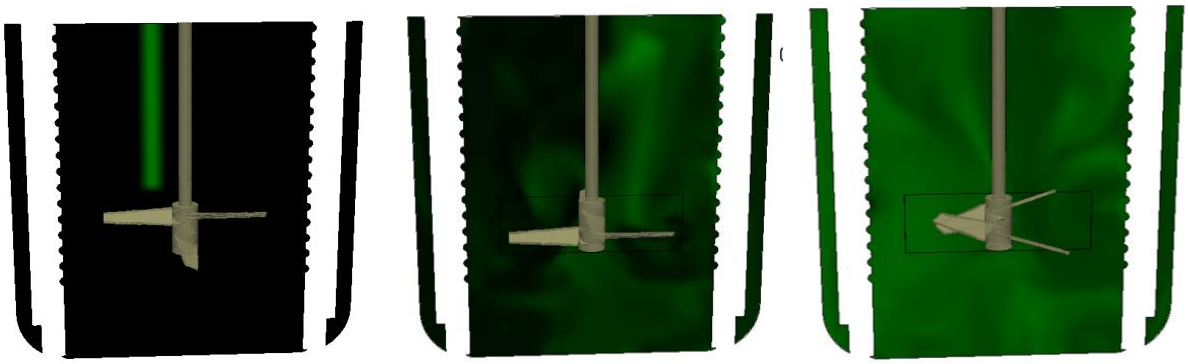

Fig. 73: Tracer transport from injection to its distribution in the reactor.

The concentration can be tracked in each computational cell of the simulation. Following the criterion of 95 % mixing goodness, all cells that have a concentration of at least 0.95 times the end concentration are extracted and the resulting volume is calculated. The end concentration is known after the division of the reactor volume by the tracer column volume. Of course, when the concentration is tracked at only some selected probe locations, the resulting time is lower than in the case where the whole domain is observed. This can be seen in Fig. 74.

Since the latter method is physically more accurate, it is clearly recommended for mixing time determinations. The evaluation of it can be performed in the post processing tool ParaView. Several filters like “calculator”, “integrate variables” and “plot selection over time” allow the visualization of tracer distribution (see Fig. 73) as well as the curve generation of the volume fraction that fulfills the extraction criterion (like in Fig. 74). On order to save memory and computational resources, it is important to know how sensitive the mixing time is to time resolution. It is known for the transient simulations, that a certain Courant number has to be considered [16]. Of course, this leads to very short time steps. Obviously, the fields are stored only for coarser time resolution, since it would otherwise exceed available memory capacities. For the passive scalar transport, on the other hand, the velocity field does not have to be solved explicitly. It is even possible to use before computed fields for

this issue. However, it is important to have them in a time resolution that permits accurate application. It could be shown on a special case, that a time resolution of *T*/6, where *T* is the revolution time of the stirrer, is sufficient and no significant deviation was noted when the time resolution is finer [75].

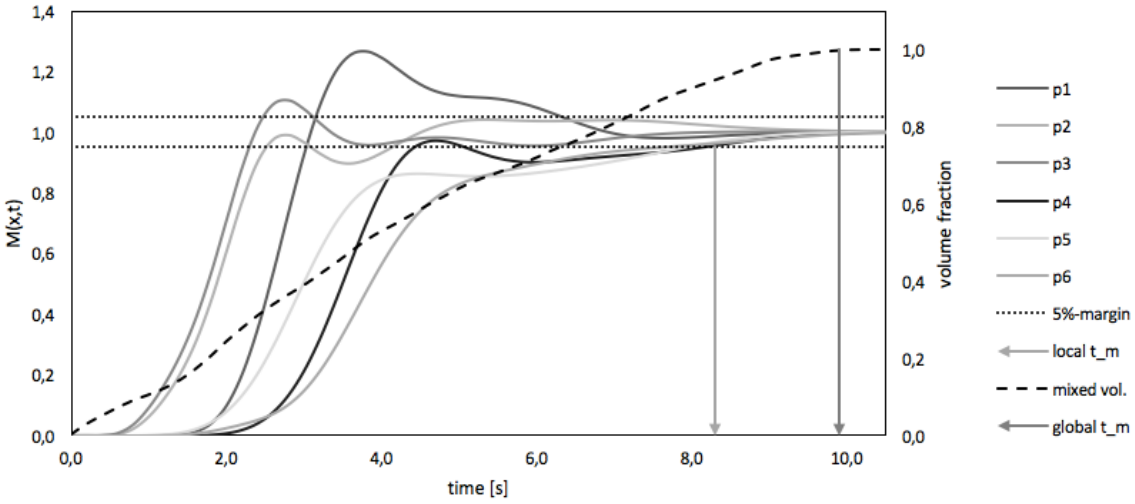

Fig. 74: Comparison of the mixing time determination methods: concentration tracing at selected probe locations (lines) and the summation of the reactor volume that fulfills the 95 %-criterion (dashed).

8.3. Validation of the simulation results

After the simulation of different stirrer types, rotating frequencies and injection spots, the results are compared to the measurements. The simulations and measurements are plotted in Fig. 75. A linear dependency is clearly visible, although there are proportionally higher mixing time results for the measurements. In these observed cases, the difference between the simulations and the measurements is in the area of factor 3. The main reason for that is the numerical diffusion which is strongly present in this complex mesh. It influences the transport equation in a strong manner, see equation (2.31). The AMI-patches imply this effect even more. The factor of 3 is only valid for the used mesh quality, hence. For all observed cases, the mesh generation was as similar as possible. Little deviations are possible since the mesh generation process is barely controllable in this manner. For other internals, setups and scales, the mesh quality can differ and the here found factor is not applicable, though. Further deviation reasons can lay in the measurement method and accuracy. The work of Hirtsiefer [73] points out these issues.

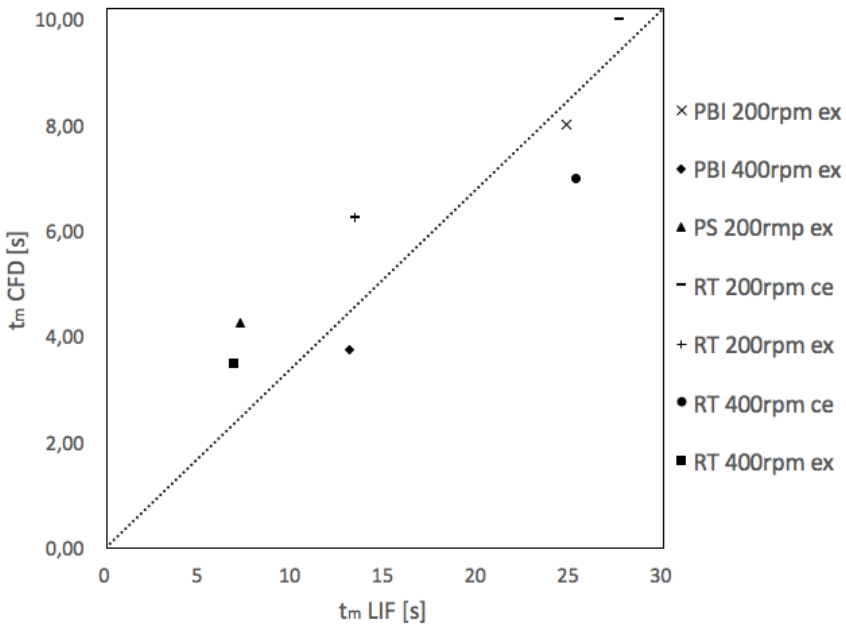

Fig. 75: Comparison of CFD and LIF results. Three different stirrer types are used: PBI – pitched plade impeller; PS – paddle stirrer; RT – rushton turbine. Two rotational frequencies and two injection spots are chosen: centic (ce) and eccentric (ex).

8.4. Conclusions for mixing time investigations

In the scope of efficiency enhancement, the mixing plays an important role, since it is one of the basis operations. However, the approach to determination of measures for mixing efficiency is highly dependent on the setup of the investigation. It is barely possible to compare different systems on a generic basis. Therefore, this work focuses on the implementation of a simulation method that is capable of depict the measured reality. The results obtained in this work encourage for further effort on this area. Still there are unresolved questions like the handling of numerical diffusion and the impact of mesh quality on it. In the range of measured data, the simulations give consistent results, considering a systematic deviation factor. At this point, generic statements are avoided – instead, references for further effort are formulated:

- The performance of investigations on the reduction of numerical diffusion will help to reduce the systematic error and minimize the deviation factor and make the determination more stable regarding the spatial resolution.
- The understanding of dependencies and correlations between mesh quality criteria and the systematic deviation factor will make the simulations more verifiable and thus controllable.
- For reliable mixing time and efficiency determinations, it is important to formulate a generic, reproducible, meaningful and standardized method.

9. Conclusions and outlook

In the scope of the present work, stirring processes were investigated with the aim to enhance the energy efficiency. The stirring process had to be seen in the context of all tasks which a stirred reactor vessel has to fulfill. Obviously, the flow patterns produced by the agitator's work are the binding points for all other aspects of stirring. The heat transfer, mixing and energy consumption can be deduced from flow patterns. Different abstractions of flow field generation were presented and evaluated concerning their worth for certain investigations. Different strategies for the evaluation of simulation result goodness were presented and applied in critical points. In addition to numerical methods, the results were approved by measurements, namely the PIV and LIF technologies. Besides simulation and measurement areas, the scope implied an industrial stirring process that served as the precedent for laboratory and simulation investigations. This is a chemical esterification reactor with immersing helical coils as heater elements. The results and principals found in simulations and laboratory experiments were transferred to the industrial process and implemented in a living plant. Apart from the industrial precedent, a further heater type was investigated for comparison. A novel and innovative design for heaters in agitated reactors was derived from the findings made during the investigation of existing precedents.

9.1. Flow fields and energy consumption

In order to investigate the flow patterns in such a complicated system as the turbulent agitated reactor with immersed heater coils and baffles, different levels of simplification have been performed and discussed. In the case of steady state simulations, the found results were discussed on the basis of horizontal fields, obtained from PIV measurements. They have the value of a preliminary study and give a good impression of the principal flow patterns. However, transient simulations are required for advanced investigations. Vortex shedding and hiking structures in the reactor require computationally expensive simulations which moreover have high memory demand. The implementation of transient simulations was performed successively and a method for time and memory saving simulations was derived. For this, an automated environment was developed and documented.

The flow fields were investigated for both, radial and axial pumping impellers in a reactor with immersing coils. Thereby, the principal flow patterns described in relevant literature for each stirrer type was confirmed by the measurements and simulations. Furthermore, the influence of the heater coils on the flow field was analyzed and discussed. Besides its decelerating function, the coil works as a separator of flow segments and promotes dead zoned in the reactor. The lack of high velocity incident flow at the major part of the heater could be identified as a main reason and bottle neck for heat exchange. Moreover, it is constituted as a risk factor for hot spot formation which is not only a hindrance for heat transport but can also have a negative influence on the product quality and the reaction kinetics. This effect is already seen at the use of a single coil.

Generally, radial pumping impellers show better characteristics in that manner because the incidentally discharge high velocity stream on the helix, where the axial pumping impeller discharges the jet stream downwards, where it is deflected by the bottom and creeps in the annular gap between the heater and the reactor wall. The pattern basically runs to the top of the reactor and loses energy until it sieves back to the suction side of the stirrer but with low velocity, however. The annular gap between the coils remains relatively calm. Even by use of three stirrer stages, like it is found in the industrial precedent, the pattern is strongly conducted by an axial profile without transferring the energy to the critical areas.

In the course of enhancement of energy efficiency, an economic solution was sought for that does not require additional equipment nor major constructive changes. Under those conditions, the modification of the stirrer stages configuration turned out to be an effective method. After the analysis of the flow fields inside the reactor, critical spots could be identified and traced back to the interactions between the stirrer and all internals. An improved configuration of the stirrer was found by means of simulations studies. The modification was realized in the industrial reactor afterwards. At the resumption of the production, several effects lead to an augmentation of the capacity of up to 12 % at 6.5 % shorter runtime. First, the temperature stability turned out to be significantly better and heating worked faster. This allowed a fast semi-batch dosing of substances without the loss of the temperature level, which is a clear indicator of higher heat flux efficiency and therefore meets the prediction made by the simulations. Second, boiling retardations lead to limitations concerning the filling level in the past. After the modification, this

problem ceased, which can be traced back to significantly lower zones of overheating and thus to a more homogeneous temperature distribution inside the reactor. A further indicator for this statement is an improved product quality. In the past, it had a strong discoloration which can be traced back to overheating. This is clearly reduced after the modification. A further reason for the latter effect can be a better dispersing of decolorizing charcoal. The reason for it is a higher interface movement, where the charcoal is dosed.

This reference project impressively demonstrates the potential of the revision of standard processes by means of fluid dynamics. Nevertheless, the industrial practice shows quite low attention for the real flow patterns at the design and operation instruction of stirred processes. There is huge potential for improvement in industrial reality and an underestimation of interaction of static and dynamic elements in the vessels.

9.2. Heat exchange

In order to investigate the heat exchange in such a complex system like the present, coupled simulation of energy, mass and momentum transport under the circumstance of complex meshes and rotating geometries could not be achieved with the used software due to instabilities and the lack of adequate solvers. Therefore, an abstracted model was developed which simplified the stirrer as a pumping black box and reduced the observation to the axial and radial component under the assumption that the tangential velocity is strongly suppressed by the overwhelming resistance of the coils and baffles. The abstraction got along without rotating meshed nor multiple reference frames by constant setting a constant discharge velocity and temperature to the stirrer black box. The heater was set to a constant wall temperature and the heat transfer occurred by means of wall functions implemented in OF. The fixed stream develops in dependence on existing geometries in the domain and then leaves it through remaining patches of the stirrer black box. Of course, the heat transfer, found in this model is useless for comparison with a real reactor, because the stirrer works as a perfect cooler which is not the case in practice and the tangential velocity is completely neglected. However, the value of the model consists in comparative investigations performed on it. Parameter studies show tendencies and principal issues of the present case. This way, the position of radial and axial

impellers in the reactors could be investigated. Furthermore, hotspots could be identified and localized.

In the next step, a completely novel heater was designed by use of this abstraction model. The principle of the development is to avoid problem zones like they can be observed in the conventional setups. In this development, the jet stream of the stirrer is used as a driver for the positioning of coil windings in the reactor. An iterative algorithm has been presented which manages to position heater coils in a way that they have the highest possible incident flow. In this procedure, the temperature fields are used for the detection of hotspots. Since it is the aim of the development to avoid them, a measure called relative homogeneity was derived which served as a quality criterion of the novel heater.

The simulations used for the development were verified and validated not only by means of numerical aspects but also by measurements after the novel heater was constructed and experimented. The abstraction model appeared to be valid for the development in this scope. However, the application to a reactor with multiple stirrer stages failed at the transfer from abstraction to the three-dimensional simulation. The conditions for simplification assumptions turned out to be invalid in that case. Further work has to be performed at that point to develop a working method for the development of adequate heaters also for that case.

The realistic and local heat exchange and its influence on reaction kinetics and product quality is still not adequately investigated in the major part of industrial applications. Inclusively small changes can enhance the efficiency of heat exchange in stirred processes, as it could be successfully shown in this work.

9.3. Mixing time

The investigation of mixing time is in a huge amount dependent on the experimental setup. This work rather focuses on the implementation of a valid method for the determination of mixing times and the observation of mixing progress. Two principles are presented to simulate the spreading of a tracer substance in the reactor domain. The handling of the tracer as a second phase turned out as an “expensive” method with low mesh convergence order whereas the implementation of a passive scalar transport equation poses a “cheap” method that can be easily integrated in the before

developed automated transient solution method without significant computational and memory costs. The validation with results from LIF measurements showed good agreement with the determined results obtained from the simulation but with a systematic deviation by the factor of three, however.

For reliable predictions, further work has to be done in this area. However, the method for evaluation and determination of the mixing time value is well described in this work.

9.4. Outlook

The interaction between an industrial precedent, measurement technology and CFD simulations is obviously beneficial for the detection and the remedy of problems known from the practice. Low budget changes can produce huge results, when the problems can be identified in a reliable way. Further investigation should intensify such corporations for maximum benefit.

In the area of CFD, further work has to be done in generation of stable solvers which can handle complex meshes, dynamic geometries, heat exchange and multiphase applications.

In the area of measurements, the technology can be extended by further features like volumetric PIV, multiple color LIF and coupled PIV/LIF possibilities. Also, further development of the investigated model is necessary concerning constructive feasibility and RIM quality.

In the area of further heater development, the jet driven design principal might be formalized and implemented in the before developed simulation environment. There still is a lack of accuracy concerning axial pumping impellers and the use of multiple stirrer stages which has to be handled for industrial use.

10. Symbols used

10.1. Latin symbols

a	[$m^2 s^{-1}$]	thermal transport
Q	[$kg\ m^2 s^{-2}$]	heat
$\dot{Q}$	[$kg\ m^2 s^{-3}$]	heat flux
u, U	[$m\ s^{-1}$]	velocity
c_p	[$kg^2 m\ s^{-2} K^{-1}$]	heat capacity
x, y, z	[m]	spatial coordinate
t	[s]	time
q_ϕ	[$kg\ s^{-1}$]	source term, e.g. formation rate of mass
$C, c_{Re}, \ldots$	[-]	coefficients of the characteristic equation
P	[$kg\ m^2 s^{-3}$]	power
M	[$kg\ m^2 s^{-2}$]	torque
n	[s^{-1}]	rotation frequency
n	[m]	normal vector
T	[K]	temperature
A	[m^2]	area
S	[m^2]	surface
V	[m^3]	volume
m	[kg]	mass
J	[$kg\ m\ s^{-1}$]	momentum
T	[$m^2 s^{-2}$]	stress tensor

I	[-]	unit tensor
D	[s^{-1}]	deformation tensor
b	[$m\,s^{-2}$]	force
g	[$m\,s^{-2}$]	gravity
k	[m^2s^{-2}]	kinetic turbulent energy
R	[$kg\,m^{-1}s^{-2}$]	Reynolds stress tensor
c	[$m^{-3}mol$]	concentration
$M(x)$	[-]	mixing quality
h, H	[m]	height
d, D	[m]	diameter
N	[-]	integer number
I_{rel}	[$kg^{-1}m^{-2}s^{-3}K$]	relative inhomogeneity

10.2. Greek symbols

ω	[s^{-1}]	angular velocity
π	[-]	mathematical constant °Pi
ρ	[$kg\,m^3$]	density
ν	[m^2s^{-1}]	kinematic viscosity
η	[$kg\,m^{-1}s$]	dynamic viscosity
α	[$kg\,s^{-3}K^{-1}$]	heat transfer coefficient
λ	[$kg\,m\,s^{-3}K^{-1}$]	heat conduction coefficient
δ	[m]	boundary layer thickness
ϕ	[kg]	extensive quantity, e.g. mass

ϕ	[]	intensive quantity – referred to ϕ, normalized by mass
Γ	[m^2s^{-1}]	diffusion coefficient
τ	[s]	concrete time
ϵ	[m^2s^{-3}]	turbulent kinetic energy dissipation rate
σ	[-]	standard deviation
ψ	[]	scalar field

10.3. Dimensionless identifiers

Ne	Newton number
Re	Reynolds number
Ne	Newton number
Vis	viscosity number
Pr	Prandtl number
Ne	Newton number

10.4. Mathematical operators and notation

d	differential operator
∂	partial differential operator
Δ	delta, difference
$\int$	integral
$\mathbf{M}$	matrix notation – bold, non-italic
$\boldsymbol{v}$	vector notation – bold, italic

10.5. Abbreviations

CFD	Computational Fluid Dynamics
FEM	Finite Element Method
FDM	Finite Differential Method
FVM	Finite Volume Method
DEM	Discrete Element Method
NSE	Navier-Stokes-Equation
CV	Control Volume
CM	Control Mass
CAE	Computer Aided Engineering
CAD	Computer Aided Design
RAS	Reynolds Averaged Simulation
RANS	Reynolds Averaged Navier-Stokes
PIV	Particle Image Velocimetry
LIF	Laser-Induced Fluorescence
PB	Population Balance
MRF	Multiple Reference Frame
AMI	Arbitrary Mesh Interface
GGI	Generalized Grid Interface
OF	OpenFOAM®
RIM	Refraction Index Matching
IA	Interrogation Area

OOP	Out-Of-Plane
DSL	Domain Specific Language
GUI	Graphical User Interface
MDX	Multidisciplinary Design Exploration
API	Axial Pumping Impeller
RPI	Radial Pumping Impeller
PBB	Pumping Black Box
rpm	rounds per minute
PBI	Pitched Blade Impeller
PS	Paddle Stirrer
RT	Rushton Turbine

11. References

[1] M. Zlokarnik, *Rührtechnik: Theorie und Praxis*. Berlin: Springer, 1999.

[2] M. Kraume and Gesellschaft Verfahrenstechnik und Chemieingenieurwesen, Eds., *Mischen und Rühren: Grundlagen und moderne Verfahren*. Weinheim: Wiley-VCH, 2003.

[3] A. Brunn and W. Nitsche, *Strömungsmesstechnik.* Dordrecht: Springer, 2006.

[4] O. Fiedler, *Strömungs- und Durchflussmesstechnik*. München; Wien: Oldenbourg, 1992.

[5] R. J. Goldstein, Ed., *Fluid mechanics measurements*, 2nd ed. Washington, DC: Taylor & Francis, 1996.

[6] P. Mavros, C. Xuereb, and J. Bertrand, “Determination of 3-D Flow Fields in Agitated Vessels by Laser-Doppler Velocimetry: Use and Interpretation of RMS Velocities,” *Chem. Eng. Res. Des.*, vol. 76, no. 2, pp. 223–233, Feb. 1998.

[7] K. Bauckhage, “Gleichzeitige Erfassung von Partikelmerkmalen und Eigenschaften mehrphasiger Strömungen mit Hilfe der Phasen-Doppler-Anemometrie: Gleichzeitige Erfassung von Partikelmerkmalen und Eigenschaften mehrphasiger Strömungen mit Hilfe der Phasen-Doppler-Anemometrie,” *Chem. Ing. Tech.*, vol. 68, no. 3, pp. 253–266, Mar. 1996.

[8] M. Sommerfeld and H.-H. Qiu, “Characterization of particle-laden, confined swirling flows by phase-doppler anemometry and numerical calculation,” *Int. J. Multiph. Flow*, vol. 19, no. 6, pp. 1093–1127, Dec. 1993.

[9] W. Bachalo, R. Rudoff, and A. Brena De La Rosa, “Mass flux measurements of a high number density spray system using the phase Doppler particle analyzer,” 1988.

[10] J. C. Bhatia, J. Domnick, F. Durst, and C. Tropea, “Phase-Doppler-Anemometry and the Log-Hyperbolic Distribution applied to Liquid Sprays,” *Part. Part. Syst. Charact.*, vol. 5, no. 4, pp. 153–164, 1988.

[11] M. Raffel, Ed., *Particle image velocimetry: a practical guide*, 2nd ed. Heidelberg ; New York: Springer, 2007.

[12] V. Bliem, “Untersuchung des Einflusses der Strömungsverhältnisse auf den Wärmeübergang in Rührreaktoren mit Rohrschlangeneinbauten mittels Particle Image Velocimetry und Laser Induced Fluorescence,” Universität Duisburg Essen, Essen, 2016.

[13] J. Kitzhofer, T. Nonn, and C. Brücker, “Generation and visualization of volumetric PIV data fields,” *Exp. Fluids*, vol. 51, no. 6, pp. 1471–1492, Dec. 2011.

[14] J. L. Kinsey, “Laser-Induced Fluorescence,” *Annu. Rev. Phys. Chem.*, vol. 28, no. 1, pp. 349–372, Oct. 1977.

[15] T. Cebeci, Ed., *Computational fluid dynamics for engineers: from panel to Navier-Stokes methods with computer programs*. Long Beach, Calif. : Berlin: Horizons Pub. Inc., ; Springer, 2005.

[16] J. H. Ferziger and M. Perić, *Computational methods for fluid dynamics*, 3rd, rev. ed ed. Berlin ; New York: Springer, 2002.

[17] S. Lecheler, *Numerische Strömungsberechnung: schneller Einstieg durch ausführliche praxisrelevante Beispiele*, 1. Aufl. Wiesbaden: Vieweg + Teubner, 2009.

[18] A. R. Paschedag, *CFD in der Verfahrenstechnik: allgemeine Grundlagen und mehrphasige Anwendungen*. Weinheim: Wiley-VCH, 2004.

[19] H. K. Versteeg and W. Malalasekera, *An introduction to computational fluid dynamics: the finite volume method*, 2nd ed. Harlow, England ; New York: Pearson Education Ltd, 2007.

[20] E. Bartholomé, Ed., *Ullmanns Encyklopädie der technischen Chemie*, 4., neubearb. u. erw. Aufl. Weinheim (Bergstr.): Verlag Chemie, 1972.

[21] J. Y. Oldshue, “Mixing theory and practice, V. M. Uhl and J. B. Gray Vol. I, Academic Press, New York(1966). 340 pages,$15.50,” *AIChE J.*, vol. 13, no. 4, pp. 826–827, Jul. 1967.

[22] P. von Böckh, *Wärmeübertragung: Grundlagen und Praxis*, 2., bearb. Aufl. Berlin: Springer, 2006.

[23] Verein Deutscher Ingenieure, S. Kabelac, and Gesellschaft Verfahrenstechnik und Chemieingenieurwesen, Eds., *VDI-Wärmeatlas: [Berechnungsunterlagen für Druckverlust, Wärme- und Stoffübergang]*, 10., bearb. und erw. Aufl. Berlin: Springer, 2006.

[24] Ekato Holding GmbH and W. Himmelsbach, Eds., *Ekato. The book*, 3. ed. Freiburg: Ekato Holding, 2012.

[25] F. Kneule, *Rühren*, 3. Aufl. Frankfurt am Main: Deutsche Gesellschaft für Chemisches Apparatewesen, Chemische Technik und Biotechnologie, 1986.

[26] G. B. Tatterson, *Fluid mixing and gas dispersion in agitated tanks*. New York: McGraw-Hill, 1991.

[27] H. Oertel and M. Böhle, *Strömungsmechanik: Grundlagen, Grundgleichungen, Lösungsmethoden, Softwarebeispiele*, 3., überarb. und erw. Aufl. Wiesbaden: Vieweg, 2004.

[28] H. Jasak, “Error Analysis and Estimation for the Finite Volume Method with Applications to Fluid Flows,” University of London, 1996.

[29] L. Biferale, M. Blank, and U. Frisch, “Chaotic Cascades with Kolmogorov 1941 Scaling,” *Journal Of Statistical Physics*, vol. Vol.75(5-6), pp. 781–795, Jun. 1994.

[30] A. N. Kolmogorov, “The Local Structure of Turbulence in Incompressible Viscous Fluid for Very Large Reynolds Numbers,” *Proc. R. Soc. Math. Phys. Eng. Sci.*, vol. 434, no. 1890, pp. 9–13, Jul. 1991.

[31] S. B. Pope, *Turbulent flows*. Cambridge ; New York: Cambridge University Press, 2000.

[32] P. S. Bernard and J. M. Wallace, *Turbulent flow: analysis, measurement, and prediction*. Hoboken, N.J: Wiley, 2002.

[33] P. A. Davidson, *Turbulence: an introduction for scientists and engineers*. Oxford, UK ; New York: Oxford University Press, 2004.

[34] D. C. Wilcox, *Turbulence modeling for CFD*. La Cãnada, CA: DCW Industries, Inc, 1993.

[35] J. Y. Luo, R. I. Issa, and A. D. Gosman, “Prediction of Impeller-Induced Flows in Mixing Vessels Using Multiple Frames of Reference,” *IChemE Symposium Series*, vol. 136, pp. 549–556, 1994.

[36] “FLUENT 6.3 User’s Guide.” [Online]. Available: https://www.sharcnet.ca/Software/Fluent6/html/ug/main_pre.htm. [Accessed: 04-Sep-2017].

[37] Z. Liu, Y. Zheng, L. Jia, J. Jiao, and Q. Zhang, “Stereoscopic PIV studies on the swirling flow structure in a gas cyclone,” *Chem. Eng. Sci.*, vol. 61, no. 13, pp. 4252–4261, Jul. 2006.

[38] “piv_stereo.jpg 384×287 Pixel.” [Online]. Available: http://www.velocimetry.net/images/piv_stereo.jpg. [Accessed: 10-Jan-2018].

[39] OpenCFD, “OpenFOAM® - Official home of The Open Source Computational Fluid Dynamics (CFD) Toolbox.” [Online]. Available: http://www.openfoam.com.

[40] “Henry Weller | OpenFOAM Expert,” *CFD Direct*. [Online]. Available: https://cfd.direct/about/henry-weller/.

[41] “Deutsche Fortran WebSite.” [Online]. Available: http://www.fortran.de/. [Accessed: 15-Aug-2017].

[42] “C++ language - cppreference.com.” [Online]. Available: http://en.cppreference.com/w/cpp/language. [Accessed: 15-Aug-2017].

[43] “Category:FOAM-Extend Version 4.0 - OpenFOAMWiki.” [Online]. Available: https://openfoamwiki.net/index.php/Category:FOAM-Extend_Version_4.0. [Accessed: 15-Aug-2017].

[44] “Engineering Simulation & 3-D Design Software | ANSYS.” [Online]. Available:

http://www.ansys.com/.

[45] “Discover Better Designs, Faster | MDX.” [Online]. Available: http://mdx.plm.automation.siemens.com/. [Accessed: 22-Aug-2017].

[46] “HELYX Advanced CFD Software Suite | engys.” [Online]. Available: http://engys.com/de/products/helyx. [Accessed: 22-Aug-2017].

[47] “Professional Meshing Solutions,” *cfmesh.com*. [Online]. Available: https://cfmesh.com/.

[48] “SimScale - CFD, FEA, and Thermal Simulation in the Cloud | CAE.” [Online]. Available: https://www.simscale.com/. [Accessed: 22-Aug-2017].

[49] “Codes -- CFD-Wiki, the free CFD reference.” [Online]. Available: https://www.cfd-online.com/Wiki/Codes. [Accessed: 22-Aug-2017].

[50] “CFD - Strömungssimulation › Wiki › ubuntuusers.de.” [Online]. Available: https://wiki.ubuntuusers.de/CFD_-_Str%C3%B6mungssimulation/. [Accessed: 22-Aug-2017].

[51] C. Greenshields, “OpenFOAM User Guide: CFD Direct, Architects of OpenFOAM,” *CFD Direct*, 02-Mar-2017. [Online]. Available: https://cfd.direct/openfoam/user-guide/. [Accessed: 12-Sep-2017].

[52] “Contrib/PyFoam - OpenFOAMWiki.” [Online]. Available: https://openfoamwiki.net/index.php/Contrib/PyFoam. [Accessed: 23-Aug-2017].

[53] “Contrib/swak4Foam - OpenFOAMWiki.” [Online]. Available: https://openfoamwiki.net/index.php/Contrib/swak4Foam. [Accessed: 23-Aug-2017].

[54] T. Marić, J. Höpken, and K. Mooney, *The OpenFOAM technology primer*. Duisburg: Sourceflux, 2014.

[55] “Welcome to Python.org,” *Python.org*. [Online]. Available: https://www.python.org/.

[56] J. Wolf and S. Kania, *Shell-Programmierung: das umfassende Handbuch ; [Einführung, Praxis, Übungsaufgaben, Kommandoreferenz ; für Bourne-, Korn- und Bourne-Again-Shell (bash) ; inkl. grep, sed, awk und GUIs mit dialog, Xdialog und gnuplot]*, 4., aktualisierte Aufl. Bonn: Galileo Press, 2013.

[57] “The StL Format | fabbers.com.” [Online]. Available: http://www.fabbers.com/tech/STL_Format. [Accessed: 24-Aug-2017].

[58] Ekato Holding GmbH, W. Himmelsbach, and Ekato Rühr- und Mischtechnik GmbH, Eds., *EKATO. the book*, 3. Aufl. Schopfheim: EKATO, 2012.

[59] E. L. Paul, V. A. Atiemo-Obeng, and S. M. Kresta, Eds., *Handbook of industrial mixing: science and practice*. Hoboken, N.J: Wiley-Interscience, 2004.

[60] B. Luczak, R. Müller, M. Ulbricht, and H. J. Schultz, “Experimental analysis of the flow conditions in spiral jet mills via non-invasive optical methods,” *Powder Technol.*, vol. 325, pp. 161–166, Feb. 2018.

[61] B. Luczak, R. Müller, and H. J. Schultz, “Untersuchungen zu Einflüssen auf die Strömungsverhältnisse und das Mahlergebnis in Spiralstrahlmühlen mittels Particle Image Velocimetry (PIV),” *Chem. Ing. Tech.*, vol. 88, no. 9, pp. 1362–1363, Sep. 2016.

[62] V. Bliem and H. J. Schultz, “Investigation of Horizontal Velocity Fields in Stirred Vessels with Helical Coils by PIV,” *Int. J. Chem. Eng.*, vol. 2014, pp. 1–8, 2014.

[63] V. Bliem, “Untersuchung der Strömungsverhältnisse in Rührreaktoren mit Rohrschlangeneinbauten mit PIV-Systemen,” Hochschule Niederrhein, Krefeld, 2013.

[64] A. Stefan, “Machbarkeitsstudie zur Implementierung eines Rührreaktors im CFD-Programm OpenFOAM,” Hochschule Niederrhein, Krefeld, 2014.

[65] K. V. Jährling, “Untersuchung von Rührprozessen mit verschiedenen Wärmetauschereinbauten und Optimierung der Strömungsregime mittels Particle Image Velocimetry (PIV),” Universität Duisburg Essen, Essen, to be published soon.

[66] K. Jährling *et al.*, “Particle Image Velocimetry Compared to CFD Simulation of Stirred Vessels with Helical Coils,” *Chem. Ing. Tech.*, vol. 89, no. 4, pp. 401–408, Apr. 2017.

[67] A. Stefan, S. Hindges, and H. J. Schultz, “Simulation of Heat Exchange in Vessels with Helical Coils and Influence of Stirrer Position,” *Chem. Ing. Tech.*, vol. 89, no. 4, pp. 470–474, Apr. 2017.

[68] M. Matzke, “Experimentelle Untersuchungen von Wärmeübergängen an Rohrschlangeneinbauten im Reaktormodell,” Hochschule Niederrhein, Krefeld, 2015.

[69] P. Kurpiers, *Wärmeübergang in Ein- und Mehrphasenreaktoren mit ein- und zweistufigen Rührern*. Weinheim (Federal Republic of Germany): VCH, 1985.

[70] P. Wünscher, “Optische Untersuchung von Suspendierungs- und Dispergierungsvorgängen in einem temperierten Rührreaktor mit eintauchenden Rohrschlangen,” Hochschule Niederrhein, Krefeld, 2016.

[71] L. Johnen, “Feedback on stirrer modification in the batch process of an esterification reaction.,” 01-Feb-2018.

[72] F. Schneider, “Ein Blick ins Innere der Ester-Anlage in Oberhausen,” *OXEA J.*, no. 01/18, pp. 24–25.

[73] M. Hirtsiefer, “Untersuchung des Wärmeaustausches und Mischverhaltens an helikalen Rohrschlangen in Rührreaktoren mittels laserinduzierter Fluoreszenz,” Hochschule Niederrhein, Krefeld, 2015.

[74] J. Volkmer, “Untersuchung der Darstellbarkeit des Mischzeitverhaltens von Rührprozessen mittels der CFD Software OpenFOAM,” Hochschule Niederrhein, Krefeld, 2016.

[75] A. Stefan and H. J. Schultz, “Use of OpenFOAM® for Investigation of Mixing Time in Agitated Vessels with Immersed Helical Coils,” in *Openfoam Selected Papers of the 11th Workshop.*, Springer Verlag, 2017.

12. Appendix

12.1. Scripts and OpenFOAM-file content

12.1.1. Mesh generation

Script – generateMesh

```
# Error treatment
if [ ! -f system/controlDict ]; then
      echo "Error: $1 is not a case."
      exit
fi
echo "Running case $( basename "$PWD" )..."
# meshing
echo "creating block mesh..."
blockMesh                                  | tee log.blockMesh
echo "extracting surface feature edges..."
surfaceFeatureExtract                      | tee log.surfaceFeatureExtract
echo "decomposing..."
decomposePar -force                              | tee log.decomposePar
echo "meshing..."
foamJob -s -p snappyHexMesh -overwrite           ; mv log log.snappyHexMesh
echo "reconstructing mesh..."
reconstructParMesh -constant -mergeTol 1e-6      | tee log.reconstructParMesh
echo "create patch..."
createPatch -overwrite                     | tee log.createPatch
# postprocessing
rm -rf 0 processor* > /dev/null 2>&1
mkdir 0
echo "checking mesh quality..."
checkMesh                              | tee log.checkMesh
// ************************************************************* //
```

OF-file – blockMesh

```
FoamFile
{
    version     2.0;
    format      ascii;
    class       dictionary;
    object      blockMeshDict;
}

convertToMeters 0.001;

vertices
(
    ( -125 -125  -1)    //0
    (  125 -125  -1)    //1
    (  125  125  -1)    //2
    ( -125  125  -1)    //3
    ( -125 -125 249)    //4
    (  125 -125 249)    //5
    (  125  125 249)    //6
    ( -125  125 249)    //7
); // those points demark the limits of the blocked mesh

blocks
(
    hex  (0  1  2  3  4  5  6  7)  (  50    50    50)  simpleGrading  (1  1  1)
); // adjustments defining the shape and resolution of the block(s)
```

```
edges
(
); // optional adjustments for other than straight edges
boundary
(
); // optional definition of boundaries and boundary types
// ************************************************************* //
```

OF-file – surfaceFeatureExtractDict

```
FoamFile
{
    version     2.0;
    format      ascii;
    class       dictionary;
    object      surfaceFeatureExtractDict;
}
// all .stl-files are generated by CAD software Blender
stirrerTip.stl
{
    #include "surfaceFeatureExtractDictDefaults"
}
stirrerStem.stl
{
    #include "surfaceFeatureExtractDictDefaults"
}
reactorWall.stl
{
    #include "surfaceFeatureExtractDictDefaults"
}
surface.stl
{
    #include "surfaceFeatureExtractDictDefaults"
}
cylinder.stl
{
    #include "surfaceFeatureExtractDictDefaults"
}
baffles.stl
{
    #include "surfaceFeatureExtractDictDefaults"
}
heater.stl
{
    #include "surfaceFeatureExtractDictDefaults"
}
// ************************************************************* //
```

OF-file – surfaceFeatureExtractDictDefaults

```
// How to obtain raw features (extractFromFile || extractFromSurface)
extractionMethod    extractFromSurface;
extractFromSurfaceCoeffs
{
    // Mark edges whose adjacent surface normals are at an angle less
    // than includedAngle as features
    // - 0  : selects no edges
    // - 180: selects all edges
    includedAngle   150;
}
trimFeatures
{
    // Remove features with fewer than the specified number of edges
    minElem         10;
}
// ************************************************************* //
```

OF-file – snappyHexMeshDict

```
FoamFile
```

```
{
    version     2.0;
    format      ascii;
    class       dictionary;
    object      autoHexMeshDict;
}
// Which of the steps to run
castellatedMesh true;
snap            true;
addLayers       false;
geometry
{
    stirrerTip.stl
    {
        type triSurfaceMesh;
        name stirrerTip;
    }
    stirrerStem.stl
    {
        type triSurfaceMesh;
        name stirrerStem;
    }
    reactorWall.stl
    {
        type triSurfaceMesh;
        name reactorWall;
    }
    surface.stl
    {
        type triSurfaceMesh;
        name surface;
    }
    cylinder.stl
    {
        type triSurfaceMesh;
        name cylinder;
    }
    baffles.stl
    {
        type triSurfaceMesh;
        name baffles;
    }
    heater.stl
    {
        type triSurfaceMesh;
        name heater;
    }
};
castellatedMeshControls
{
    maxLocalCells 1000000;
    maxGlobalCells 10000000;
    minRefinementCells 0;
    maxLoadUnbalance 0.10;
    nCellsBetweenLevels 1;
    features
    (
        {
            file "stirrerTip.eMesh";
            level 0;
        }
        {
            file "stirrerStem.eMesh";
            level 0;
        }
        {
            file "reactorWall.eMesh";
            level 0;
        }
        {
            file "surface.eMesh";
            level 0;
```

```
        }
        {
            file "cylinder.eMesh";
            level 0;
        }
        {
            file "baffles.eMesh";
            level 0;
        }
        {
            file "heater.eMesh";
            level 0;
        }
    );
    refinementSurfaces
    {
        reactorWall
        {
            level (2 2);
        }
        surface
        {
            level (1 1);
        }
        stirrerTip
        {
            level (2 3);
        }
        stirrerStem
        {
            level (2 2);
        }
        cylinder
        {
            level       (3 3);
            //faceType    boundary;
            cellZone cylinder;
            faceZone cylinder;
            cellZoneInside  inside;
        }
        baffles
        {
            level (2 2);
        }
        heater
        {
            level (2 2);
        }
    }
    resolveFeatureAngle 30;
    refinementRegions
    {
    }
    allowFreeStandingZoneFaces true;
}
snapControls
{
    nSmoothPatch 3;
    tolerance 4.0;
    nSolveIter 300;
    nRelaxIter 10;
        nFeatureSnapIter 10;
        implicitFeatureSnap true;
        explicitFeatureSnap false;
        multiRegionFeatureSnap true;
}
addLayersControls
{
    relativeSizes true;
    layers
    {
      heater
```

```
        {
            nSurfaceLayers 3;
        }
    }
    expansionRatio 1.0;
    finalLayerThickness 0.3;
    minThickness 0.25;
    nGrow 0;
    featureAngle 30;
    nRelaxIter 5;
    nSmoothSurfaceNormals 1;
    nSmoothNormals 3;
    nSmoothThickness 10;
    maxFaceThicknessRatio 0.5;
    maxThicknessToMedialRatio 0.3;
    minMedianAxisAngle 70;
    nBufferCellsNoExtrude 0;
    nLayerIter 50;
    nRelaxedIter 10;
}
meshQualityControls
{
    maxNonOrtho 65;
    maxBoundarySkewness 20;
    maxInternalSkewness 4;
    maxConcave 80;
    minVol 1e-13;
    minTetQuality -1;
    minArea -1;
    minTwist 0.01;
    minDeterminant 0.001;
    minFaceWeight 0.05;
    minVolRatio 0.01;
    minTriangleTwist -1;
    nSmoothScale 4;
    errorReduction 0.75;
    relaxed
    {
        maxNonOrtho 75;
    }
}
debug 0;
mergeTolerance 1E-6;
// ************************************************************* //
```

12.1.2. Generic simulation scripts

Script – Allclean

```
rm -rf log* procTime > /dev/null 2>&1
rm -rf processor* > /dev/null 2>&1
foamListTimes -withZero -rm > /dev/null 2>&1
rm -rf constant/polyMesh > /dev/null 2>&1
// ************************************************************* //
```

Script – runCase.Pre

```
./Allclean
# Option catching
usage() {
echo "
Usage: ${0##*/} [OPTIONS]
options:
 --meshSource 'local|shared'  Where to get mesh from. Default is 'shared'.
                              Source info is specified in 'caseDict'
 --dynamicMesh                splits mesh if DyM is used.  ${0##*/} looks
                              it up by default in controlDict.application
 --help                       print the usage
```

```
 gets mesh and prepares for solving
"
}
mS=local
dyM=false
solver=`foamDictionary -entry application -value system/controlDict`
if [ "$(echo $solver)" == "$(echo $solver | grep DyM )" ]; then
   dyM=true
fi
while [ "$#" -gt 0 ]
do
  case $1 in
    --meshSource)
      mS=$2; shift; shift;;
    --dynamicMesh)
      dyM=true; shift;;
    --help)
      usage
      exit 0;;
    *)
      usage
      echo "
--> AGS FATAL ERROR:
Unexpexted argument $1
"
      exit;;
  esac
done
#- get mesh from local or shared source. Shared source is not treated in
#- the scope of this appendix
if [ "$mS" == "local" ]; then
   lMP=../mesh/constant/polyMesh
   if [ -d $lMP ] && [ "$(basename $lMP)" == "polyMesh" ]; then
     echo "getting local mesh from `dirname $(dirname $lMP)`..."
     rm -rf constant/polyMesh
     cp -r  $lMP constant
   else
     echo "
--> AGS FATAL ERROR:
expected path to a 'polyMesh' directory, found $lMP
"
     exit 1
   fi
elif [ "$mS" == "shared" ]; then
   gen=`foamDictionary -entry sharedMeshInfo.generator -value caseDict`
   sc=`foamDictionary -entry sharedMeshInfo.scale -value caseDict`
   rea=`foamDictionary -entry sharedMeshInfo.reactor -value caseDict`
   st=`foamDictionary -entry sharedMeshInfo.stirrer -value caseDict`
   clea=`foamDictionary -entry sharedMeshInfo.clearance -value caseDict`
   hea=`foamDictionary -entry sharedMeshInfo.heater -value caseDict`
   baf=`foamDictionary -entry sharedMeshInfo.baffles -value caseDict`
   mCS=`foamDictionary -entry sharedMeshInfo.maxCellSize -value caseDict`
   $AGS_UTIL/getMesh --generator $gen --scale $sc --reactor $rea --stirrer
$st\
    --clearance $clea --heater $hea --baffles $baf --maxCellSize $mCS ||
exit 1
else
   echo "
--> AGS FATAL ERROR:
wrong meshSource, expected 'local' or 'shared', found $mS
"
   exit 1
fi
#- reset start conditions from original
echo "resetting start conditions and speed properties..."
rm -rf 0; cp -r 0.org 0 || exit 1
$AGS_UTIL/setSpeedProperties || exit 1
#- split mesh. Only use if solver contains DyM..
if $dyM; then
  echo "splitting mesh..."
  foamJob -s createBaffles -overwrite               > log.createBaffles
  foamJob -s mergeOrSplitBaffles -split -overwrite> log.mergeOrSplitBaffles
```

```
fi
echo "finished preprocessing."
// ********************************************************** //
```

Script – runCase

```
#- Error treatment and option catching
usage() {
echo "
Usage: ${0##*/} [OPTIONS]
options:
 --solver <OFsolver>   run specified OpenFOAM solver
 --noPreprocessing     skips preprocessing
 --noPreprocessing     skips postprocessing
 --continue            skip preprocessing and continue at latest time
 --fromStart           sets controlDict entry 'startFrom' to 'startTime'
 --parallel            perform decomposing, renumbering and parallel run
 --help                print the usage
Runs case as scripted
"
}
if [ ! -f system/controlDict ]; then
  echo "Error: $( basename "$PWD" ) is not a case."
  exit
fi
tP=0 #- previously consumed time. Only usefull, if --continue is set...
solver=`foamDictionary -entry application -value system/controlDict`
nC=`foamDictionary -entry nCores -value caseDict`
if [ $nC -le 1 ]; then p=false; else p=true; fi
pre=true
post=true
while [ "$#" -gt 0 ]
do
  case $1 in
    --solver)
      solver=$2; shift; shift;;
    --noPreprocessing)
      pre=false; shift;;
    --noPostprocessing)
      post=false; shift;;
    --continue)
      foamDictionary system/controlDict -entry startFrom -set latestTime
      pre=false;
      tP=$( cat procTime )
      shift;;
    --fromStart)
      foamDictionary system/controlDict -entry startFrom -set startTime
      shift;;
    --parallel)
      p=true; shift;;
    --help)
      usage
      exit 0;;
    *)
      usage
      echo "
--> AGS FATAL ERROR:
Unexpexted argument $1
"
      exit 1;;
  esac
done
echo "running case $( basename "$PWD" )..."
#- preprocessing
if $pre; then
  echo "preprocessing..."
  ./runCase.pre || exit 1
else
  echo "skip preprocessing..."
fi
#- solving
```

```
if $p; then
  #- only if using parallel run!!!
  echo "parallel processing..."
  echo "  decomposing..."
  foamJob -s decomposePar -latestTime -force > log.decomposePar   || exit 1
  echo "  renumbering..."
  foamJob -s -p renumberMesh -overwrite      > log.renumberMesh
  echo   "  solving..."
  foamJob -s -p $solver                      > log.$solver        || exit 1
  echo   "  reconstruct..."
  foamJob -s reconstructPar                  > log.reconstructPar || exit 1
  rm -rf processor*
else
  #- only if not using parallel run!!!
  echo   "solving..."
  foamJob -s $solver                         > log log.$solver    || exit 1
fi
rm -f log
#- postprocessing
if $post && [ -f runCase.post ]; then
  echo "postprocessing..."
  ./runCase.post || echo "failed postprocessing..."
else
  echo "skip postprocessing..."
fi
echo "finished case run."
// ************************************************************* //
```

12.1.3. Steady-state simulation

OF-file – caseDict

```
FoamFile
{
    version     2.0;
    format      ascii;
    class       dictionary;
    object      caseDict;
}
// <<<<<<<<<<<<<<<<<<< GENERAL SETTINGS >>>>>>>>>>>>>>>>>>> //
// set number of cores to run the simulation on.
//nCores            1; // no parallel run
nCores            20;
// rotation frequency [1/min]
rpm               200;
// stirrer radius [m]
r                 0.035;
// <<<<<<<<<<<<<<<<<<<<<<<<<<<<<<<<<<<<<<<<<<<<<<<<<<<<<<<<<< //

// <<<<<<<<<<<<<<<<<<<<<< MESH SETTINGS >>>>>>>>>>>>>>>>>>>>>> //
//meshSource        localMesh;
meshSource        sharedMesh;
localMeshPath     "../mesh/constant/polyMesh";
sharedMeshInfo
{
    generator         snappyHexMesh;
    scale             labI;
    reactor           flat190;
    stirrer           rushton;
    clearance         70;
    heater            novelR10;
    baffles           novelR10;
    maxCellSize       5;
};
// ************************************************************* //
```

OF-file – epsilon

```
FoamFile
{
    version     2.0;
    format      ascii;
    class       volScalarField;
    location    "0";
    object      epsilon;
}
dimensions      [0 2 -3 0 0 0 0];
internalField   uniform 20;
boundaryField
{
    ".*"
    {
        type            epsilonWallFunction;
        value           $internalField;
    }
    top
    {
        type            slip;
    }
    "AMI.*"
    {
        type            cyclicAMI;
        value           $internalField;
    }
}
// ************************************************************* //
```

OF-file – k

```
FoamFile
{
    version     2.0;
    format      ascii;
    class       volScalarField;
    location    "0";
    object      k;
}
dimensions      [0 2 -2 0 0 0 0];
internalField   uniform 1;
boundaryField
{
    ".*"
    {
        type            kqRWallFunction;
        value           uniform 0;
    }
    top
    {
        type            slip;
    }
    "AMI.*"
    {
        type            cyclicAMI;
        value           $internalField;
    }
}
// ************************************************************* //
```

OF-file – nut

```
FoamFile
{
    version     2.0;
    format      ascii;
    class       volScalarField;
    location    "0";
    object      nut;
}
```

```
dimensions      [0 2 -1 0 0 0 0];
internalField   uniform 0;
boundaryField
{
    ".*"
    {
        type            nutkWallFunction;
        value           uniform 0;
    }
    top
    {
        type            slip;
    }
    "AMI.*"
    {
        type            cyclicAMI;
    }
}
// ************************************************************* //
```

OF-file – p

```
FoamFile
{
    version     2.0;
    format      ascii;
    class       volScalarField;
    object      p;
}
dimensions      [0 2 -2 0 0 0 0];
internalField   uniform 0;
boundaryField
{
    ".*"
    {
        type            zeroGradient;
    }
    top
    {
        type            slip;
    }
    "AMI.*"
    {
        type            cyclicAMI;
        value           $internalField;
    }
}
// ************************************************************* //
```

OF-file – U

```
FoamFile
{
    version     2.0;
    format      ascii;
    class       volVectorField;
    object      U;
}
#include "../constant/speedProperties"
dimensions      [0 1 -1 0 0 0 0];
internalField   uniform (0 0 0);
boundaryField
{
    ".*"
    {
        type            fixedValue;
        value           uniform (0 0 0);
    }
    stirrerTip
    {
```

```
        type            movingWallVelocity;
        value           uniform (0 0 0);
    }
    stirrerStem
    {
        type            rotatingWallVelocity;
        origin          (0 0 0);
        axis            (0 0 1);
        omega           $omega;
    }
    top
    {
        type            slip;
    }
    "AMI.*"
    {
        type            cyclicAMI;
        value           $internalField;
    }
}
// ************************************************************* //
```

OF-file – speedProperties

```
FoamFile
{
    version     2.0;
    format      ascii;
    class       dictionary;
    location    "constant";
    object      speedProperties;
}
// rpm        =200 ;
// r          =0.035 ;
// omega      = 2*pi*rps = 2*pi*rpm/60
// T          = 60/rpm   = 2*pi/omega
// steadyTime = 25*T     = 25*60/rpm
// U_tip      = omega*r  = 2*pi*r*rpm/60
omega       -20.94395102;
T           .30000000;
steadyTime  7.50000000;
dT          .05000000;
U_tip       .73303828;
// ************************************************************* //
```

OF-file – MRFProperties

```
FoamFile
{
    version     2.0;
    format      ascii;
    class       dictionary;
    location    "constant";
    object      MRFProperties;
}
#include "speedProperties"
MRF1
{
    cellZone    cylinder;
    active      yes;
    // Fixed patches (by default they 'move' with the MRF zone)
    nonRotatingPatches ();
    origin    (0 0 0);
    axis      (0 0 1);
    omega     $omega;
}
// ************************************************************* //
```

OF-file – transportProperties

```
FoamFile
{
    version     2.0;
    format      ascii;
    class       dictionary;
    location    "constant";
    object      transportProperties;
}
    transportModel  Newtonian;
    nu              nu [0 2 -1 0 0 0 0] 1e-06;
// ************************************************************* //
```

OF-file – turbulentProperties

```
FoamFile
{
    version     2.0;
    format      ascii;
    class       dictionary;
    location    "constant";
    object      turbulenceProperties;
}
simulationType  RAS;
RAS
{
    RASModel        kEpsilon;
    turbulence      on;
    printCoeffs     on;
    delta           smooth;
    cubeRootVolCoeffs
    {
        deltaCoeff      1;
    }
    PrandtlCoeffs
    {
        delta           cubeRootVol;
        cubeRootVolCoeffs
        {
            deltaCoeff      1;
        }
        smoothCoeffs
        {
            delta           cubeRootVol;
            cubeRootVolCoeffs
            {
                deltaCoeff      1;
            }
            maxDeltaRatio   1.1;
        }
        Cdelta          0.158;
    }
    vanDriestCoeffs
    {
        delta           cubeRootVol;
        cubeRootVolCoeffs
        {
            deltaCoeff      1;
        }
        smoothCoeffs
        {
            delta           cubeRootVol;
            cubeRootVolCoeffs
            {
                deltaCoeff      1;
            }

            maxDeltaRatio   1.1;
        }
```

```
        Aplus           26;
        Cdelta          0.158;
    }
    smoothCoeffs
    {
        delta           cubeRootVol;
        cubeRootVolCoeffs
        {
            deltaCoeff      1;
        }
        maxDeltaRatio   1.1;
    }
}
// ************************************************************* //
```

OF-file – controlDict

```
FoamFile
{
    version         2;
    format          binary;
    class           dictionary;
    location        "system";
    object          controlDict;
}
application     simpleFoam;
startFrom       latestTime;
startTime       0;
stopAt          endTime;
endTime         20000;
deltaT          1;
writeControl    timeStep;
writeInterval   250;
purgeWrite      4;
writeFormat     binary;
writePrecision  6;
writeCompression off;
timeFormat      general;
timePrecision   6;
runTimeModifiable true;
// ************************************************************* //
```

OF-file – decomposeParDict

```
FoamFile
{
    version     2.0;
    format      ascii;
    class       dictionary;
    location    "system";
    object      decomposeParDict;
}
#include "../caseDict"
numberOfSubdomains   $nCores;
method               scotch;
// ************************************************************* //
```

OF-file – fvSchemes

```
FoamFile
{
    version     2.0;
    format      ascii;
    class       dictionary;
    location    "system";
    object      fvSchemes;
}
ddtSchemes
{
    default         steadyState;
```

```
}
gradSchemes
{
    default         Gauss linear;
}
divSchemes
{
    default         none;
    div(phi,U)      bounded Gauss limitedLinearV 1;
    div(phi,k)      bounded Gauss limitedLinear 1;
    div(phi,epsilon) bounded Gauss limitedLinear 1;
    div((nuEff*dev2(T(grad(U))))) Gauss linear;
}
laplacianSchemes
{
    default         Gauss linear corrected;
}
interpolationSchemes
{
    default         linear;
}
snGradSchemes
{
    default         corrected;
}
// ************************************************************* //
```

OF-file – fvSolution

```
FoamFile
{
    version     2.0;
    format      ascii;
    class       dictionary;
    location    "system";
    object      fvSolution;
}
solvers
{
    p
    {
        solver          GAMG;
        tolerance       1e-08;
        relTol          0.05;
        smoother        GaussSeidel;
        cacheAgglomeration true;
        nCellsInCoarsestLevel 20;
        agglomerator    faceAreaPair;
        mergeLevels     1;
    }
    U
    {
        solver          smoothSolver;
        smoother        GaussSeidel;
        nSweeps         2;
        tolerance       1e-07;
        relTol          0.1;
    }
    k
    {
        solver          smoothSolver;
        smoother        GaussSeidel;
        nSweeps         2;
        tolerance       1e-07;
        relTol          0.1;
    }
    epsilon
    {
        solver          smoothSolver;
        smoother        GaussSeidel;
        nSweeps         2;
```

```
        tolerance       1e-07;
        relTol          0.1;
    }
}

SIMPLE
{
    nNonOrthogonalCorrectors 0;
    pRefCell        0;
    pRefValue       0;
}
relaxationFactors
{
    fields
    {
        p               0.3;
    }
    equations
    {
        U               0.7;
        k               0.5;
        epsilon         0.5;
    }
}
// ************************************************************* //
```

12.1.4. Transient simulation

OF-file – dynamicMeshDict

```
FoamFile
{
    version     2.0;
    format      ascii;
    class       dictionary;
    location    "constant";
    object      dynamicMeshDict;
}
#include "speedProperties"
dynamicFvMesh   solidBodyMotionFvMesh;
motionSolverLibs ( "libfvMotionSolvers.so" );
solidBodyMotionFvMeshCoeffs
{
    cellZone        cylinder;
    solidBodyMotionFunction  rotatingMotion;
    rotatingMotionCoeffs
    {
        origin        (0 0 0);
        axis          (0 0 1);
        omega         $omega; // 2*pi*n/60
    }
}
// ************************************************************* //
```

OF-file – controlDict

```
FoamFile
{
    version         2;
    format          ascii;
    class           dictionary;
    location        "system";
    object          controlDict;
}
#include "../constant/speedProperties"
application     pimpleDyMFoam;
startFrom       latestTime;
```

```
startTime       0;
stopAt          endTime;
endTime         7.5;
deltaT          1e-05;
writeControl    adjustableRunTime;
writeInterval   $dT;
purgeWrite      0;
writeFormat     binary;
writePrecision  6;
writeCompression uncompressed;
timeFormat      general;
timePrecision   10;
runTimeModifiable yes;
adjustTimeStep  yes;
maxCo           4;
// ************************************************************* //
```

OF-file – fvSchemes

```
FoamFile
{
    version     2.0;
    format      ascii;
    class       dictionary;
    location    "system";
    object      fvSchemes;
}
ddtSchemes
{
    default         Euler;
}
gradSchemes
{
    default         Gauss linear;
    grad(p)         Gauss linear;
    grad(U)         cellLimited Gauss linear 1;
}
divSchemes
{
    default         none;
//    div(phi,U)      Gauss upwind;
    div(phi,U)      Gauss linearUpwind grad(U);
    div(phi,k)      Gauss upwind;
    div(phi,epsilon) Gauss upwind;
    div((nuEff*dev(T(grad(U))))) Gauss linear;
    div((nuEff*dev2(T(grad(U))))) Gauss linear;
}
laplacianSchemes
{
    default         Gauss linear limited 0.33;
}
interpolationSchemes
{
    default         linear;
}
snGradSchemes
{
    default         limited corrected 0.33;
}
fluxRequired
{
    default         no;
    pcorr           ;
    p               ;
}
// ************************************************************* //
```

OF-file – fvSolution

```
FoamFile
{
    version     2.0;
    format      ascii;
    class       dictionary;
    object      fvSolution;
}
solvers
{
    pcorr
    {
        solver          GAMG;
        tolerance       1e-2;
        relTol          0;
        smoother        DICGaussSeidel;
        cacheAgglomeration no;
        nCellsInCoarsestLevel 10;
        agglomerator    faceAreaPair;
        mergeLevels     1;
        maxIter         50;
    }
    p
    {
        $pcorr;
        tolerance       1e-5;
        relTol          0.01;
    }
    pFinal
    {
        $p;
        tolerance       1e-6;
        relTol          0;
    }
    "(U|k|epsilon)"
    {
        solver          smoothSolver;
        smoother        symGaussSeidel;
        tolerance       1e-6;
        relTol          0;
      nSweeps           1;
    }
    "(U|k|epsilon)Final"
    {
        solver          smoothSolver;
        smoother        symGaussSeidel;
        tolerance       1e-6;
        relTol          0;
      nSweeps           1;
    }
}
PIMPLE
{
    momentumPredictor   yes;
    correctPhi          yes;
    nOuterCorrectors    1;
    nCorrectors         3;
    nNonOrthogonalCorrectors 0;
    pRefCell  0;
    pRefValue 0;
}
relaxationFactors
{
    "(U|k|epsilon).*"   1;
}
cache
{
    grad(U);
}
// ************************************************************* //
```

OF-file – createBafflesDict

```
FoamFile
{
    version     2.0;
    format      ascii;
    class       dictionary;
    object      createBafflesDict;
}
// Whether to convert internal faces only (so leave boundary faces intact).
// This is only relevant if your face selection type can pick up boundary
// faces.
internalFacesOnly true;
// Baffles to create.
baffles
{
    cylinder
    {
        //- Use predefined faceZone to select faces and orientation.
        type        faceZone;
        zoneName    cylinder;
        patches
        {
            master
            {
                //- Master side patch
                name            AMI1;
                type            cyclicAMI;
                matchTolerance  0.0001;
                neighbourPatch  AMI2;
                transform       noOrdering;
            }
            slave
            {
                //- Slave side patch
                name            AMI2;
                type            cyclicAMI;
                matchTolerance  0.0001;
                neighbourPatch  AMI1;
                transform       noOrdering;
            }
        }
    }
}
// ************************************************************* //
```

OF-file – createPatchDict

```
FoamFile
{
    version     2.0;
    format      ascii;
    class       dictionary;
    object      createPatchDict;
}
// Do a synchronisation of coupled points after creation of any patches.
// Note: this does not work with points that are on multiple coupled
patches
//       with transformations (i.e. cyclics).
pointSync false;
// Patches to create.
patches
(
);
// ************************************************************* //
```

12.1.5. Pseudo-2D simulation – heat transfer

Script – runCase.Pre

```
#- meshing
echo "creating block mesh..."
blockMesh                           | tee log.blockMesh
echo "extract surface features..."
surfaceFeatureExtract                     | tee log.surfaceFeatureExtract
echo "run meshing..."
snappyHexMesh -overwrite                  | tee log.snappyHexMesh
echo "extruding 2D mesh..."
extrudeMesh                         | tee log.extrudeMesh
echo "creating boundaries..."
createPatch -overwrite                    | tee log.createPatch
echo "remove empty faces..."
collapseEdges -collapseFaces -overwrite        | tee log.collapseEdges
echo "check mesh quality..."
checkMesh                           | tee log.checkMesh
rm -rf 0; cp -r 0.org 0
// ************************************************************* //
```

Script – runCase.post

```
#- post-processing
wallHeatFlux | tee log.wallHeatFlux
reconstructPar
rm -r processor*
#paraFoam >/dev/null 2>&1 &
pvpython batch.py
mv screen.png $(basename "$PWD").png
mv video1.ogv $(basename "$PWD").ogv
// ************************************************************* //
```

Script – batch.py

```
#- do not miss to change path when state file is copied from elsewhere
servermanager.LoadState("state.pvsm")
actView=GetRenderView()
actView.ViewSize = [1000, 700]
SetActiveView(actView)
animationScene1 = GetAnimationScene()
#animationScene1.GoToFirst()
#animationScene1.GoToNext()
animationScene1.GoToLast()
#- save screenshot
SaveScreenshot('screen.png', magnification=3, quality=100, view=actView)
WriteAnimation('video1.ogv')
// ************************************************************* //
```

OF-file – alphat

```
FoamFile
{
    version     2.0;
    format      ascii;
    class       volScalarField;
    location    "0";
    object      alphat;
}
dimensions      [1 -1 -1 0 0 0 0];
internalField   uniform 0;
boundaryField
{
    top
    {
        type            slip;
    }
    "heater.*"
    {
        type            compressible::alphatWallFunction;
        Prt             0.85;
        value           uniform 0;
    }
    reactorWall
```

```
    {
        type            compressible::alphatWallFunction;
        Prt             0.85;
        value           uniform 0;
    }
    stirrerStem
    {
        type            compressible::alphatWallFunction;
        Prt             0.85;
        value           uniform 0;
    }
    baffles
    {
        type            compressible::alphatWallFunction;
        Prt             0.85;
        value           uniform 0;
    }
    stirrerTipOut
    {
        type            calculated;
        value           uniform 0;
    }
    stirrerTipIn
    {
        type            calculated;
        value           uniform 0;
    }
    #include "defaultBoundaries"
}
// ************************************************************* //
```

OF-file – T

```
FoamFile
{
    version     2.0;
    format      ascii;
    class       volScalarField;
    object      T;
}
dimensions      [0 0 0 1 0 0 0];
internalField   uniform 293;
boundaryField
{
    top
    {
      type        slip;
    }
    "heater.*"
    {
        type            fixedValue;
        value           uniform 333;
    }
    reactorWall
    {
        type            zeroGradient;
    }
    stirrerStem
    {
        type            zeroGradient;
    }
    baffles
    {
        type            zeroGradient;
    }
    stirrerTipOut
    {
        type            fixedValue;
        value           $internalField;
    }
    stirrerTipIn
    {
        type            zeroGradient;
```

```
    }
    #include "defaultBoundaries"
}
// ************************************************************* //
```

OF-file – U

```
FoamFile
{
    version     2.0;
    format      ascii;
    class       volVectorField;
    object      U;
}
dimensions      [0 1 -1 0 0 0 0];
internalField   uniform (0 0 0);
boundaryField
{
    top
    {
      type        slip;
    }
    "heater.*"
    {
      type            fixedValue;
        value           uniform (0 0 0);
    }
    reactorWall
    {
      type            fixedValue;
        value           uniform (0 0 0);
    }
    stirrerStem
    {
      type            fixedValue;
        value           uniform (0 0 0);
    }
    baffles
    {
      type            fixedValue;
        value           uniform (0 0 0);
    }
    stirrerTipOut
    {
        type            fixedValue;
        value           uniform (-0.7 0 0);
    }
    stirrerTipIn
    {
            type         zeroGradient;
    }
    #include "defaultBoundaries"
}
// ************************************************************* //
```

OF-file – defaultValues

```
front
{
      type        wedge;
}
back
{
      type        wedge;
}
zAxis
{
      type        symmetry;
}
// ************************************************************* //
```

OF-file – thermophysicalProperties

```
FoamFile
{
    version     2.0;
    format      ascii;
    class       dictionary;
    object      thermophysicalProperties;
}
thermoType
{
    type            heRhoThermo;
    //Energy for a mixture based on density
    mixture         pureMixture;
    transport       polynomial;
    //Transport package using polynomial functions for mu and kappa
    thermo          hPolynomial;
    //Thermodynamics package templated on the equation of state, using
polynomial
    //functions for cp, h and s
    //Polynomials for h and s derived from cp
    equationOfState icoPolynomial;
    //Incompressible, polynomial form of equation of state, using a
polynomial
    //function for density.
    specie          specie;
    energy          sensibleEnthalpy;
    //Thermodynamics mapping class to expose the sensible enthalpy function
    //as the standard enthalpy function h(T).
}
mixture
{
    // coefficients for water
    specie
    {
        nMoles          1;
        molWeight       18;
    }
    equationOfState
    {
        rhoCoeffs<8>     (762.9905923634 1.8271604010 -0.0034991891 0 0 0 0
0 );
      //rhoCoeffs<8> (1000 0 0 0 0 0 0 0);
    }
    thermodynamics
    {
        Hf              0;
        Sf              0;
        CpCoeffs<8>      ( 5413.5533746131 -7.8014112487 0.0123245614 0 0 0
0 0);
      //CpCoeffs<8>     ( 4183 0 0 0 0 0 0 0);
    }
    transport
    {
        muCoeffs<8>     ( 0.0199331594 -0.0001086515 0.0000001505 0 0 0 0 0
);
        kappaCoeffs<8>   (-0.5876034855 0.0064656194 -0.0000082451 0 0 0 0
0);
       // muCoeffs<8>     ( 0.001 0 0 0 0 0 0 0 );
        //kappaCoeffs<8>  (0.58 0 0 0 0 0 0 0);
    }
}
// ************************************************************* //
```

12.1.6. C++ code

C++-file – meltFields.cpp

```
#include<stdio.h>
#include<stdlib.h>
```

```
#include<iostream>
#include<fstream>
#include<sstream>
#include<string>
using namespace std;

template<class T> string toString(const T& t) {
    ostringstream stream;
    stream << t;
    return stream.str();
} // konvertiert zahl zu string

template<class T> T fromString(const string& s) {
    istringstream stream (s);
    T t;
    stream >> t;
    return t;
} // konverts string to number

int main(int argc, char *argv[]) {
    if ( argc != 2 ) {
        cout << "expected 1 argument (maxAngle), found " << argc - 1 <<
endl;
        return 0;
    }

    double comp;
    double internal[6][95800];
    double surface[6][8716];
    int n;

    int minAngle = 0;
    int maxAngle = fromString<int>( argv[1] );
    int deltaAngle = (maxAngle-minAngle)/5;
    int angle=minAngle;

    string angleS;
    string dateiS;
    const char * dateiName;

    fstream f;
    fstream r;
    r.precision( 10 );

        while ( angle <= maxAngle ){
            angleS = toString<int>( angle );

            dateiS = "zi" + angleS; // analog for x, y and p
                   dateiName = dateiS.c_str();
            f.open( dateiName , ios::in);
            n=0;
            while ( f >> comp )
            {
                internal[ angle/deltaAngle ][n] = comp;
                n++;
            } // read values
            f.close();

            dateiS = "zs" + angleS;
             dateiName = dateiS.c_str();
            f.open( dateiName, ios::in);
            n=0;
            while ( f >> comp )
            {
                surface[ angle/deltaAngle ][n] = comp;
                n++;
            } // read values
            f.close();

            angle += deltaAngle;
        } // loop all files
```

```
        dateiS = "zi";
        dateiName = dateiS.c_str();
        r.open( dateiName, ios::out);
        for (int i = 0; i < 95800 ; i++) {
            double mittel = 0;
            for (int j = 0; j < 6; j++) {
                mittel += internal[j][i];
            }

            r << mittel/6 << endl;
        }
        r.close();

        dateiS = "zs";
        dateiName = dateiS.c_str();
        r.open( dateiName, ios::out);
        for (int i = 0; i < 8716; i++) {
            double mittel = 0;
            for (int j = 0; j < 6; j++) {
                mittel += surface[j][i];
            }
            r << mittel/6 << endl;
        }
        r.close();
} // main
```

12.2. Workspace for effective use of OpenFOAM for stirred processes

The workspace is not available in the online version.

12.3. Animation: juxtaposition of measurement and simulation of a transient stirring process

The workspace is not available in the online version.

12.4. List of publications

Lead author publications

09/2016 Stefan A, Wuenscher P, Schultz HJ, Ulbricht M (2016), Untersuchung der Gasdichteverteilung in begasten Ruehrkesseln mit eintauchenden Rohrschlangen. Chem. Ing. Tech. 88(9):1385-1386. doi:10.1002/cite.201650341

04/2017 Stefan A, Schultz HJ (2016), Simulation of the Heat Exchange in Vessels with Helical Coils and the Influence of Stirrer Position. Chem. Ing. Tech. 89(4):470-474. doi:10.1002/cite.201600146

01/2018 A. Stefan and H. J. Schultz, "Use of OpenFOAM® for Investigation of Mixing Time in Agitated Vessels with Immersed Helical Coils," in Openfoam Selected Papers of the 11th Workshop., Springer Verlag, 2017. ISBN: 978-3-319-60845-7

Co-author publications

09/2016 Schultz HJ, Matzke M, Kessel C, Jährling K, Stefan A, Bliem V (2016), Experimente und gekoppelte CFD-Simulationen von Wärmeübergängen an Rohrschlangen in Fermentern und Rührreaktoren. Chem. Ing. Tech. 88(9):1380. doi:10.1002/cite.201650216

04/2017 K. Jährling et al., "Particle Image Velocimetry Compared to CFD Simulation of Stirred Vessels with Helical Coils," Chem. Ing. Tech., vol. 89, no. 4, pp. 401–408, Apr. 2017. doi:10.1002/cite.201600145

Conferences – oral presentations

03/2015 Interaktive Untersuchung von Rührprozessen am Bespiel eines Reaktors mit komplexen Einbauten Teil 2: Implementierung des Modells im CFD-Werkzeug OpenFOAM und Validierung; Stefan, A., Bliem, V., Schultz, H. J., Jahrestreffen der Fachgruppen Computational Fluid Dynamics und Mehrphasenströmungen, 2015, Lüneburg, Germany.

06/2016 Use of OpenFOAM® for Investigation of Mixing Time in Agitated Vessels with immersed helical coils; Stefan, A., Ulbricht, M., Schultz, H. J., OpenFOAM Workshop 11, 2016, Guimaraes, Portugal.

12.5. Curriculum vitae

The CV is not available in the online version based on data-legal reasons.